University of South Carolina
Scholar Commons

Theses and Dissertations

2018

Design, Synthesis, Characterization, And Applications Of Matrix Free Polymer Nanocomposites

Yucheng Huang
University of South Carolina

Follow this and additional works at: https://scholarcommons.sc.edu/etd

 Part of the Chemistry Commons

Recommended Citation

Huang, Y.(2018). *Design, Synthesis, Characterization, And Applications Of Matrix Free Polymer Nanocomposites.* (Doctoral dissertation). Retrieved from https://scholarcommons.sc.edu/etd/4831

This Open Access Dissertation is brought to you by Scholar Commons. It has been accepted for inclusion in Theses and Dissertations by an authorized administrator of Scholar Commons. For more information, please contact dillarda@mailbox.sc.edu.

DESIGN, SYNTHESIS, CHARACTERIZATION, AND APPLICATIONS OF MATRIX FREE POLYMER NANOCOMPOSITES

by

Yucheng Huang

Bachelor of Science
Nanjing University, 2008

Master of Science
Nanjing University, 2011

Submitted in Partial Fulfillment of the Requirements

For the Degree of Doctor of Philosophy in

Chemistry

College of Arts and Sciences

University of South Carolina

2018

Accepted by:

Brian C. Benicewicz, Major Professor

Chuanbing Tang, Committee Member

Andrew B. Greytak, Committee Member

Rosemarie M. Booze, Committee Member

Cheryl L. Addy, Vice Provost and Dean of the Graduate School

© Copyright by Yucheng Huang, 2018
All Rights Reserved

ACKNOWLEDGMENTS

I would like to express my gratitude to my advisor, Dr. Brian C. Benicewicz, for his mentoring, knowledge, and support currently and in future. He always encourages and supports me to be an independent scientist. He is supportive to my accidental discovery and gives full freedom to explore a new research area. Thank my committee members, Dr. Chuanbing Tang, Dr. Andrew B. Greytak, and Dr. Rosemarie M. Booze for their helpful discussions and guidance.

Special thanks are owed to the collaborators of Columbia University, Dr. Sanat K. Kumar, Dr. Eileen Buenning, and Connor R. Bilchak. I would like to thank Dr. Yang Zheng, Dr. Lei Wang, Dr. Amrita Sarkar, Dr. Morgan Stefik, Dr. Zhongkai Wang, Dr. Jifu Wang, Julia Pribyl, Zaid Abbas, Massimo Tawfilas, Andrew Pingitore, Susan Hipp, Laura Murdock, Dr. Guoqing Qian, Dr. Warren Steckle, Karl Golian, Maan Al-Ali, Dr. Fei Huang, Dr. Lihui Wang, Dr. Mohammad Khani, Dr. Michael Bell, Dr. Tony Neely, Dr. Kayley Fishel, Dr. Xin Li, Dr. Anand Viswanath, and all the other Benicewicz group members.

I am also grateful to my friends, Qingfeng Zhang, Lichao Sun, Ting Pan, Linghang Zeng, Guangfang Li, Kangmin Xie, Ping Li, Yi Shen, Li Wang, Zhengrui Miao, Xinyi Guo, Gang Wang, and Hongkun Lin, for their friendship.

Finally I would like to thank my wife, Yanmei Xu, and my family for their countless support and love in my life.

ABSTRACT

This dissertation focuses on the design, synthesis, characterization and application of matrix free polymer nanocomposites. Reversible addition-fragmentation chain transfer (RAFT) polymerization was used to synthesize block copolymers and polymer grafted silica nanoparticles with precise control over architectures.

In the first chapter, thermoplastic elastomer (TPE) grafted nanoparticles were prepared by grafting block copolymer poly(styrene-*block*-(n-butyl acrylate)) onto silica nanoparticles (NPs) (~15nm) via surface initiated RAFT polymerization. The effects of polymer chain length and graft density on the mechanical properties were investigated using films made solely from the grafted NPs. The ultimate tensile stress and elastic modulus increased with the increase of PS chain length. The dispersion of silica NPs and the microphase separation of block copolymers in the matrix-free polymer nanocomposite were investigated using small angle X-ray scattering (SAXS), transmission electron microscopy (TEM), differential scanning calorimetry (DSC) and dynamic mechanical analysis (DMA). The higher polymer graft density TPEs exhibited better microphase separation of block copolymers and more uniform silica NP dispersion than lower polymer graft density TPEs with similar polymer chain length and compositions.

In the following chapter, we investigated the application of matrix-free polymer nanocomposites in the gas separation area. Polymer membranes have wide applications in gas separation. Poly(methyl acrylate) (PMA) and poly(methyl methacrylate) (PMMA)

grafted silica NPs were synthesized by surface initiated RAFT polymerization. A versatile protocol was developed to remove ungrafted PMA from PMA grafted silica NPs from RAFT polymerization, which was implemented in place of a traditional ultracentrifuge procedure. The membranes from neat polymer grafted silica NPs exhibited an enhanced gas permeability over neat polymers, which was related to the increased free volume. The permeability can also be tuned by the grafted polymer molecular weight, which showed a "volcano plot" in permeability versus molecular weight. There was no aging effect on the membranes from polymer grafted NPs in the experimental measurement time line, which is important for practical applications in designing stable gas separation membranes.

Finally, the synthesis and applications of matrix free polymer grafted silica nanoplatelets as photonic crystals were investigated. One-dimensional photonic crystals can be formed by self-assembly of block copolymers, which typically need large molecular weight polymers. A new strategy for two different photonic crystals was constructed with different solvent responses and reflecting colors from the films of a single block copolymer. Initially, films made from poly(3-(triethoxysilyl)propyl methacrylate)-*block*-poly(stearyl methacrylate) with moderate molecular weight ($PTEPM_{666}$-*b*-$PSMA_{553}$ film) were responsive to alcohol with an observed stop band change from 365 nm (dry film) to 458 nm (film in ethanol), displaying a blue color. After conversion of the PTEPM domain to form SiO_2 nanoplatelets, the $PSMA_{553}$-g-SiO_2 nanoplatelet film showed a larger stop band change from 365 nm (dry film) to 591 nm (film in THF), which reflected a bright orange color.

TABLE OF CONTENTS

LIST OF TABLES

LIST OF FIGURES

List of Abbreviations

AIBN ..... Azobisisobutyronitrile

ATRP ..... Atom transfer radical polymerization

BA ..... Butyl acrylate

BCP ..... Block copolymer

CPDB ..... 4-cyanopentanoic acid dithiobenzoate

CDPA ..... 4-Cyano-4-(((dodecylthio)carbonothioyl)thio)pentanoic acid

CRP ..... Controlled radical polymerization

DCC ..... N,N'-Dicyclohexylcarbodiimide

DCM ..... Dichloromethane

DMA ..... Dynamic mechanical analysis

DMAP 4-Dimethylaminopyridine

DMF ..... N,N-dimethylformamide

DoPAT ..... 2-(((dodecylthio)carbonothioyl)thio)propanoic acid

DSC ..... Differential scanning calorimetry

ESAXS ..... Extreme-small angle X-ray scattering

FT-IR ..... Fourier transform infrared spectroscopy

FWHM ..... Full width at half maximum

GPC ..... Gel permeation chromatography

NMP ..... Nitroxide mediated polymerization

NMR ..... Nuclear Magnetic Resonance

NP ..... Nanoparticle

MA ..... Methyl acrylate

MMA..... Methylmethacrylate

MP..... Melting point

PALS..... Positron annihilation lifetime spectroscopy

PBA..... Poly(butyl acrylate)

PDMS..... Polydimethylsiloxane

PC..... Photonic crystal

PMA..... Poly(methyl acrylate)

PMMA ..... Poly(methyl methacrylate)

PS ..... Polystyrene

PSMA..... Poly(stearyl methacrylate)

PTEPM..... Poly(3-(triethoxysilyl)propyl methacrylate)

P2VP ..... Poly(2-vinylpyridine)

QCM ..... Quartz crystal microbalance

RAFT ..... Reversible addition-fragmentation chain transfer

RDRP ..... Reversible-deactivation radical polymerization

ROMP ..... Ring-opening metathesis polymerization

RPM..... Rotations per minute

SBS ..... Poly(styrene-block-butadiene-block-styrene)

SEM ..... Scanning electron microscope

SIS..... Poly(styrene-block-isoprene-block-styrene)

TEM ..... Transmission electron microscopy

TEOS..... Tetraethoxysilane

THF ..... Tetrahydrofuran

TPE ..... Thermoplastic elastomer

TGA ..... Thermogravimetric Analysis

SAXS ..... Small-angle X-ray scattering

SI ..... Surface initiated

UV-vis..... Ultraviolet visible spectroscopy

LIST OF SCHEMES

CHAPTER 1

INTRODUCTION

1.1 Polymer nanocomposites

Polymer nanocomposites (PNCs) from the blending of inorganic nanoparticle (NP) and polymer matrix have attracted more and more interests both in academia and industry.[1-19] Incorporation of inorganic nanoparticles into the polymer matrix could bring the combined properties from each. The interface between inorganic nanoparticles and organic polymer matrix increases the unfavorable enthalpy interaction, which most of time results in an agglomeration of NPs in the matrix. This deteriorates the properties of the polymer materials.

Surface modification of NPs by ligands or polymers has been reported to improve the compatibility of NPs with polymer matrices. However, mere surface modification cannot guarantee to create a well dispersed NP morphology in the matrix. Polymer grafted nanoparticles, also known as polymer brushes on nanoparticles, could form different morphorlogies in a polymer matrix. Kumar et al. reported that polystyrene (PS) grafted silica nanoparticles self-assembled into isotropic and anisotropic morphologies with well dispersed, strings, sheets, and agglomeration in a polystyrene matrix.[20] The morphology was tuned by the polymer chain graft density and polymer chain length ratio of grafted and matrix polymer. An experimental morphology diagram is illustrated in **Figure 1.1**, which indicates a high graft density and high grafted to matrix polymer chain length ratio was necessary for nanoparticles to obtain well dispersed morphology in the polymer nanocomposite.

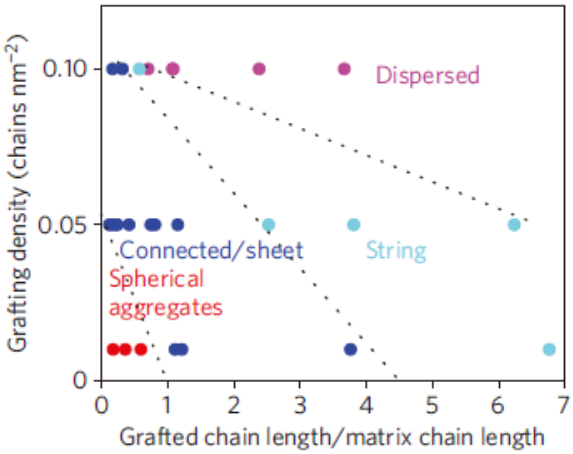

Figure 1.1 Experimental morphology diagram of polymer grafted nanoparticles in polymer matrix.[20]

Practically the randomly well dispersed nanoparticles in polymer matrix was important to achieve enhanced mechanical and other desired properties.[2,5,7,8,10,12,16-18,21] Benicewicz et al. reported an improved strategy to obtain well dispersed nanoparticles in polymer matrix with bimodal polymer brushes.[22] Bimodal polymer brushes on nanoparticles contained two populations of grafted polymers: a low graft density long brush and another high graft density short brush. The long polymer brush can entangle with the polymer matrix while the dense short brush can screen nanoparticle-nanoparticle core attractions. The bimodal PS grafted silica nanoparticles showed better NP dispersion and improved mechanical properties than monomodal PS grafted NPs in a PS matrix.[22,23] The bimodal polymer brushes on nanoparticles are not limited to the same chemical polymer. Mixed bimodal brushes have been designed and synthesized with different functionalities. [22,24-26]

1.2 RAFT polymerization

Reversible addition-fragmentation chain transfer (RAFT) polymerization was firstly reported by CSIRO researchers in 1998.[27] It is a controlled radical polymerization

technique and has been widely used for polymer synthesis.[28-32] It is difficult to synthesize polymers with a low dispersity (Đ) of molecular weights in conventional free radical polymerization due to chain transfer and radical termination. In order to alleviate the chain transfer and radical termination, it's crucial to control the concentration of active radicals at a low level. RAFT polymerization afforded precise control over the molecular weight with narrow Đ and well-defined architectures. RAFT polymerization is different from conventional free radical polymerization by using a specially designed chain transfer agent. Chain transfer agents are typically dithioesters or trithiocarbonates, which have high chain transfer constants. The mechanism of RAFT polymerization is illustrated in **Scheme 1.1**.[32,33] After initiation, the propagating radical P_n· reacts with the RAFT agent to form intermediate **B**, which fragments to form **C** and a new radical R：R·reinitiates monomer to form a new propagating radical P_m：The main equilibrium is established quickly between P_m；P_n·and dormant polymer **C**. Also the termination step can produce some dead polymers. After the polymerization is stopped, most polymer chains are dormant **C** with thiocarbonylthio end groups, which can be used for the synthesis of block copolymers[34] and further modifications.[35-38] Different kinds of RAFT agents with R and Z groups were reported to have good control over the polymerization for different monomer types (styrenes, (meth)acrylates, (meth)acrylamides, vinyl esters, vinyl amides etc). The end group could also be reduced to generate a thiol for thiol-ene "click" reactions.[39-42] The polymers synthesized by RAFT always result in a pink or yellow color, which is due to the color of RAFT agent. This color can be removed by reacting with excess initiator.[43,44]

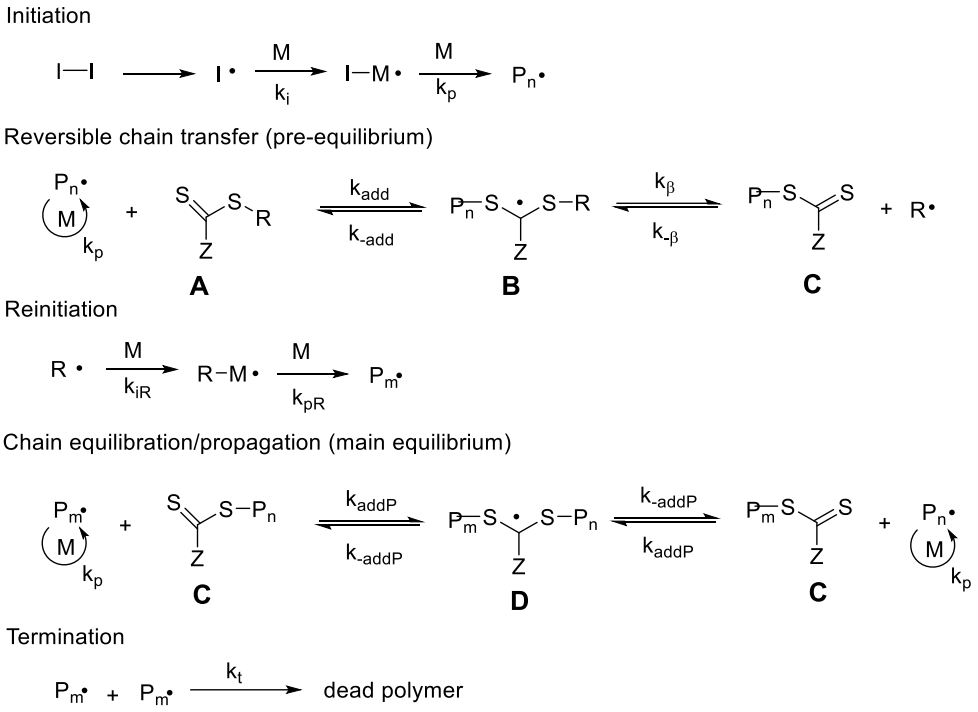

Scheme 1.1 Mechanism of RAFT polymerization

RAFT polymerization also uses mild polymerization conditions, which is similar to free radical polymerization. RAFT polymerization has been reported to occur in different mediums like organic solvents, supercritical carbon dioxide,[45] ionic liquids[46] and water[47]. RAFT polymerization can be applied in solution, bulk[48], suspension,[49-51] and emulsion[52] conditions. RAFT polymerization is sensitive to trace oxygen, so degassing is necessary for a controlled polymerization. Stevens et al. reported the use of glucose oxidase (GOx) enzyme to deoxygenate for RAFT polymerization, which showed control over the polymerization in an open vessel.[53] Boyer et al. reported photo-induced electron transfer-reversible addition-fragmentation chain transfer (PET-RAFT) polymerization with a photoredox catalyst, which was tolerant to oxygen without the degassing step.[54,55]

1.3 Surface modification of nanoparticles by polymers

The surface modification of nanoparticles by polymers can be achieved by grafting to and grafting from strategies (**Figure 1.2**).[48,56-60] The grafting to approach was accomplished by either physical absorption or chemical bonding of polymers to the surface. The physical absorption technique used non-covalent interactions between polymers and the NP surface, such as electronic interaction, Van der Waals interaction, and hydrogen bonding, which was susceptible to environmental stimulus (temperature, pH, ion, light, electric filed, ultrasound etc.). The chemically covalent grafting to approach involved the reaction between a functional group in the polymer chains and the nanoparticle surface. However, the grafting to strategy suffered from difficulty to get high graft density of polymer chains on the surface, which resulted from the steric hindrance of successive polymer chains to approach the nanoparticle surface. The polymer molecular weight also affected the modification efficiency, with lower graft densities for high molecular weight polymers.

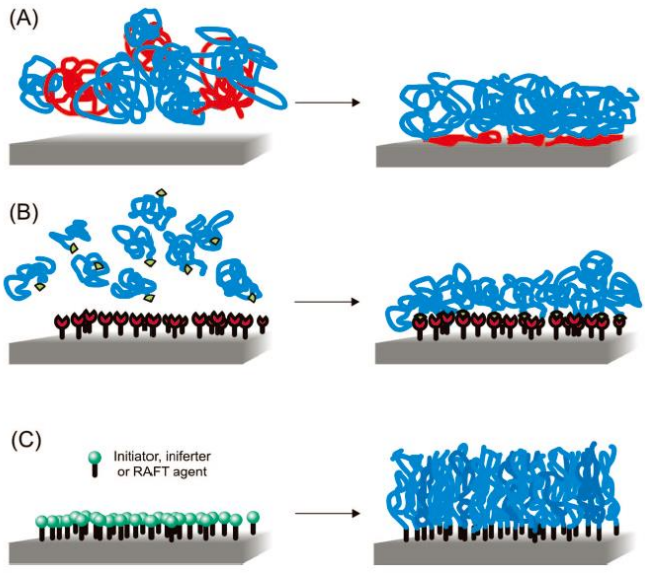

Figure 1.2 Surface modification by polymer strategies. (a) physisorption; (b) chemical grafting to; (c) grafting from. [56]

Grafting from strategy started by attaching initiator or RAFT agent onto the surface, which was followed by surface initiated polymerization of adding monomers. Anionic, cationic, ring-opening, and ring-opening metathesis polymerizations have been used for surface initiated polymerization.[48,56-59,61] Recent developments of controlled radical polymerization techniques (RAFT, atom-transfer radical-polymerization (ATRP), and nitroxide-mediated radical polymerization (NMP)) enabled new strategies to modify the surface, which expanded the graft density range compared to the grafting to strategy.[37,62-71] In addition, the grafting polymer composition and molecular weight can be well controlled to investigate the structure property relationships.

The nanoparticles widely reported as nanofillers in polymer composites were mainly silica and metal oxide nanoparticles. Functional organic silanes were used to modify the silica nanoparticles surface, which formed covalent Si-O-Si bonding with initiator or RAFT agent for a grafting from approach. A wide range of metal oxide and metal nanoparticles has been reported for surface modification with different inherent properties including aluminium oxide, magnesium oxide, zinc oxide, zirconium dioxide, cerium oxide, titanium dioxide, iron oxide, tin oxide, indium tin oxide, copper oxide, yttrium oxide, lanthanum oxide, barium titanate, tungsten trioxide, indium oxide, gold, silver, and quantum dots.[56,72,73] The surface modification of metal oxide nanoparticles made use of reactivity of the –OH groups on the surface by reacting with silanes, phosphonates, carboxylates, catechols, alkenes and alkynes, amines and others.[74] Silanes were often used to modify metal oxide surfaces. However, this approach was limited by the fact that the bonding was susceptible to hydrolysis.[75] The carboxylates, catechols, and amines bondings were mainly through non-covalent interactions. The alkenes and alkynes were through

photo-induced reactions. The phosphonates approach was mostly used to modify metal oxide surfaces through chemisorption to form strong covalent P-O-M bonding.[76-79]

1.4 Surface modification by RAFT polymerization

Surface initiated RAFT (SI-RAFT) polymerization has been widely used to modify nanoparticles or substrate surfaces with excellent control over the polymerization to obtain different architectures due to its versatility, simplicity, and being free of metal contamination.[56,57,59] The grafting from approach was mainly used to modify surfaces to get high graft densities. Initiator, RAFT agent and monomer were involved in the polymerization process, so initiator or RAFT agent can be anchored onto the surface for polymerization (**Scheme 1.2**).

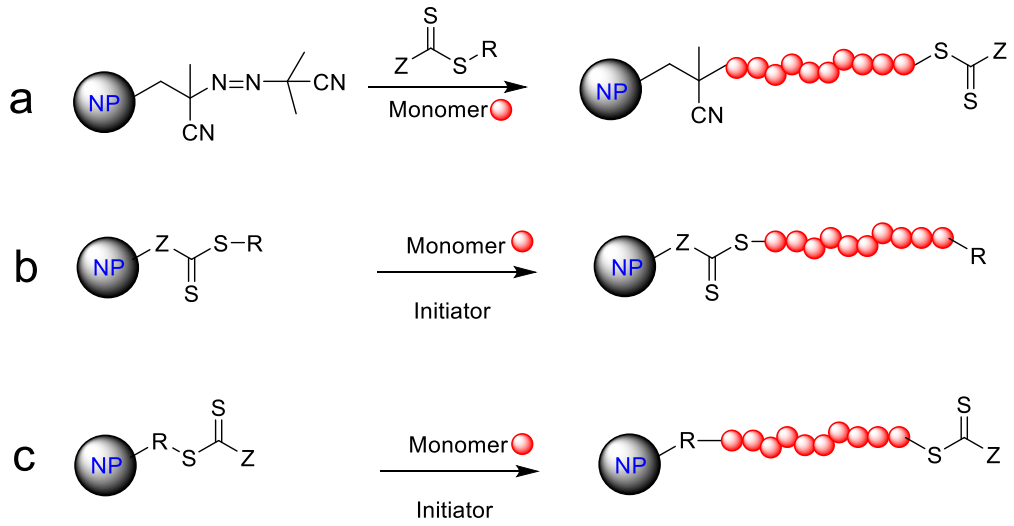

Scheme 1.2 Different approaches for surface initiated RAFT polymerization with grafting from strategy. (a) Initiator attached; (b) Z-group attached; (c) R-group attached.

The initiator immobilization approach was used to modify surface for different monomers.[80-82] However, it was limited by the thermal stability as well as large amount of ungrafted free polymers generated from the polymerization. The free polymers can be

easily washed away by solvent for large flat surface (silicon wafer, glass) and large size particles while it was difficult for nanoparticles. For the immobilization of the RAFT agent, both Z- and R-group approaches were reported. The the Z-group strategy was less investigated by researchers than R-group strategy.[83] In Z-group approach, the RAFT agent was located near the surface, which limited the propagation of polymer chains due to steric hindrance of surrounding polymer chains.[84] Benicewicz et al. firstly reported the use of a silane functional RAFT agent to modify silica nanoparticles with the R-group grafting from approach.[84] It showed good control over polymerization of monomers on the silica nanoparticle surface with high graft density. However, the synthesis of the silane functional RAFT agent was tedious with low yield. A versatile approach was developed later by Benicewicz et al. for SI-RAFT polymerization (**Scheme 1.3**).[85]

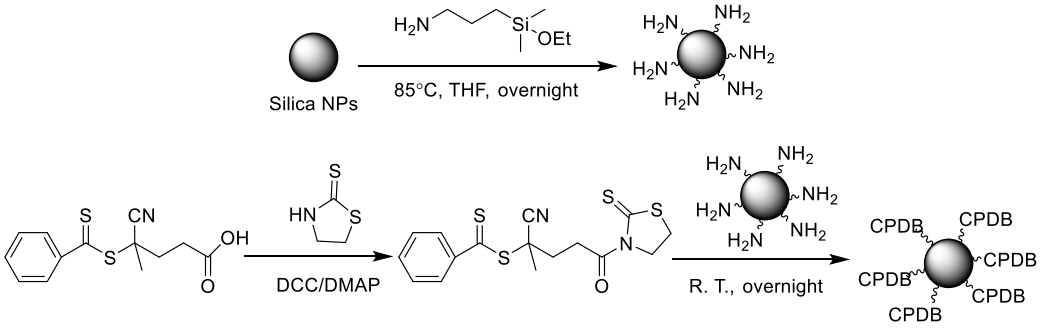

Scheme 1.3 Synthesis procedures for CPDB modified silica nanoparticles.

The silica NPs reacted with aminopropyldimethylethoxysilane to get an amino-functional surface. The RAFT agent, 4-cyanopentanoic acid dithiobenzoate (CPDB), with –COOH group was activated by mercaptothiazoline to prepare activated CPDB. The activated CPDB reacted with amine-functional silica NPs to yield RAFT modified silica NPs. The graft density was tuned by the relative amount of aminosilane to NPs, which

ranged from 0.01 to 0.7 chain/nm^2. The CPDB anchored silica NPs showed controlled polymerization with styrene (St) and methyl methacrylate (MMA) monomers. This versatile approach enabled the researchers to tether different RAFT agents with a –COOH group and polymerize different monomers.

1.5 Matrix-free polymer nanocomposites

The mechanical properties of polymer materials can be improved by adding inorganic nanofillers into the polymer matrix to form polymer composites. Often, the Young's modulus and yield stress were improved by the fillers relative to neat polymer while the fracture strain sacrificed.[10] The morphology of nanoparticles (well dispersed, strings, sheets, and aggregations) in the composite, is crucial to the mechanical properties of the polymer nanocomposite. Kumar et al. reported the mechanical properties of thin glassy PS films with PS grafted silica nanoparticles. The films with different silica NPs morphologies showed different mechanical properties with the same silica content loading (**Figure 1.3**).[86]

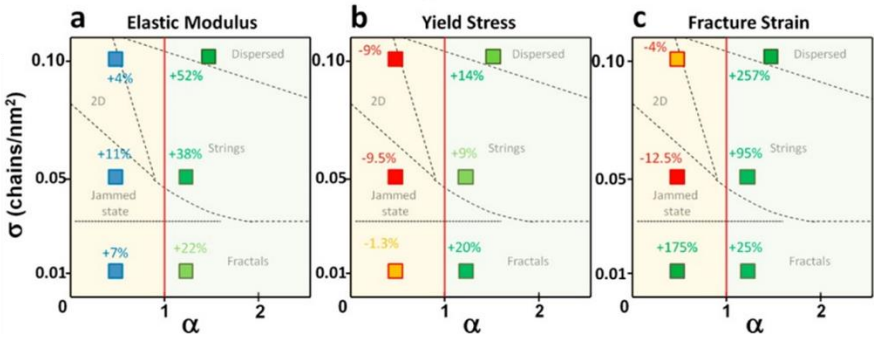

Figure 1.3 Reinforcement percentage of the (a) elastic modulus, (b) yield stress, and (c) failure strain of PS-g-SiO_2 NPs relative to the pure polymer depending on grafting density and grafted/ matrix chain length ratio.[86]

The elastic modulus, yield stress and fracture strain increased for the nanocomposite film with well dispersed NPs compared to neat PS. Interestingly, all the fracture strains increased when the grafted/matrix chain length ratio was larger than 1, which indicated a more entangled interaction from the grafted PS chains penetrating into the matrix polymer.

The traditional polymer nanocomposites form by mixing polymer matrix with nanoparticles. As discussed above, the dispersion state of nanoparticles is important to the nanocomposite properties. In addition, the NPs loading is another parameter we need to consider for enhancing properties. The chemical modification of the NPs surface by polymers enabled tunability of morphologies of the NPs in the composite, which was summarized by Kumar et al. with the experimental 'morphology diagram' of polymer grafted nanoparticles mixed with polymer matrix.[20,87] In order to attain a well dispersed morphology regime, high polymer graft density and high grafted/matrix chain length are necessary. This resulted in a low content of inorganic nanoparticles in the polymer grafted NPs, which further limited a high loading of NPs in the polymer nanocomposites. However, in some cases, high loading of NPs is necessary for good performance, such as polymer nanocomposites for optical[88], conductive, dieletric,[77] and magnetic applications with properties associated to the NPs.

Matrix-free polymer nanocomposites, as the term suggests, are formed solely by polymer grafted nanoparticles without extra polymer matrix. This architecture has advantages over traditional inorganic nanofiller/polymer matrix with inherently good NP dispersion.[89] This enabled the high loading of inorganic NP while maintaining good NPs dispersion. In matrix free polymer nanocomposites, the grafted polymers provide functionality for the mechanical properties and the inorganic core adds functionality to

their intrinsic properties. Vaia et al. investigated the dielectric properties of matrix-free polystyrene grafted titanium dioxide (TiO_2) with inorganic content from 60-80 wt%.[77] The film obtained from solvent casting was optically transparent even at 60-80 wt% TiO_2 content, which indicated a good dispersion of NPs in the composite. Li et al. reported matrix-free bimodal grafted polydimethylsiloxane (PDMS)/zirconium dioxide for LEDs to enhance light extraction efficiency.[88] The bimodal architecture used a dense short polymer brush to screen core-core attractions while the long brush imparted effective chain entanglement. Wang et al. reported a matrix-free magnetic thermoplastic elastomer from poly(n-butyl acrylate-co-methyl methacrylate) grafted Fe_3O_4 nanoparticles.[90] The bulk film exhibited thermoplastic elastomer properties and the superparamagnetic behavior for Fe_3O_4 nanoparticles was illustrated by dispersing the polymer grafted Fe_3O_4 in DMF solution.

1.6 Dissertation outline

This dissertation focuses on the design, synthesis, characterization, and application of the matrix-free polymer nanocomposites with different architectures. Reversible addition fragmentation chain transfer (RAFT) polymerization was used to construct the various polymer nanocomposites.

In Chapter 2, a diblock copolymer, poly(styrene-block-(n-butyl acrylate)) (PS-b-PBA), was covalently tethered onto 15nm silica nanoparticles by surface initiated RAFT polymerization, which mimicked the polymer structure of traditional ABA triblock copolymer thermoplastic elastomers (TPEs). The films were prepared by hot pressing of PS-b-PBA grafted silica NPs, without extra polymer matrix. The effects of polymer chain

length and graft density on the mechanical properties were investigated. The results indicated that the ultimate tensile stress and elastic modulus increased with the increase of PS chain length. The stress, strain at break and elastic modulus were independent of the silica content. The highest ultimate tensile strength of PS-*b*-PBA-*g*-SiO_2 (*ca*. 17 MPa) was higher than the highest value of TPEs from triblock PS-*b*-PBA-*b*-PS (*ca*. 12 MPa) prepared by emulsion RAFT polymerization. The dispersion of the silica NPs and the microphase separation of the block copolymer in the matrix-free polymer nanocomposite were investigated using SAXS, TEM, DSC and DMA. The higher polymer graft density TPEs exhibited better microphase separation of the block copolymers and more uniform silica NP dispersion than lower polymer graft density TPEs with similar polymer chain length and composition.

In Chapter 3, we focused on another application of matrix-free polymer nanocomposites in the gas separation area. Many gas separation membranes have been previously synthesized and investigated. However, most of them were limited by the Robeson upper bound due to limited ability to tune the polymer free volume. Polymer composites obtained from traditional blending of silica nanoparticles with polymer matrix showed a decrease in permeability, which was consistent with traditional composite theories. Thus it was interesting to investigate the performance of membranes formed solely by polymer grafted nanoparticles. 2-(Dodecylthiocarbonothioylthio)propanoic acid (DoPAT) RAFT agent was used for SI-RAFT polymerization to prepare poly(methyl acrylate) (PMA) grafted silica nanoparticles. A versatile protocol was developed to remove ungrafted PMA from PMA grafted silica NPs from RAFT polymerization, which was used instead of the traditional ultracentrifuge procedure. The membranes from neat polymer grafted silica NPs exhibited

an enhanced gas permeability of CO_2 over neat polymers with a 10-fold increase while there was a slight decrease of selectivity of CO_2/CH_4 in PMA grafted silica membranes. The permeability can also be tuned by the grafted polymer molecular weight, which showed a "volcano plot" behavior in permeability versus molecular weight. There was no aging effect on the membranes from polymer grafted NPs in the experimental measurement time line, which has practical applications in designing stable gas separation membranes.

Finally, Chapter 4 focused on the applications of block copolymers and the in situ generated matrix free polymer grafted silica nanoplatelets as photonic crystals. A block copolymer, poly(3-(triethoxysilyl)propyl methacrylate)-block-poly(stearyl methacrylate) with moderate molecular weight ($PTEPM_{666}$-*b*-$PSMA_{553}$) was synthesized by RAFT polymerization. The film self-assembled into a lamellar structure and the casted film was colorless. However, the film was blue after immersion into ethanol with an observed stop band change from 365 nm (dry film) to 458 nm (film in ethanol). This was due to the swelling of PTEPM layer in ethanol, which increased the layer thickness to reflect blue light. After gelation of the PTEPM domain by hydrochloric acid to form SiO_2 nanoplatelets, the $PSMA_{553}$ grafted SiO_2 nanoplatelet film showed a larger stop band change from 365 nm (dry film) to 591 nm (film in THF), which reflected a bright orange color. This resulted from the swelling of the grafted PSMA in THF. Different molecular weight block copolymers were investigated to construct different colors of photonic crystals.

1.7 References

(1) Kumar, S. K.; Benicewicz, B. C.; Vaia, R. A.; Winey, K. I. *Macromolecules* **2017**, *50*, 714.

(2) Hussain, F.; Hojjati, M.; Okamoto, M.; Gorga, R. E. *J. Compos. Mater.* **2006**, *40*, 1511.

(3) Kao, J.; Thorkelsson, K.; Bai, P.; Rancatore, B. J.; Xu, T. *Chem. Soc. Rev.* **2013**, *42*, 2654.

(4) Lenart, W. R.; Hore, M. J. A. *Nano-Structures & Nano-Objects* **2017**.

(5) Sanchez, C. B., P.; Popall, M.; Nicole, L. *Chem. Soc. Rev.* **2011**, *40*, 696.

(6) Sanchez, C.; Julián, B.; Belleville, P.; Popall, M. *J. Mater. Chem.* **2005**, *15*, 3559.

(7) Kickelbick, G. *Prog. Polym. Sci.* **2003**, *28*, 83.

(8) Jancar, J.; Douglas, J. F.; Starr, F. W.; Kumar, S. K.; Cassagnau, P.; Lesser, A. J.; Sternstein, S. S.; Buehler, M. J. *Polymer* **2010**, *51*, 3321.

(9) Schadler, L. S. K., S.K.; Benicewicz, B.C.; Lewis, S.L.; Harton, S.E. *MRS Bull.* **2007**, *32*, 335.

(10) Jordan, J.; Jacob, K. I.; Tannenbaum, R.; Sharaf, M. A.; Jasiuk, I. *Mater. Sci. Eng. A* **2005**, *393*, 1.

(11) Schaefer, D. W. J., R. S. *Macromolecules* **2007**, *40*, 8501.

(12) Kumar, S. K.; Krishnamoorti, R. *Annu. Rev. Chem. Biomol. Eng.* **2010**, *1*, 37.

(13) Fischer, H. *Mater. Sci. Eng. C* **2003**, *23*, 763.

(14) Crosby, A. J.; Lee, J. Y. *Polym. Rev.* **2007**, *47*, 217.

(15) Paul, D. R.; Robeson, L. M. *Polymer* **2008**, *49*, 3187.

(16) Rittigstein, P.; Torkelson, J. M. *J. Polym. Sci., Part B: Polym. Phys.* **2006**, *44*, 2935.

(17) Muller, K.; Bugnicourt, E.; Latorre, M.; Jorda, M.; Echegoyen Sanz, Y.; Lagaron, J. M.; Miesbauer, O.; Bianchin, A.; Hankin, S.; Bolz, U.; Perez, G.; Jesdinszki, M.; Lindner, M.; Scheuerer, Z.; Castello, S.; Schmid, M. *Nanomaterials (Basel)* **2017**, *7*.

(18) Tjong, S. C. *Mater. Sci. Eng., R* **2006**, *53*, 73.

(19) Balazs, A. C.; Emrick, T.; Russell, T. P. *Science* **2006**, *314*, 1107.

(20) Akcora, P.; Liu, H.; Kumar, S. K.; Moll, J.; Li, Y.; Benicewicz, B. C.; Schadler, L. S.; Acehan, D.; Panagiotopoulos, A. Z.; Pryamitsyn, V.; Ganesan, V.; Ilavsky, J.; Thiyagarajan, P.; Colby, R. H.; Douglas, J. F. *Nat. Mater.* **2009**, *8*, 354.

(21) Fu, S.-Y.; Feng, X.-Q.; Lauke, B.; Mai, Y.-W. *Composites, Part B* **2008**, *39*, 933.

(22) Rungta, A.; Natarajan, B.; Neely, T.; Dukes, D.; Schadler, L. S.; Benicewicz, B. C. *Macromolecules* **2012**, *45*, 9303.

(23) Natarajan, B.; Neely, T.; Rungta, A.; Benicewicz, B. C.; Schadler, L. S. *Macromolecules* **2013**, *46*, 4909.

(24) Zhao, D.; Di Nicola, M.; Khani, M. M.; Jestin, J.; Benicewicz, B. C.; Kumar, S. K. *ACS Macro Lett.* **2016**, *5*, 790.

(25) Zhao, D.; Di Nicola, M.; Khani, M. M.; Jestin, J.; Benicewicz, B. C.; Kumar, S. K. *Soft Matter* **2016**, *12*, 7241.

(26) Zheng, Y.; Huang, Y.; Abbas, Z. M.; Benicewicz, B. C. *Polym. Chem.* **2016**, *7*, 5347.

(27) Chiefari, J. C., Y. K.; Ercole, F.; Krstina, J.; Jeffery, J.; Le, T. P. T.; Mayadunne, R. T. A.; Meijs, G. F.; Moad, C. L.; Moad, G.; Rizzardo, E.; Thang, S. H. *Macromolecules* **1998**, *31*, 5559.

(28) Moad, G. R., E.; Thang, S. H. *Acc. Chem. Res.* **2008**, *41*, 1133.

(29) Moad, G. R., E.; Thang, S. H. *Aust. J. Chem.* **2005**, *58*, 379.

(30) Moad, G.; Rizzardo, E.; Thang, S. H. *Aust. J. Chem.* **2012**, *65*, 985.

(31) Hill, M. R.; Carmean, R. N.; Sumerlin, B. S. *Macromolecules* **2015**, 5459.

(32) Moad, G. *Macromol. Chem. Phys.* **2014**, *215*, 9.

(33) Barner-Kowollik, C.; Buback, M.; Charleux, B.; Coote, M. L.; Drache, M.; Fukuda, T.; Goto, A.; Klumperman, B.; Lowe, A. B.; McLeary, J. B.; Moad, G.; Monteiro, M. J.; Sanderson, R. D.; Tonge, M. P.; Vana, P. *J. Polym. Sci., Part A: Polym. Chem.* **2006**, *44*, 5809.

(34) Keddie, D. J. *Chem. Soc. Rev.* **2014**, *43*, 496.

(35) M. Alyse Harvison, A. P. J. R., A Thomas P. Davis,A; Lowe, a. A. B. *Aust. J. Chem.* **2011**, *64*, 992.

(36) Moad, G.; Rizzardo, E.; Thang, S. H. *Polym. Int.* **2011**, *60*, 9.

(37) Gregory, A.; Stenzel, M. H. *Prog. Polym. Sci.* **2012**, *37*, 38.

(38) Roth, P. J.; Boyer, C.; Lowe, A. B.; Davis, T. P. *Macromol. Rapid Commun.* **2011**, *32*, 1123.

(39) Lowe, A. B. *Polym. Chem.* **2010**, *1*, 17.

(40) Lowe, A. B. *Polym. Chem.* **2014**, *5*, 4820.

(41) Hoyle, C. E.; Bowman, C. N. *Angew. Chem. Int. Ed.* **2010**, *49*, 1540.

(42) Nair, D. P.; Podgórski, M.; Chatani, S.; Gong, T.; Xi, W.; Fenoli, C. R.; Bowman, C. N. *Chem. Mater.* **2014**, *26*, 724.

(43) Willcock, H.; O'Reilly, R. K. *Polym. Chem.* **2010**, *1*, 149.

(44) Perrier, S.; Takolpuckdee, P.; Mars, C. A. *Macromolecules* **2005**, *38*, 2033.

(45) Jennings, J.; Beija, M.; Kennon, J. T.; Willcock, H.; O'Reilly, R. K.; Rimmer, S.; Howdle, S. M. *Macromolecules* **2013**, *46*, 6843.

(46) Perrier, S.; Davis, T. P.; Carmichael, A. J.; Haddleton, D. M. *Chem. Commun.* **2002**, 2226.

(47) Mc Cormick, C. L.; Lowe, A. B. *Acc. Chem. Res.* **2004**, *37*, 312.

(48) Edmondson, S.; Osborne, V. L.; Huck, W. T. *Chem. Soc. Rev.* **2004**, *33*, 14.

(49) Zetterlund, P. B.; Thickett, S. C.; Perrier, S.; Bourgeat-Lami, E.; Lansalot, M. *Chem. Rev.* **2015**, 9745.

(50) Cunningham, M. F. *Prog. Polym. Sci.* **2008**, *33*, 365.

(51) Zetterlund, P. B.; Kagawa, Y.; Okubo, M. *Chem. Rev.* **2008**, *108*, 3747.

(52) Luo, Y.; Wang, X.; Zhu, Y.; Li, B.-G.; Zhu, S. *Macromolecules* **2010**, *43*, 7472.

(53) Chapman, R.; Gormley, A. J.; Herpoldt, K.-L.; Stevens, M. M. *Macromolecules* **2014**, *47*, 8541.

(54) Xu, J.; Jung, K.; Atme, A.; Shanmugam, S.; Boyer, C. *J. Am. Chem. Soc.* **2014**, *136*, 5508.

(55) Xu, J.; Jung, K.; Boyer, C. *Macromolecules* **2014**, *47*, 4217.

(56) Barbey, R. L., L.; Paripovic, D.; Schuwer, N.; Sugnaux, C.; Tugulu, S.; Klok, H.-A. *Chem. Rev.* **2009**, *109*, 5437.

(57) Chen, W.-L.; Cordero, R.; Tran, H.; Ober, C. K. *Macromolecules* **2017**.

(58) Zoppe, J. O.; Ataman, N. C.; Mocny, P.; Wang, J.; Moraes, J.; Klok, H. A. *Chem. Rev.* **2017**.

(59) Moraes, J.; Ohno, K.; Maschmeyer, T.; Perrier, S. *Chem. Commun.* **2013**, *49*, 9077.

(60) Kango, S.; Kalia, S.; Celli, A.; Njuguna, J.; Habibi, Y.; Kumar, R. *Prog. Polym. Sci.* **2013**, *38*, 1232.

(61) Wu, L.; Glebe, U.; Böker, A. *Polym. Chem.* **2015**, *6*, 5143.

(62) Braunecker, W. A.; Matyjaszewski, K. *Prog. Polym. Sci.* **2007**, *32*, 93.

(63) Lutz, J. F.; Ouchi, M.; Liu, D. R.; Sawamoto, M. *Science* **2013**, *341*, 628.

(64) Patten, T. E.; Matyjaszewski, K. *Adv. Mater.* **1998**, *10*, 901.

(65) Coessens, V.; Pintauer, T.; Matyjaszewski, K. *Prog. Polym. Sci.* **2001**, *26*, 337.

(66) Hawker, C. J. *Acc. Chem. Res.* **1997**, *30*, 373.

(67) Hadjichristidis, N.; Iatrou, H.; Pitsikalis, M.; Mays, J. *Prog. Polym. Sci.* **2006**, *31*, 1068.

(68) Yagci, Y.; Tasdelen, M. A. *Prog. Polym. Sci.* **2006**, *31*, 1133.

(69) Vauthier, C.; Bouchemal, K. *Pharm. Res.* **2009**, *26*, 1025.

(70) Nicolas, J.; Guillaneuf, Y.; Lefay, C.; Bertin, D.; Gigmes, D.; Charleux, B. *Prog. Polym. Sci.* **2013**, *38*, 63.

(71) Yamago, S. *Chem. Rev.* **2009**, *109*, 5051.

(72) Yan, J.; Pan, X.; Wang, Z.; Lu, Z.; Wang, Y.; Liu, L.; Zhang, J.; Ho, C.; Bockstaller, M. R.; Matyjaszewski, K. *Chem. Mater.* **2017**, *29*, 4963.

(73) Viswanath, A.; Shen, Y.; Green, A. N.; Tan, R.; Greytak, A. B.; Benicewicz, B. C. *Macromolecules* **2014**, *47*, 8137.

(74) Pujari, S. P.; Scheres, L.; Marcelis, A. T.; Zuilhof, H. *Angew. Chem. Int. Ed.* **2014**, *53*, 6322.

(75) Pujari, S. P.; Li, Y.; Regeling, R.; Zuilhof, H. *Langmuir* **2013**, *29*, 10405.

(76) Mutin, P. H.; Guerrero, G.; Vioux, A. *J. Mater. Chem.* **2005**, *15*, 3761.

(77) Tchoul, M. N.; Fillery, S. P.; Koerner, H.; Drummy, L. F.; Oyerokun, F. T.; Mirau, P. A.; Durstock, M. F.; Vaia, R. A. *Chem. Mater.* **2010**, *22*, 1749.

(78) Maliakal, A.; Katz, H.; Cotts, P. M.; Subramoney, S.; Mirau, P. *J. Am. Chem. Soc.* **2005**, *127*, 14655.

(79) Guerrero, G.; Mutin, P. H.; Vioux, A. *Chem. Mater.* **2001**, *13*, 4367.

(80) Baum, M.; Brittain, W. J. *Macromolecules* **2002**, *35*, 610.

(81) Bain, E. D.; Dawes, K.; Özçam, A. E.; Hu, X.; Gorman, C. B.; Šrogl, J.; Genzer, J. *Macromolecules* **2012**, *45*, 3802.

(82) Kondo, T.; Gemmei-Ide, M.; Kitano, H.; Ohno, K.; Noguchi, H.; Uosaki, K. *Colloids Surf. B Biointerfaces* **2012**, *91*, 215.

(83) Zhao, Y.; Perrier, S. *Macromolecules* **2006**, *39*, 8603.

(84) Li, C.; Benicewicz, B. C. *Macromolecules* **2005**, *38*, 5929.

(85) Li, C.; Han, J.; Ryu, C. Y.; Benicewicz, B. C. *Macromolecules* **2006**, *39*, 3175.

(86) Maillard, D.; Kumar, S. K.; Fragneaud, B.; Kysar, J. W.; Rungta, A.; Benicewicz, B. C.; Deng, H.; Brinson, L. C.; Douglas, J. F. *Nano Lett.* **2012**, *12*, 3909.

(87) Kumar, S. K.; Jouault, N.; Benicewicz, B.; Neely, T. *Macromolecules* **2013**, *46*, 3199.

(88) Li, Y.; Wang, L.; Natarajan, B.; Tao, P.; Benicewicz, B. C.; Ullal, C.; Schadler, L. S. *RSC Adv.* **2015**, *5*, 14788.

(89) Fernandes, N. J.; Koerner, H.; Giannelis, E. P.; Vaia, R. A. *MRS Commun.* **2013**, *3*, 13.

(90) Jiang, F.; Zhang, Y.; Wang, Z.; Wang, W.; Xu, Z.; Wang, Z. *ACS Appl. Mater. Interfaces* **2015**, *7*, 10563.

CHAPTER 2

MATRIX-FREE POLYMER NANOCOMPOSITE THERMOPLASTIC ELASTOMERS*

*This chapter was adapted from Huang et al., *Macromolecules*, **2017**, *50*, 4742.

2.1 Abstract

Thermoplastic elastomer (TPE) grafted nanoparticles were prepared by grafting block copolymer poly(styrene-*block*-(n-butyl acrylate)) onto silica nanoparticles (NPs) via surface initiated reversible addition-fragmentation chain transfer (RAFT) polymerization. The effects of polymer chain length and graft density on the mechanical properties were investigated using films made solely from the grafted NPs. The ultimate tensile stress and elastic modulus increased with increasing PS chain length. The dispersion of the silica NPs and the microphase separation of the block copolymer in the matrix-free polymer nanocomposite were investigated using small angle X-ray scattering (SAXS), transmission electron microscopy (TEM), differential scanning calorimetry (DSC) and dynamic mechanical analysis (DMA). The higher polymer graft density TPEs exhibited better microphase separation of the block copolymers and more uniform silica NP dispersion than lower polymer graft density TPEs with similar polymer chain length and composition.

2.2 Introduction

Thermoplastic elastomers (TPEs) have broad applications in a variety of fields as footware, paving, replacement of vulcanized rubber, adhesives, sealants, coatings, automotive, medical, etc.[1,2] The traditional and widely used TPEs are made from triblock copolymers such as poly(styrene-*block*-butadiene-*block*-styrene) (SBS) and poly(styrene-*block*-isoprene-*block*-styrene) (SIS), which are synthesized by living anionic polymerization.[2,3] Traditional ABA type TPEs contain a glassy domain dispersed within a rubbery domain formed from microphase separation of the block copolymer. Recent developments in controlled radical polymerization techniques have added additional tools for the design and synthesis of new architectures of polymer materials.[4-8] Jerome et al.

reported TPEs formed from poly(methyl methacrylate-*block*-(n-butyl acrylate)-*block*-methyl methacrylate) (PMMA-*b*-PBA-*b*-PMMA) by atom transfer radical polymerization (ATRP).[9] They also compared the differences in morphology and mechanical properties with an identical block copolymer prepared by anionic polymerization. Luo et al. prepared a series of thermoplastic elastomers of poly(styrene-*block*-(n-butyl acrylate)-*block*-styrene) (PS-*b*-PBA-*b*-PS) by reversible addition-fragmentation chain transfer (RAFT) emulsion polymerization.[10] In addition to the traditional TPEs formed by ABA triblock copolymers, new architectures of thermoplastic elastomers have been reported, such as star block copolymers[11-13], comb multigrafted copolymers,[14-16] etc. Matyjaszewski et al. reported a thermoplastic elastomer formed by 10- and 20-arm starlike block copolymers, poly(n-butyl acrylate-*block*-methyl methacrylate) (PBA-*b*-PMMA), from short linear multifunctional initiators.[17] The ultimate tensile strength and the elastic modulus increased as the number of arms increased. Tang et al. prepared a thermoplastic elastomer by random copolymer-grafted cellulose with the rigid cellulose backbone dispersed in soft matrix random copolymer PBA-*co*-PMMA (0.9-3.4 wt% cellulose).[18]

Inorganic nanoparticles can be added to polymer matrices as nanofillers to tune the mechanical properties.[19,20] The dispersion of nanoparticles in the matrix was crucially important to the mechanical properties of polymer nanocomposites.[21-26] Polymer grafted nanoparticles can self-assemble into well-defined structures[27-30] and increase the compatibility of nanoparticles with the polymer matrix.[31,32] The dispersion of the nanoparticles in polymer nanocomposites was mainly dependent on polymer graft density, and the ratio of molecular weights of grafted polymer and matrix polymer.[33-36] Mondragon et al. reported the use of polystyrene grafted magnetic nanoparticles to improve the

dispersion of magnetic nanoparticles in a SBS thermoplastic elastomer matrix.[37] Polymer nanocomposites formed by one-component polymer grafted NPs, which were also referred to as matrix-free nanocomposites, had advantages over the traditional nanoparticle filled matrix systems. The matrix-free nanocomposite overcame the demixing issue because the polymers were chemically tethered to the NPs.[38] However, there are very few reports of thermoplastic elastomers formed by matrix-free organic/inorganic polymer nanocomposites. Recently Wang et al. reported thermoplastic elastomer composites formed by PBA-*co*-PMMA grafted multiwalled carbon nanotubes[39,40] and Fe_3O_4 nanoparticles[41] prepared using ATRP. The magnetic polymer nanocomposite exhibited higher tensile strength and elastic recovery than the counterpart linear copolymers. To the best of our knowledge, there are no reports of polymer architecture effects (including polymer grafting density and chain length) on the microphase separation and mechanical properties of films formed by block copolymer grafted inorganic nanoparticles.

Herein we report on thermoplastic elastomers formed by block copolymer grafted silica NPs without additional polymer matrix. The block copolymer, poly(styrene-*block*- (n-butyl acrylate)) (PS-*b*-PBA), tethered to 15 nm silica nanoparticles was prepared by RAFT polymerization using a grafting-from strategy.[42-44] In addition to the PS glassy domains dispersed in the rubbery PBA matrix, the silica nanoparticles also acted as crosslinking sites in the thermoplastic elastomers formed by PS-*b*-PBA grafted silica nanoparticles (PS-*b*-PBA-*g*-SiO_2). Three main parameters were used to tune the mechanical properties of the polymer nanocomposite film: chain length of PBA, chain length of PS, and graft density of the polymer chains. We investigated the impacts of these parameters on the mechanical properties of TPEs formed by PS-*b*-PBA-*g*-SiO_2 (**Figure 2.1**).

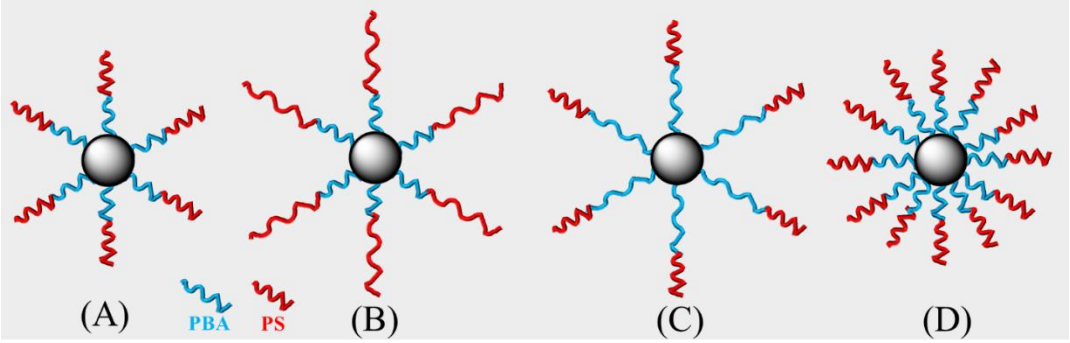

Figure 2.1 Comparison of block copolymer PS-*b*-PBA grafted silica nanoparticles with different chain lengths of PS (**A** *vs* **B**), chain lengths of PBA (**A** *vs* **C**) and chain grafted densities (**A** *vs* **D**).

2.3 Experimental

Materials.

All chemicals were purchased from Sigma-Aldrich or Fisher unless otherwise specified. Styrene (>99%) and n-butyl acrylate (>99%) were purified by passing each through a column of activated basic alumina column to remove the inhibitor. 4-Cyano-4-(((dodecylthio)carbonothioyl)thio)pentanoic acid (CDPA, >97%) was purchased from Boron Molecular. Colloidal silica particles (~15nm diameter, 30 wt% in MEK) were supplied by Nissan Chemical. 3-Aminopropyldimethylethoxysilane was purchased from Gelest Inc. 2-Mercaptothiazoline (98%) was purchased from Alfa Aesar. Azobisisobutyronitrile (AIBN) was recrystallized from ethanol twice before use.

Characterization.

Polymer Characterization.

^{1}H NMR (Bruker Avance III-HD 300 MHz and 400 MHz) were conducted using $CDCl_3$ as solvent. Molecular weights (Mn) and dispersities (Đ) were determined using a gel permeation chromatograph (GPC) equipped with a Varian 290-LC pump, a Varian 390-

LC refractive index detector, and three Styragel columns(HR1, HR3 and HR4, molecular weight range of 100-5000, 500-30000, and 5000-500000, respectively). THF was used as eluent for GPC at 30 ℃ and a flow rate of 1.0 mL/min. GPC was calibrated with polystryrene (PS) standards obtained from Polymer Laboratories. UV−vis absorption spectra were recorded on a Shimadzu UV-2450. Thermogravimetric analysis (TGA) measurements were carried out on a TA Q5000 thermogravimetric analyzer (TA Instruments). All the samples were preheated to 150 ℃ and kept at this temperature for 10 min to remove residual solvents. After cooling to 40 ℃, the samples were heated to 800 ℃ with a heating rate of 10 ℃/min in a nitrogen atmosphere. Differential scanning calorimetry (DSC) was conducted using a TA Q2000 DSC (TA Instruments) under nitrogen atmosphere at a heating rate of 10 ℃/min from -80 ℃ to 180 ℃. Tensile testing was conducted using an Instron 5500 tensile tester with a 100 N load cell with a crosshead speed of 20 mm/min. The dog-bone shaped samples for tensile testing were cut from hot pressed samples with 22 mm length and 5 mm width. Each sample was tested at least three times for tensile testing. Dynamic mechanical analysis (DMA) was conducted using a RSA3 DMA (TA Instruments) in tensile mode. The DMA data were collected by testing with a frequency of 1.0 Hz, 0.1% strain and a heating rate of 3 ℃ /min from -100 ℃ to 150 ℃.

Film preparation.

Polymer grafted silica nanocomposites were hot pressed on a Carver hotpress at 150 ℃ and 1500 psi for 5 min then 3000 psi for 30 min to get films with *ca.* 0.3 mm thickness.

X-ray measurement.

Small-angle X-ray scattering (SAXS) experiments were conducted using a SAXSLab Ganesha instrument at the South Carolina SAXS Collaborative. A Xenocs GeniX3D microfocus source was used with a Cu target to generate a monochromic beam with a 0.154 nm wavelength. The instrument was calibrated using National Institute of Standard and Technology (NIST) reference material 640c silicon powder with the peak position at total scattering angle of 2θ of 28.44˚. A Pilatus 300 K detector (Dectris) was used to collect the two-dimensional (2D) scattering pattern. The 2D images were azimuthally integrated to yield the scattering vector and intensity. All SAXS experiments were conducted for 1 hour with an X-ray flux of 4.1 M photons/s incident up on the sample with a sample-to-detector distance of 1052 mm.

Electron Microscopy.

Transmission electron microscopy (TEM) was performed on a Hitachi H8000 TEM at an accelerating voltage of 200 KV. The microsectioned sample for TEM was prepared by embedding the film in epoxy resin followed by ultramicrotomy with diamond knife at room temperature to a thickness of *ca.* 100 nm and transferred to a copper TEM grid.

Surface initiated RAFT polymerization was used to synthesize PS-*b*-PBA grafted silica nanoparticles (**Scheme 2.1)**. Briefly, the silica nanoparticles were reacted with 3-aminopropyldimethylethoxysilane to obtain a primary amine functionalized surface, which was further reacted with activated CDPA RAFT agent. The block copolymer grafted silica nanoparticles were synthesized by sequential polymerization of n-butyl acrylate and styrene on the surface of silica nanoparticles.

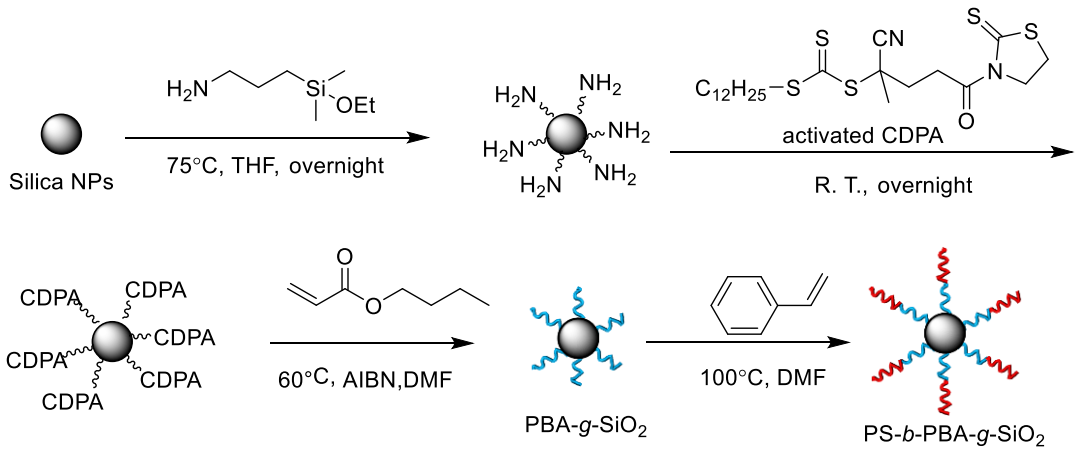

Scheme 2.1 Synthesis of PS-*b*-PBA grafted silica nanoparticles.

Activation of RAFT Agent CDPA.

CDPA (4.07 g, 0.01 mol), 2-mercaptothiazoline (1.31 g, 0.011 mol) and 4-dimethylaminopyridine (DMAP) (0.122 g, 0.001 mol) were dissolved in 100 ml dichloromethane. The solution was cooled in ice bath and N, N'-dicyclohexylcarbodiimide (DCC) (2.48 g, 0.012 mol) was added slowly into the solution. The solution was warmed to room temperature and stirred for 1 hour. After the precipitate was filtered, the solution was concentrated and purified by silica gel column chromatography (hexane: ethyl acetate=3:1) to get activated CDPA (4.32 g, 86%) as yellow solid (MP = 58-59 ˚C). ^{1}H NMR (300 MHz, $CDCl_3$):δ (ppm) 4.60 (t, 2H, *J*=7.5 Hz), 3.68-3.49 (m, 2H), 3.34 (t, 2H, *J*=7.5 Hz), 2.68-2.44 (m, 2H), 1.90 (s, 3H), 1.71 (quint, 2H, *J*=7.5 Hz), 1.43-1.27 (m, 18H), 0.89 (t, 3H, *J*=6.6 Hz); ^{13}C NMR (75MHz, $CDCl_3$):δ (ppm) 271.1, 201.7, 172.4, 119.2, 56.0, 46.3, 37.1, 34.4, 33.9, 31.9, 29.64, 29.57, 29.44, 29.36, 29.1, 29.0, 28.5, 27.7, 24.9, 22.7, 14.2. HRMS (EI) (m/z) calc for $C_{22}H_{36}N_2OS_5$: 504.1439; found: 504.1431.

Synthesis of CDPA Anchored Silica Nanoparticles.

Colloid silica nanoparticles (50 g, 30% in MEK), 3-aminopropyldimethylethoxysilane (360 μL) and 50 mL THF were added to 250 mL round bottom flask. After purging with N_2 for 30 min, the solution was heated to 75 ℃ overnight and then cooled to room temperature. The solution was poured into 400 mL hexanes and amino-functionalized silica nanoparticles were recovered by centrifugation at 3000 rpm for 10 min. The dispersion-precipitation process was repeated another two times. The amino-functionalized silica nanoparticles were dispersed in 50 mL THF and added to the activated CDPA (0.5 g) THF solution slowly. After stirring overnight, the solution was poured into 200 mL hexanes and the CDPA functionalized silica nanoparticles were recovered by centrifugation. The dispersion-precipitation was repeated until the supernatant was colorless after centrifugation. Finally, the CDPA anchored silica nanoparticles (CDPA-SiO_2) were dried in vacuum at room temperature. The graft density of CDPA on silica nanoparticle was analyzed by UV-Vis spectra as 55.7 μmol/g (0.24 ch/nm^2).

Synthesis of Poly (n-butyl acrylate) (PBA) Grafted Silica Nanoparticles (PBA-*g*-SiO_2).

CDPA-SiO_2 (2.0 g, 55.7 μmol/g) was dispersed in 16 mL N, N-dimethylformamide (DMF) and n-butyl acrylate (BA) (16.3 mL, 0.114 mol). The solution was added to a 50 mL Schlenk flask and sonicated for 1min. AIBN (1.14 mL 0.01M in DMF) was added to the flask and the solution was degassed by four freeze-pump-thaw cycles, backfilled with nitrogen, and then placed in an oil bath at 60 ℃ for 3.25 h. The polymerization was quenched by placing the flask in an ice bath. The solution was poured into 120 mL methanol to precipitate the PBA grafted NPs. The PBA-*g*-SiO_2 was recovered by

centrifugation at 5000 rpm for 10 min and re-dispersed in DMF. The dispersion-precipitation process was repeated another two times. The molecular weight of PBA was measured by treating 50 mg nanoparticles in 2 mL THF with HF (0.2 mL of a 51% solution in water) and the resulting cleaved polymer chains were analyzed by GPC. The cleaved PBA had molecular weight Mn=40100 and dispersity Đ=1.14.

Synthesis of Poly(styrene-*block*-(n-butyl acrylate)) Grafted Silica Nanoparticles (PS-*b*-PBA-*g*-SiO_2).

PBA-*g*-SiO_2 (0.9 g) was dispersed in 20 mL DMF in a 50 mL Schlenk flask. Styrene (10 mL) was added to the flask and degassed by four freeze-pump-thaw cycles, backfilled with nitrogen, and then placed in an oil bath at 100 ℃ for 3h. The polymerization was stopped by placing the flask in an ice bath. The solution was poured into 100 mL cold methanol and PS-*b*-PBA-*g*-SiO_2 was recovered by centrifugation at 5000 rpm for 10 min. This was re-dispersed in 25mL THF and the dispersion-precipitation process was repeated for another two times. The purified PS-*b*-PBA-*g*-SiO_2 was dried in a vacuum oven for 24 h. The molecular weight for the block copolymer PS-*b*-PBA was Mn=81500 and dispersity Đ=1.25.

2.4 Results and Discussion

Synthesis and Characterization of PS-*b*-PBA-*g*-SiO_2. The RAFT agent CDPA was used for the polymerization of n-butyl acrylate. Thermal-initiated RAFT polymerization of styrene was used to synthesize the block copolymer grafted silica nanoparticles. A series of block copolymer grafted silica nanoparticles with different graft densities and molecular weights were synthesized by using different ratios of monomer to the CDPA terminated

PBA-*g*-SiO_2. GPC was used to characterize the molecular weight and dispersity of grafted polymer chains (**Figure 2.2**). In addition, ^{1}H NMR was used to characterize the composition of the block copolymers (**Figure 2.3**). In the ^{1}H NMR spectra, the chemical shift (δ) at 7.09-6.36 ppm was from the aromatic protons of polystyrene while the δ at 4.04 ppm originated from C(=O)O-CH_2 in PBA. The ratio of repeat units of styrene and n-butyl acrylate was calculated from the two integrations. TGA was used to characterize the weight percent of silica in the PS-*b*-PBA-*g*-SiO_2. Higher molecular weights resulted in lower silica weight percent with the same graft density. The characteristic data of the block copolymer grafted silica nanoparticles are listed in **Table 2.1**.

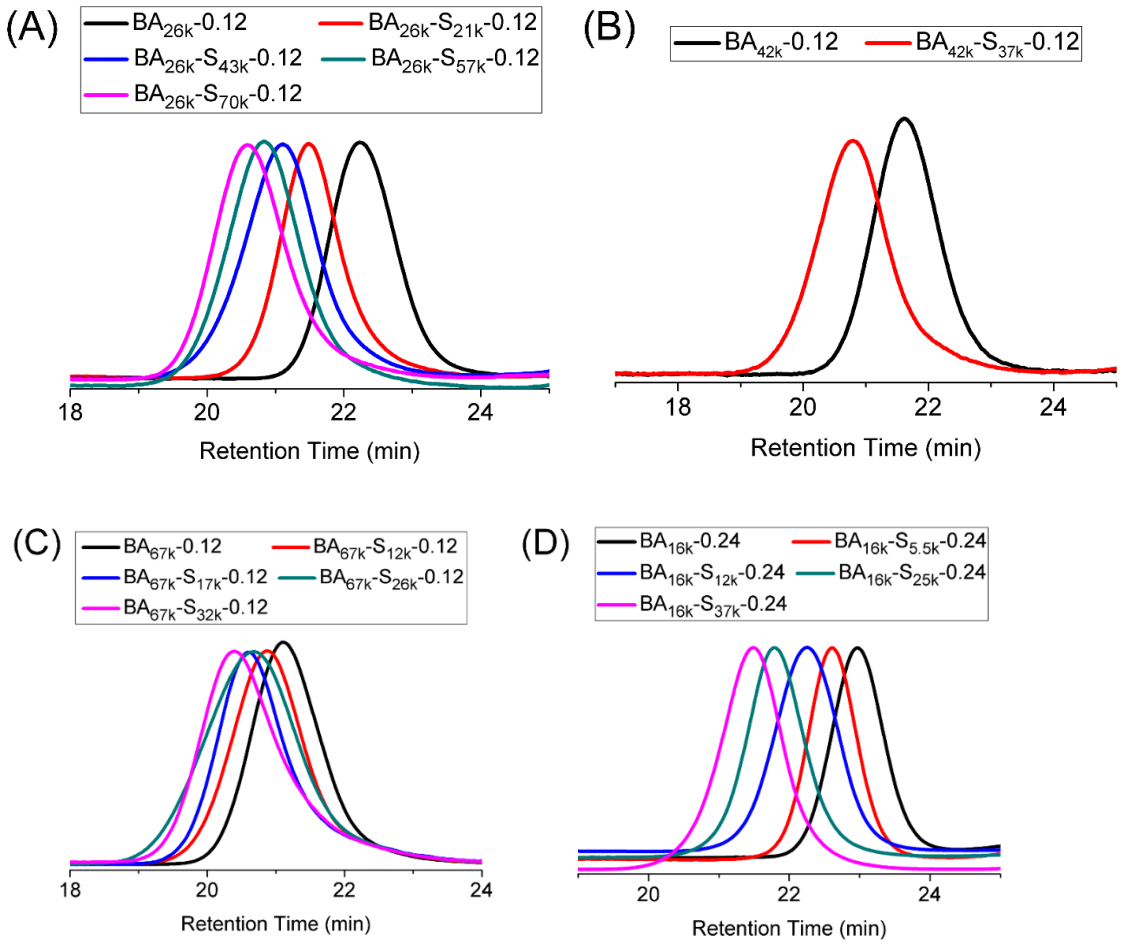

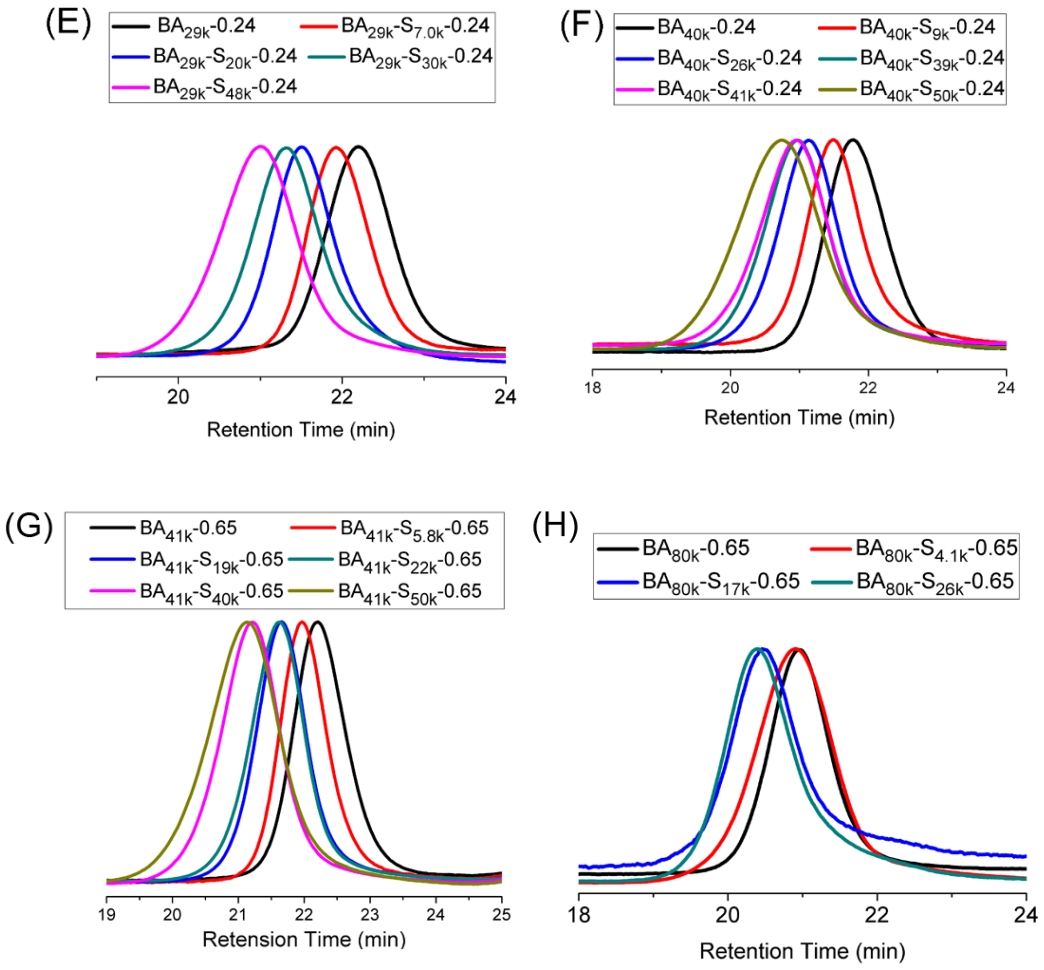

Figure 2.2 GPC curves of PS-*b*-PBA-*g*-SiO_2 with different graft densities.

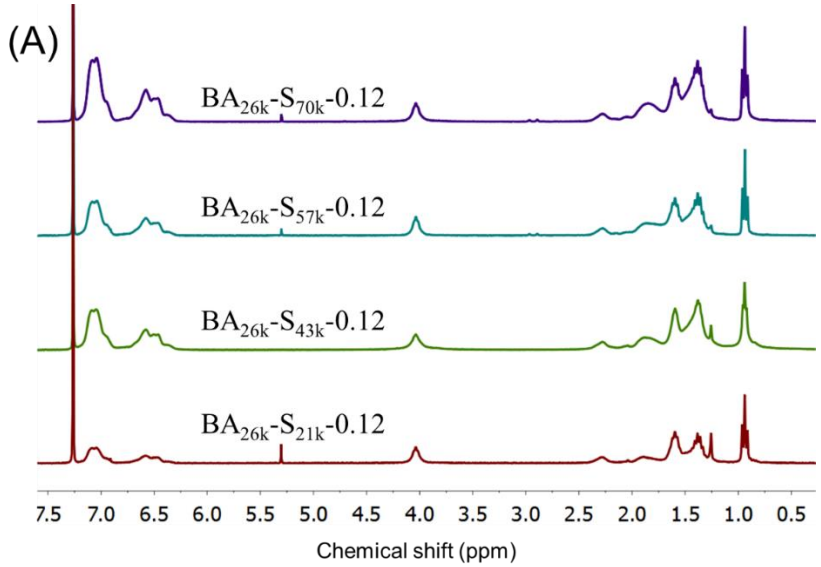

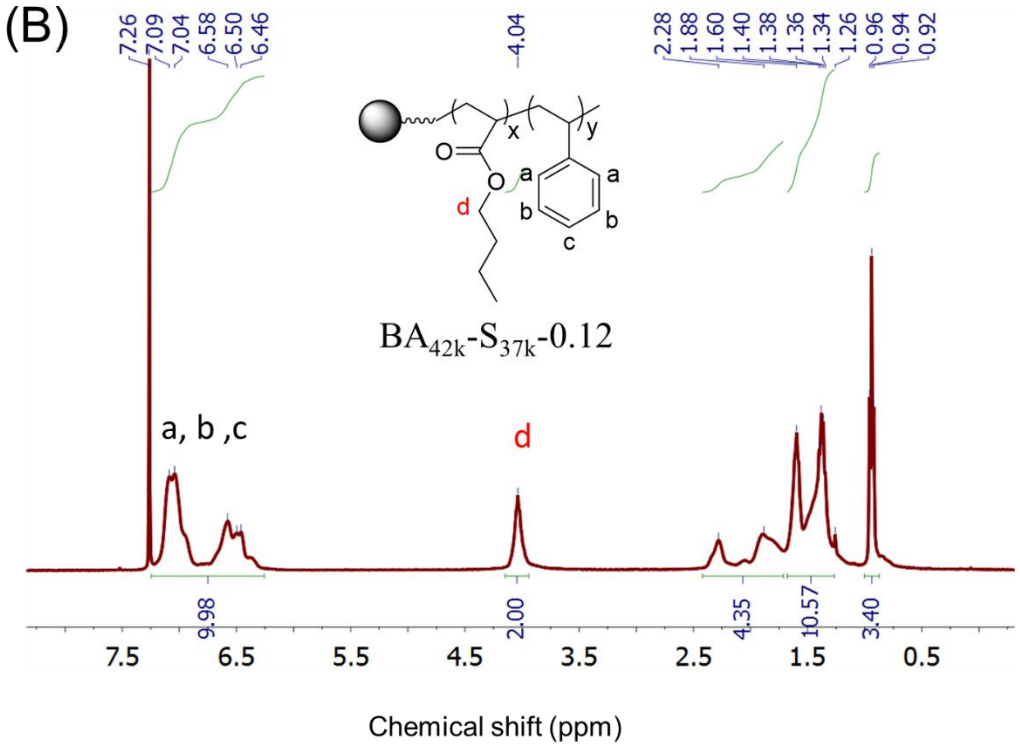
(B)
7.26
7.09
7.04
6.58
6.50
6.46
4.04
2.28
1.88
1.60
1.40
1.38
1.36
1.34
1.26
0.96
0.94
0.92
x
y
O
O
a
a
b
b
c
d
BA42k-S37k-0.12
a, b ,c
d
9.98
2.00
4.35
10.57
3.40
7.5
6.5
5.5
4.5
3.5
2.5
1.5
0.5
Chemical shift (ppm)

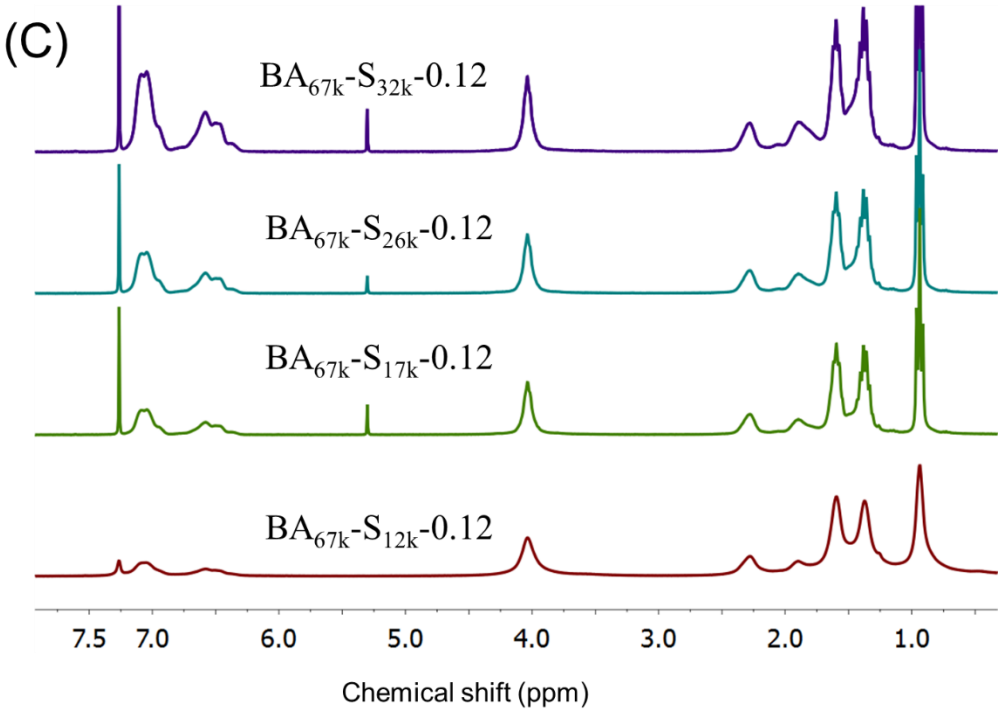
(C)
BA67k-S32k-0.12
BA67k-S26k-0.12
BA67k-S17k-0.12
BA67k-S12k-0.12
7.5
7.0
6.0
5.0
4.0
3.0
2.0
1.0
Chemical shift (ppm)

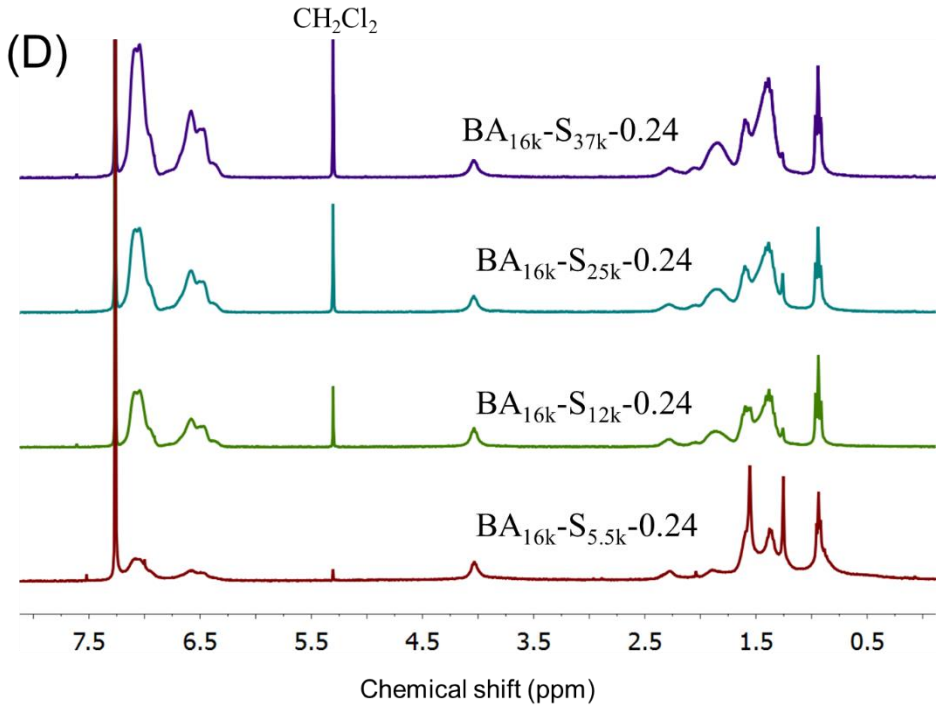
(D)
CH_2Cl_2
BA_{16k}-S_{37k}-0.24
BA_{16k}-S_{25k}-0.24
BA_{16k}-S_{12k}-0.24
BA_{16k}-$S_{5.5k}$-0.24
7.5
6.5
5.5
4.5
3.5
2.5
1.5
0.5
Chemical shift (ppm)

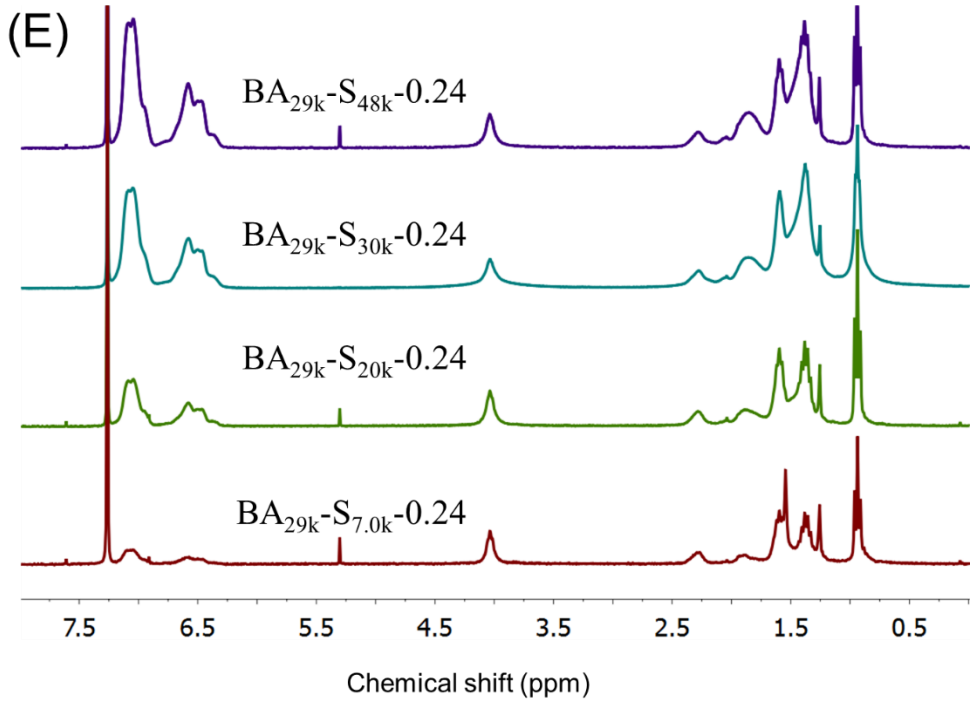
(E)
BA_{29k}-S_{48k}-0.24
BA_{29k}-S_{30k}-0.24
BA_{29k}-S_{20k}-0.24
BA_{29k}-$S_{7.0k}$-0.24
7.5
6.5
5.5
4.5
3.5
2.5
1.5
0.5
Chemical shift (ppm)

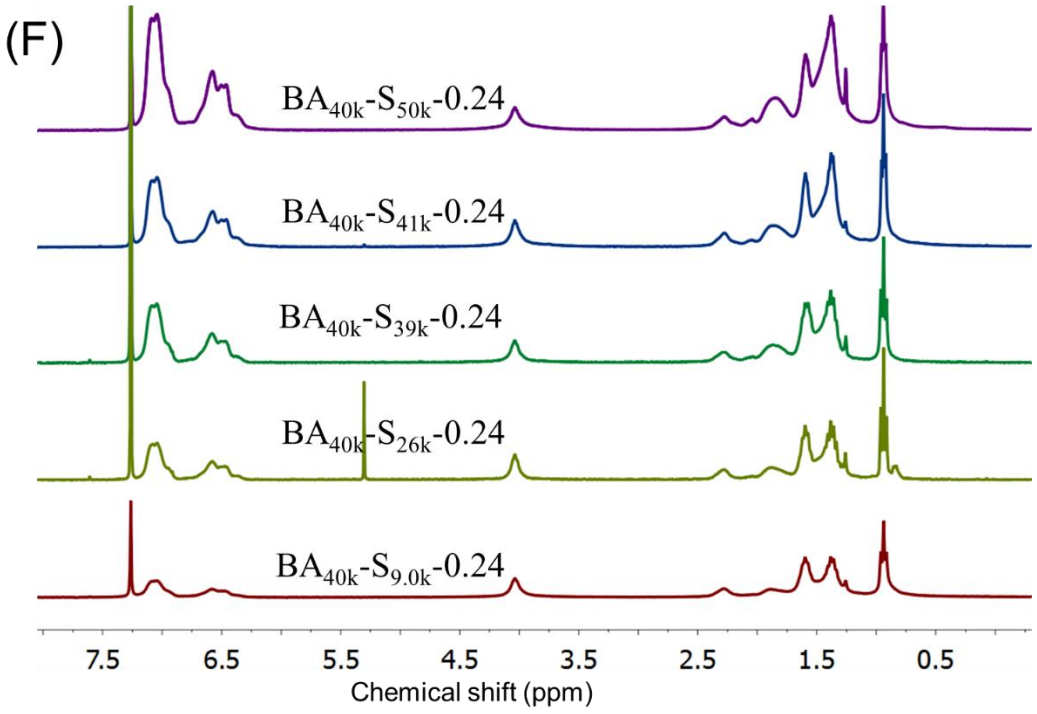
(F)
BA40k-S50k-0.24
BA40k-S41k-0.24
BA40k-S39k-0.24
BA40k-S26k-0.24
BA40k-S9.0k-0.24
7.5
6.5
5.5
4.5
3.5
2.5
1.5
0.5
Chemical shift (ppm)

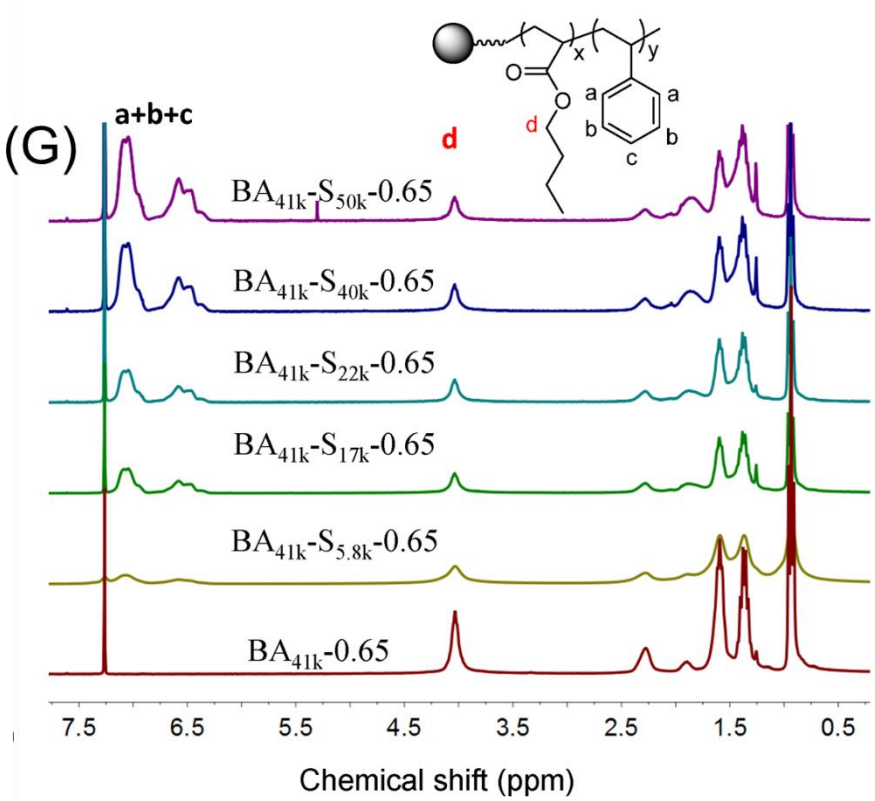
(G)
a+b+c
d
x
y
O
O
a
a
b
b
c
d
BA41k-S50k-0.65
BA41k-S40k-0.65
BA41k-S22k-0.65
BA41k-S17k-0.65
BA41k-S5.8k-0.65
BA41k-0.65
7.5
6.5
5.5
4.5
3.5
2.5
1.5
0.5
Chemical shift (ppm)

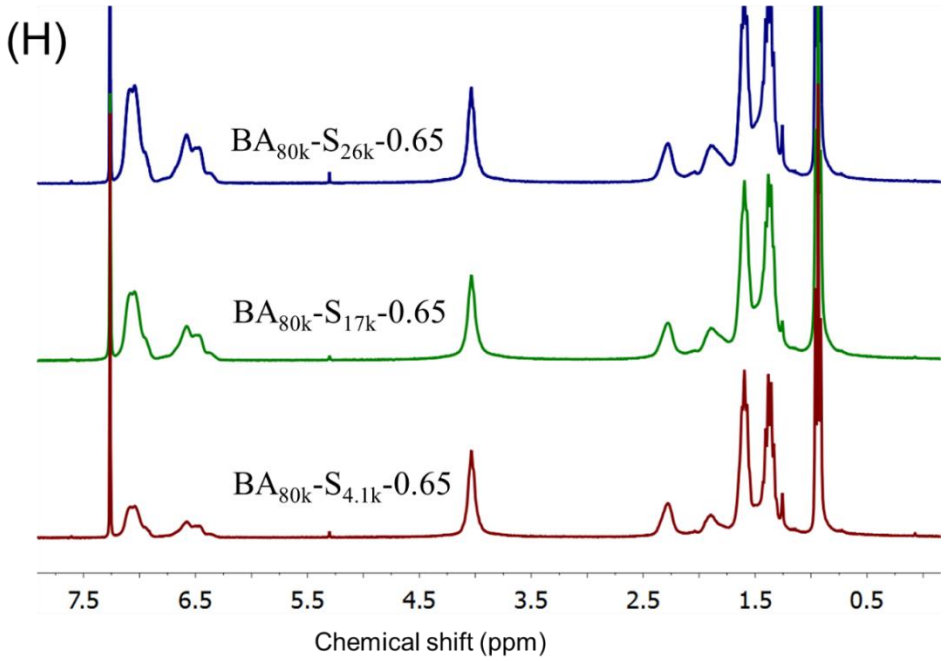

Figure 2.3 ^{1}H NMR spectra of PBA-*g*-SiO_2 and PS-*b*-PBA-*g*-SiO_2 with different graft densities.

Table 2.1 Characterization of PS-*b*-PBA-*g*-SiO_2.

Sample[a]	Mn (PBA)[b]	Đ (PBA)[b]	Mn (PS-*b*-PBA)[b]	Đ (PS-*b*-PBA)[b]	DP(S) /DP(BA)[c]	SiO_2 (wt%)[d]	PS (wt%)[e]
BA_{26k}-S_{21k}-0.12	26400	1.17	47800	1.21	1.29	47.0	27.1
BA_{26k}-S_{43k}-0.12	26400	1.17	69600	1.27	2.15	37.4	39.8
BA_{26k}-S_{57k}-0.12	26400	1.17	83300	1.28	2.58	32.7	45.6
BA_{26k}-S_{70k}-0.12	26400	1.17	96100	1.28	3.83	27.1	55.2

BA_{42k}-S_{37k}-0.12	42100	1.18	79400	1.28	2.00	30.5	43.0
BA_{67k}-S_{12k}-0.12	66500	1.20	78200	1.29	0.26	30.9	12.1
BA_{67k}-S_{17k}-0.12	66500	1.20	83900	1.38	0.54	30.1	21.3
BA_{67k}-S_{26k}-0.12	66500	1.20	92000	1.41	0.82	27.0	29.2
BA_{67k}-S_{32k}-0.12	66500	1.20	98300	1.39	1.29	21.5	40.2
BA_{16k}-$S_{5.5k}$-0.24	15700	1.09	21200	1.09	1.31	53.2	24.1
BA_{16k}-S_{12k}-0.24	15700	1.09	28100	1.15	3.43	40.9	43.5
BA_{16k}-S_{25k}-0.24	15700	1.09	40400	1.14	5.52	35.2	53.0
BA_{16k}-S_{37k}-0.24	15700	1.09	52800	1.19	7.10	28.0	61.4
BA_{29k}-$S_{7.0k}$-0.24	29100	1.11	36100	1.10	0.52	41.8	17.3
BA_{29k}-S_{20k}-0.24	29100	1.11	49200	1.15	1.43	32.3	36.4
BA_{29k}-S_{30k}-0.24	29100	1.11	59100	1.16	2.01	27.7	44.8
BA_{29k}-S_{48k}-0.24	29100	1.11	77100	1.24	3.46	21.3	58.1
BA_{40k}-$S_{9.0k}$-0.24	40100	1.14	49100	1.18	0.83	31.5	27.6
BA_{40k}-S_{26k}-0.24	40100	1.14	66500	1.23	1.78	23.7	45.1
BA_{40k}-S_{39k}-0.24	40100	1.14	79300	1.22	2.06	20.6	49.7

BA_{40k}-S_{41k}-0.24	40100	1.14	81500	1.25	2.19	20.3	51.0
BA_{40k}-S_{50k}-0.24	40100	1.14	90400	1.38	3.38	16.9	60.9
BA_{41k}-$S_{5.8k}$-0.65	40800	1.11	46600	1.12	0.26	16.6	14.5
BA_{41k}-S_{19k}-0.65	40800	1.11	60300	1.14	0.98	12.8	38.7
BA_{41k}-S_{22k}-0.65	40800	1.11	62500	1.17	1.27	11.9	44.7
BA_{41k}-S_{40k}-0.65	40800	1.11	80300	1.23	2.27	9.4	58.8
BA_{41k}-S_{50k}-0.65	40800	1.11	90800	1.28	3.23	8.9	66.0
BA_{80k}-$S_{4.1k}$-0.65	79900	1.15	84000	1.24	0.41	8.7	22.8
BA_{80k}-S_{17k}-0.65	79900	1.15	97100	1.36	0.73	8.1	34.2
BA_{80k}-S_{26k}-0.65	79900	1.15	105400	1.33	1.01	7.1	41.9

[a]Sample defined as follows: BA represents n-butyl acrylate, S represents styrene. The number subscripted is the molecular weight of n-butyl acrylate and styrene measured by GPC; the number after the second dash represents the graft density of polymer chains. Graft density was calculated based on UV-Vis spectrum. [b]Molecular weight and dispersity were measured by GPC. [c]DP represents degree of polymerization. The ratio of repeat units of styrene and n-butyl acrylate was measured by ^{1}H NMR of PS-*b*-PBA-g-SiO_2. [d]The weight percent of silica in PS-*b*-PBA-*g*-SiO_2 was measured by TGA. [e]The weight percent of PS and PBA in PS-*b*-PBA-*g*-SiO_2 was calculated by TGA and ^{1}H NMR.

Table 2.2 Tensile test results of PS-*b*-PBA grafted silica nanoparticles.

Sample	Tensile Stress (MPa)[a]	Strain at Break (%)[a]	Modulus (MPa)[a]	Yield Strength (MPa)[a]	Yield Strain (%)[a]
BA_{26k}-S_{21k}-0.12	7.8 ± 0.6	232 ± 19	10.5 ± 0.3	2.5 ± 0.1	21.3 ± 0.9
BA_{26k}-S_{43k}-0.12	13.9 ± 0.6	137 ± 8	184.0 ± 21.4	7.2 ± 0.6	9.5 ± 0.6
BA_{26k}-S_{57k}-0.12	15.8 ± 0.4	115 ± 15	326.0 ± 13.5	11.4 ± 0.1	5.5 ± 0.2
BA_{26k}-S_{70k}-0.12	16.8 ± 0.3	63 ± 12	567.6 ± 26.5	19.5 ± 0.1	6.2 ± 0.5
BA_{42k}-S_{37k}-0.12	14.0 ± 0.2	164 ± 3	194.9 ± 4.0	6.8 ± 0.2	7.1 ± 0.1
BA_{67k}-S_{12k}-0.12	2.3 ± 0.1	429 ± 12	0.6 ± 0.04	-[b]	-
BA_{67k}-S_{17k}-0.12	6.1 ± 0.2	485 ± 22	1.0 ± 0.2	-	-
BA_{67k}-S_{26k}-0.12	6.2 ± 0.2	259 ± 17	2.5 ± 0.1	-	-
BA_{67k}-S_{32k}-0.12	11.1 ± 0.2	240 ± 5	70.8 ± 5.0	3.1 ± 0.3	12.6 ± 0.4
BA_{16k}-$S_{5.5k}$-0.24	3.7 ± 0.3	134 ± 10	27.8 ± 3.0	-	-
BA_{16k}-S_{12k}-0.24	12.8 ± 0.8	72 ± 8	427.1 ± 17.6	9.0 ± 0.4	4.5 ± 0.2
BA_{16k}-S_{25k}-0.24	16.7 ± 0.4	64 ± 7	509.8 ± 16.2	16.4 ± 0.4	6.0 ± 0.05
BA_{16k}-S_{37k}-0.24	22.3 ± 0.6	26 ± 4	878.4 ± 6.1	27.6 ± 0.7	5.4 ± 0.1

BA_{29k}-$S_{7.0k}$-0.24	1.2 ±0.2	189 ±28	0.4 ±0.02	-	-
BA_{29k}-S_{20k}-0.24	10.4 ±0.6	206 ±10	106.1 ±9.2	3.3 ±0.05	8.1 ±0.6
BA_{29k}-S_{30k}-0.24	13.4 ±0.5	152 ±5	272.2 ±18.0	7.3 ±0.3	6.2 ±1.0
BA_{29k}-S_{48k}-0.24	17.2 ±0.5	83 ±22	592.0 ±10.2	19.0 ±0.2	5.1 ±0.05
BA_{40k}-$S_{9.0k}$-0.24	7.2 ±0.2	317 ±13	2.1 ±0.1	-	-
BA_{40k}-S_{26k}-0.24	13.7 ±0.6	225 ±13	153.4 ±5.3	4.4 ±0.1	6.7 ±0.4
BA_{40k}-S_{41k}-0.24	14.2 ±0.5	148 ±5	366.8 ±10.1	9.4 ±0.2	5.0 ±0.1
BA_{40k}-S_{50k}-0.24	15.4 ±0.2	48 ±13	620.0 ±44.6	16.7 ±0.5	5.7 ±0.3
BA_{41k}-$S_{5.8k}$-0.65	0.8 ±0.03	290 ±23	0.4 ±0.04	-	-
BA_{41k}-S_{19k}-0.65	8.0 ±0.5	241 ±9	102.2 ±2.7	2.3 ±0.1	5.0 ±0.1
BA_{41k}-S_{22k}-0.65	7.3 ±0.7	177 ±15	207.4 ±3.9	4.3 ±0.2	4.4 ±0.3
BA_{41k}-S_{40k}-0.65	14.3 ±0.4	180 ±5	433.3 ±13.4	12.3 ±0.6	4.2 ±0.2
BA_{41k}-S_{50k}-0.65	14.4 ±0.5	116 ±30	501.4 ±26.9	16.3 ±0.3	5.4 ±0.6
BA_{80k}-$S_{4.1k}$-0.65	3.7 ±0.02	413 ±14	0.6 ±0.02	-	-
BA_{80k}-S_{17k}-0.65	6.5 ±0.3	326 ±13	13.4 ±3.2	0.4 ±0.1	4.4 ±0.8
BA_{80k}-S_{26k}-0.65	4.1 ±0.1	142 ±10	72.4 ±5.4	1.5 ±0.3	3.8 ±0.6

[a]Mean value ±standard error. [b] No yielding

Mechanical Properties of Films Formed by PS-*b*-PBA-*g*-SiO_2.

Films formed by hot pressing samples of PS-*b*-PBA-*g*-SiO_2 resulted in transparent matrix-free nanocomposites which were used to characterize the mechanical properties. The stress-strain curves were obtained on dog-bone specimens cut from the films (**Figure 2.4**).

Figure 2.4 Dog-bone shaped film for tensile test

The ultimate tensile strength, strain at break, modulus, yield strength and strain are summarized in **Table 2.2**. The ultimate tensile stress, strain at break and modulus varied significantly with changes in graft density and polymer chain length of the PBA and PS.

The Effect of Chain Length on Mechanical Properties. The films formed by hot pressing of PS-*b*-PBA-*g*-SiO_2 showed typical properties of thermoplastic elastomers with both elastomeric and plastic behavior (**Figure 2.5A-G**). Most of the films with the same graft density and polymer chain length of PBA showed similar trends in mechanical behavior: the ultimate tensile stress increased and strain at break decreased as the corresponding PS chain length increased. Moreover, the elastic modulus increased as the PS chain length increased, which is consistent with typical TPEs.[2,10] These relationships were also

confirmed by the ultimate tensile stress, strain at break and modulus versus PS content plots (**Figure 2.6**). Luo et al. reported the ultimate tensile strength of TPEs of PS-*b*-PBA-*b*-PS increased linearly with PS content at less than 50 wt% PS with the highest stress about 12 MPa.[10] This work introduced the concept of polymers covalently bound to silica NPs, which act as crosslinking sites. However, there was no clear relationship between the silica content and the mechanical properties in the nanocomposites, which was illustrated by the random distribution of points in the ultimate tensile stress vs silica content plot (**Figure 2.6**). The yield properties of the films were largely determined by the PS content and the yield strength increased with increasing PS content. All the films with PS content less than 27 wt% did not exhibit yield behavior while the silica content varied from 8.7-53.2 wt%. The films with low PS content (BA_{67k}-S_{12k}-0.12, BA_{16k}-$S_{5.5k}$-0.24, BA_{29k}-$S_{7.0k}$-0.24 and BA_{41k}-$S_{5.8k}$-0.65) behaved more like elastomers with low elastic modulus. This is likely indicative of the structure with few continuous glassy domains dispersed in the soft PBA matrix. The effect of PBA chain length on the mechanical properties is illustrated in **Figure 2.5H** by comparing films with similar PS chain length and the same graft density (BA_{16k}-S_{25k}-0.24, BA_{29k}-S_{30k}-0.24 and BA_{40k}-S_{26k}-0.24). The elastic modulus and yield strength decreased while elongation at break increased with increasing PBA chain length. The highest ultimate tensile stress for the TPEs formed by hot pressing PS-*b*-PBA-*g*-SiO_2 was *ca.* 17 MPa, which was higher than that reported for TPEs from the triblock copolymer PS-*b*-PBA-*b*-PS (*ca.* 12 MPa) synthesized by RAFT emulsion polymerization.[10]

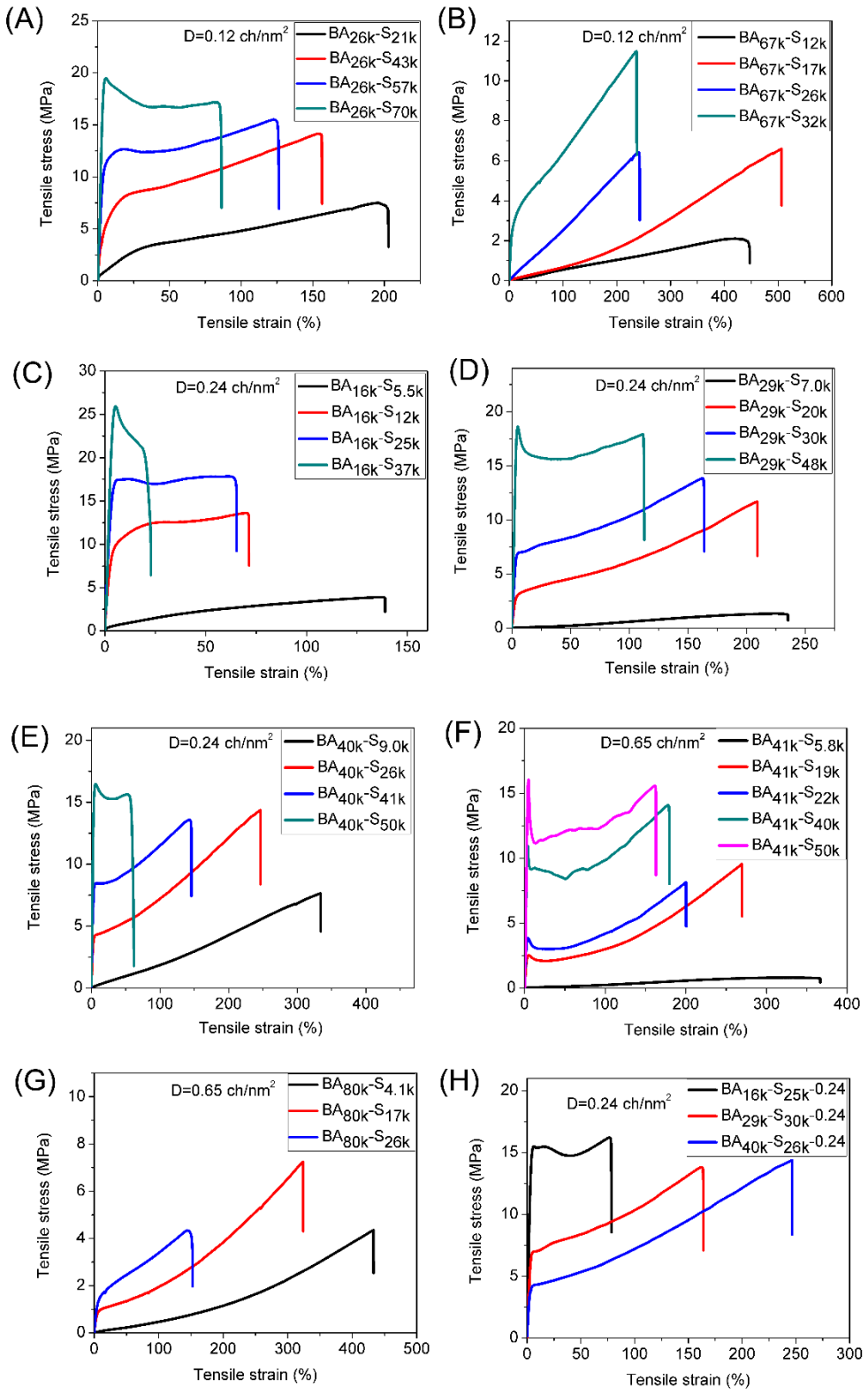

Figure 2.5 Stress-strain curves of films formed by hot pressing of PS-*b*-PBA-*g*-SiO_2.

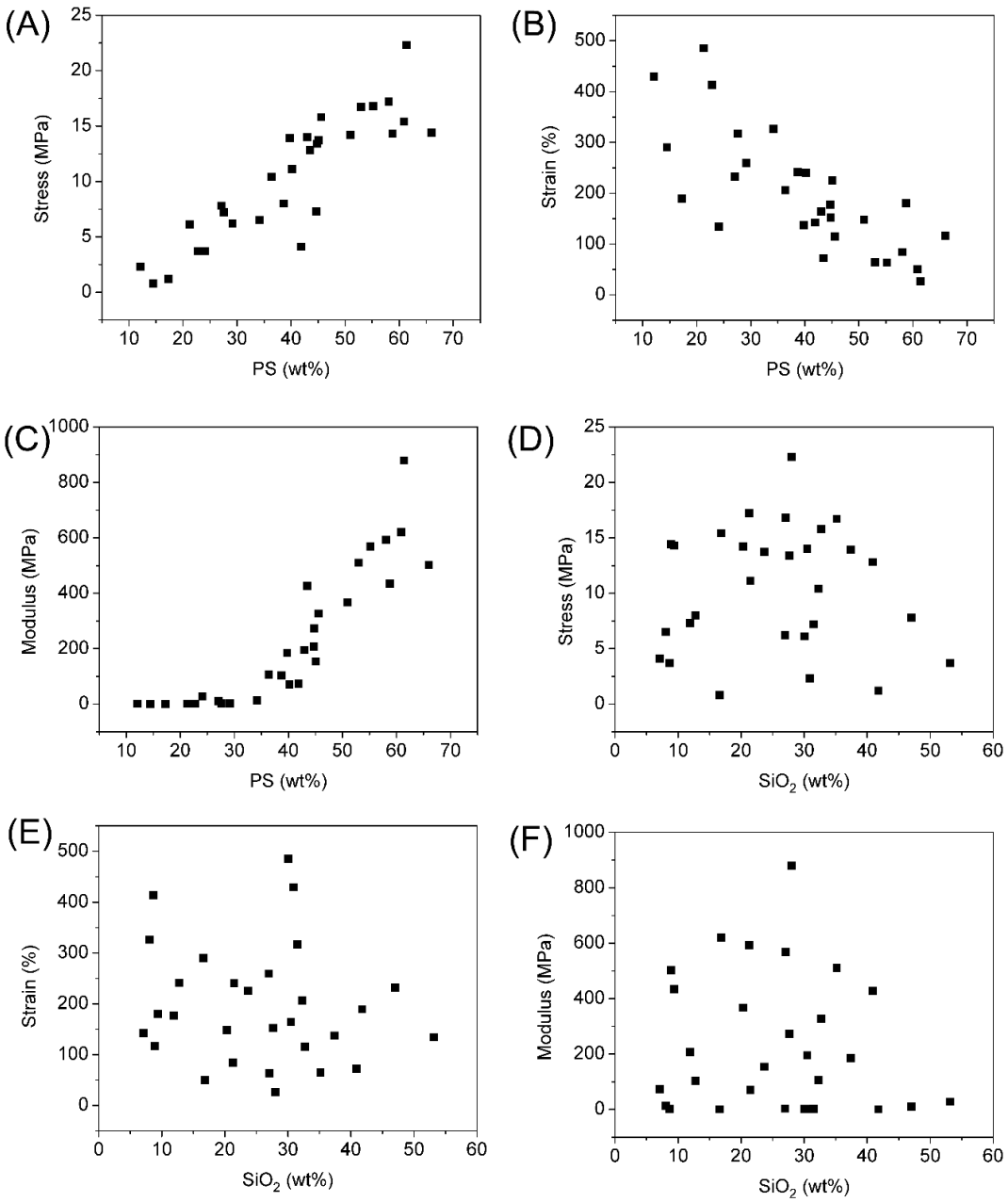

Figure 2.6 Mechanical properties of film formed by hot pressing PS-b-PBA-*g*-SiO_2 against PS and silica content. (A) Ultimate tensile stress vs PS content; (B) strain at break vs PS content; (C) Elastic modulus vs PS content; (D) ultimate tensile stress vs silica content; (E) strain vs silica content and (F) modulus vs silica content

Effect of Polymer Chain Graft Density on Mechanical Properties. The films formed from grafted NPs with similar graft molecular weights and composition of the block

copolymers but differing graft densities (BA_{42k}-S_{37k}-0.12, BA_{40k}-S_{41k}-0.24 and BA_{41k}-S_{40k}-0.65) exhibited similar ultimate tensile stress (*ca.* 14.0 MPa) and strain at break (150-180% elongation) (**Figure 2.7**).

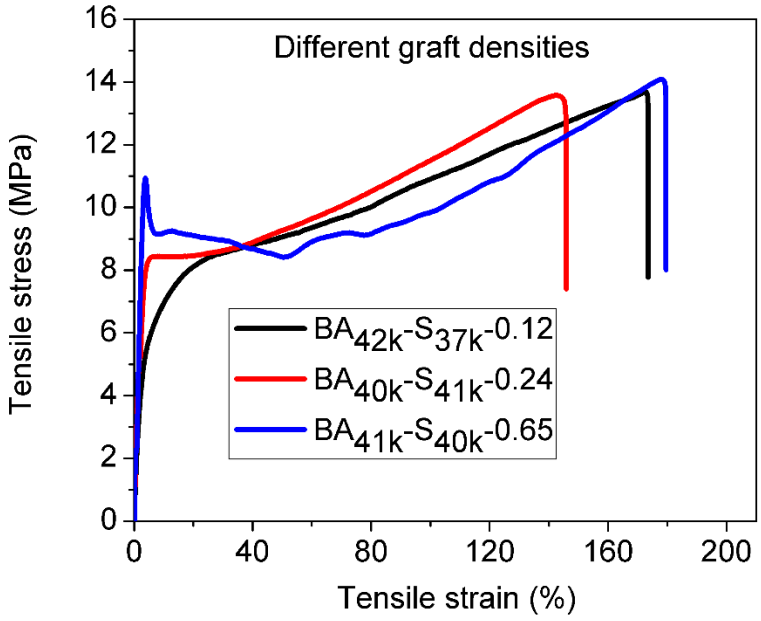

Figure 2.7 Stress-strain curves of films with similar chain length and different graft densities

The elastic modulus increased as the graft density increased, with 194.9 ± 4.0, 366.8 ± 10.1 and 433.3 ± 13.4 MPa for 0.12, 0.24 and 0.65 ch/nm^2, respectively. Additionally, all of them showed yielding and the yield strength increased with an increase in graft density. The yield strength was 6.8 ± 0.2, 9.4 ± 0.2 and 12.3 ± 0.6 MPa for 0.12, 0.24 and 0.65 ch/nm^2 with 43.0, 51.0 and 58.8 wt% PS content respectively. This indicated there were more continuous glassy domains in the high graft density composites than the low graft density composites.

DSC of PS-*b*-PBA-*g*-SiO_2.

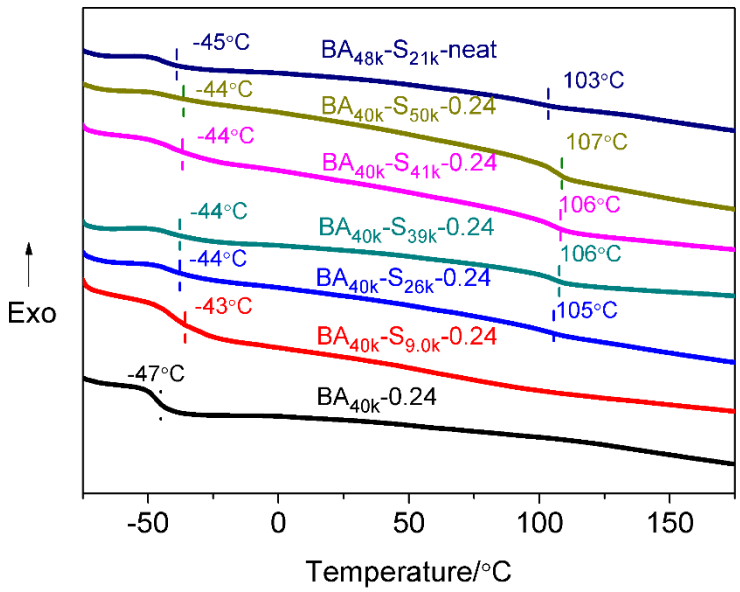

Figure 2.8 DSC curves of PS-*b*-PBA-*g*-SiO_2 with graft density of 0.24 ch/nm^2 and neat PS-*b*-PBA.

DSC was used to characterize the glass transition temperature (T_g) of PS-*b*-PBA-*g*-SiO_2 with 0.24 ch/nm^2 graft density and neat block copolymer PS-*b*-PBA (**Figure 2.8**). All the PS-*b*-PBA-*g*-SiO_2, except BA_{40k}-$S_{9.0k}$-0.24, showed two clear glass transition temperatures at *ca.* -44 ℃ and *ca.* 106 ℃ for PBA and PS blocks respectively. The lack of an observable high T_g for PS in the BA_{40k}-$S_{9.0k}$-0.24 sample was attributed to the low PS content in the sample.[10] The two distinct T_gs indicated microphase separation between PBA and PS in the PS-*b*-PBA-*g*-SiO_2 samples. There was a single T_g at -47 ℃ for PBA grafted silica sample PBA_{40k}-0.24, which was lower than the T_g of PBA in PBA-*b*-PS-0.24 samples. The PBA chain in PS-*b*-PBA-*g*-SiO_2 was restricted by both PS and silica nanoparticles while PBA in PBA-*g*-SiO_2 was merely restricted by silica nanoparticles. This resulted in an increase of T_g of PBA in PS-*b*-PBA-*g*-SiO_2.[45] The neat block copolymer,

PBA_{48k}-*b*-PS_{21k} also showed microphase separation with T_gs at -45 ℃ and 103 ℃. The T_gs of polymer grafted silica nanoparticles were slightly higher than the neat block copolymer, which resulted from lower mobility of polymer chains grafted to silica nanoparticles.[45,46]

SAXS and TEM Characterization.

The dispersion of inorganic nanoparticles in polymer nanocomposites is crucial to their mechanical properties.[22,33] The dispersion of silica nanoparticles in matrix-free polymer nanocomposites was characterized by SAXS and TEM of microtomed films formed by PS-*b*-PBA-*g*-SiO_2. We used the sample BA_{40k}-S_{39k}-0.24 as an example to investigate the dispersion of the silica nanoparticles and microphase separation. The SAXS profile of BA_{40k}-S_{39k}-0.24 films showed scattering peaks at 0.126 nm^{-1} and 0.316 nm^{-1}, which corresponded to domain spacing (d) at 49.9 nm and 19.9 nm respectively ($d=2\pi/q$) (**Figure 2.9A**). No-higher ordered scattering peaks were observed, which suggested the lack of a highly ordered morphology beyond disordered phase separation. In comparison, the sample of PBA grafted silica nanoparticle BA_{40k}-0.24, with the same graft density (0.24 ch/nm^2) and molecular weight of PBA, had a scattering peak at 0.290 nm^{-1} with corresponding d-spacing of 21.7 nm. Krishnamoorti et al. reported that thin films formed by PBA grafted silica nanoparticles with a higher graft density (~0.8 ch/nm^2) showed an ordered liquid lattice with q_1^*: q_2^* =1:$\sqrt{3}$.[47]

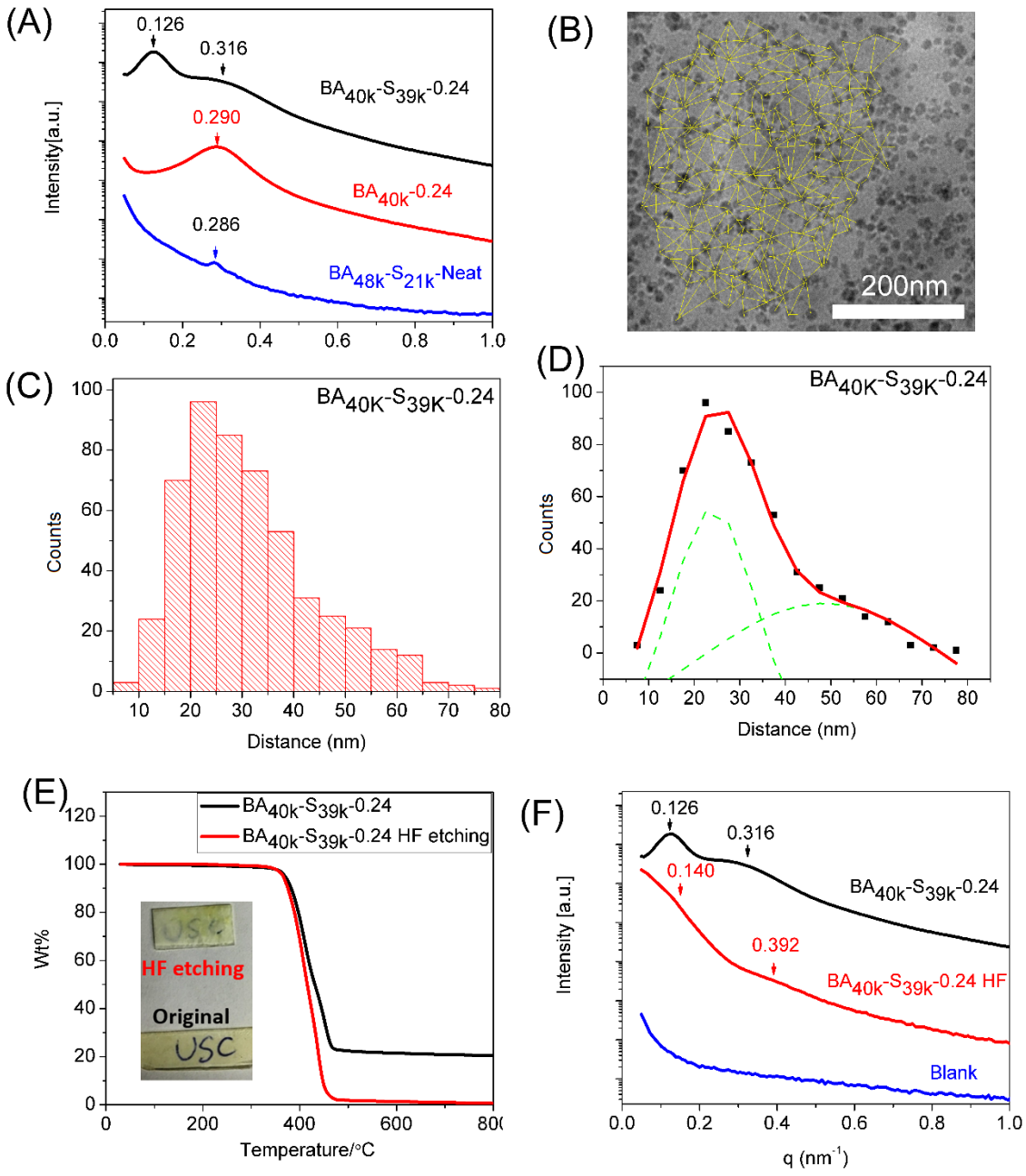

Figure 2.9 Characterization of the film formed by PS-*b*-PBA grafted silica nanoparticles. (A) SAXS of BA_{40k}-S_{39k}-0.24, BA_{40k}-0.24 and neat block copolymer BA_{48k}-S_{21k}; (B) TEM image of microtome sectioned film of BA_{40k}-S_{39k}-0.24. The thickness of TEM sample was *ca.* 100 nm. The yellow lines in the image were the labels used for the inter-particle distances analyzed by ImageJ; (C) Histograms of inter-particle distances in TEM image; (D) Distribution of inter-particle distances. The curve was fitted with Gaussian distribution; (E) TGA data of BA_{40k}-S_{39k}-0.24 before and after HF etching. Inset is the photograph of films before and after etching; (F) SAXS profile of BA_{40k}-S_{39k}-0.24 before and after HF etching.

The TEM image of a sectioned BA_{40k}-S_{39k}-0.24 bulk film indicated that silica nanoparticles were randomly dispersed in the matrix-free polymer nanocomposite (**Figure 2.9B**). The distances of adjacent silica nanoparticles were analyzed by ImageJ (~500 distances were analyzed). Statistical histograms and distribution of the interparticle distances were generated from the TEM image (**Figure 2.9C-D**). The distribution of interparticle distance showed two peaks at ~25 nm and ~55 nm, which were close to the two d-spacings (19.9 nm and 49.9 nm) obtained from the SAXS profile. This indicated the inter-particle distances from both TEM and SAXS were consistent with each other.

The DSC measurement of BA_{40k}-S_{39k}-0.24 clearly indicated there was microphase separation of PBA and PS (**Figure 2.8**). However, it was difficult to characterize the microphase separation of the block copolymer in the matrix-free polymer nanocomposite by SAXS due to the strong electron density contrast between inorganic silica and the polymers. The strong scattering peaks confirmed the silica nanoparticle dispersion. To eliminate the silica NP effect on the nanocomposite while maintaining micro-phase separation behavior of the block copolymer, excess HF was used to etch the silica component in the PS-*b*-PBA-*g*-SiO_2 film at room temperature. The film after etching showed almost no silica component, which was confirmed by TGA. The original BA_{40k}-S_{39k}-0.24 film formed by hot pressing was transparent with 20.6 wt% silica. The film after etching was semitransparent with 0.5 wt% residual (**Figure 2.9E**). The SAXS data showed that the two strong scattering peaks disappeared after the silica was etched by HF. This confirmed that these two strong scattering peaks were derived from phase separation of SiO_2 and polymer. Consequently, two weak broad scattering peaks at 0.140 nm^{-1} and 0.392 nm^{-1} were retained after SiO_2 etching (**Figure 2.9F**). This retained intensity resulted from

the electron density contrast between PBA and the void space in the film (originated from the pristine silica NP). The SAXS data of the neat block copolymer PBA_{48k}-*b*-PS_{21k} exhibited a weak scattering peak at 0.286 nm^{-1} due to the microphase separation of the blocks (**Figure 2.9A**). Thus, the microphase separation of PBA and PS in the nanocomposite BA_{40k}-S_{39k}-0.24 may also contribute to the retained scattering peak at 0.392 nm^{-1} after HF etching. The SAXS data of BA_{41k}-S_{40k}-0.65 showed a similar result with weak scattering peaks at 0.139 nm^{-1} and 0. 343 nm^{-1} after HF etching, in comparison with strong peaks at 0. 132 nm^{-1} and 0. 245 nm^{-1} before HF etching (**Figure 2.10**).

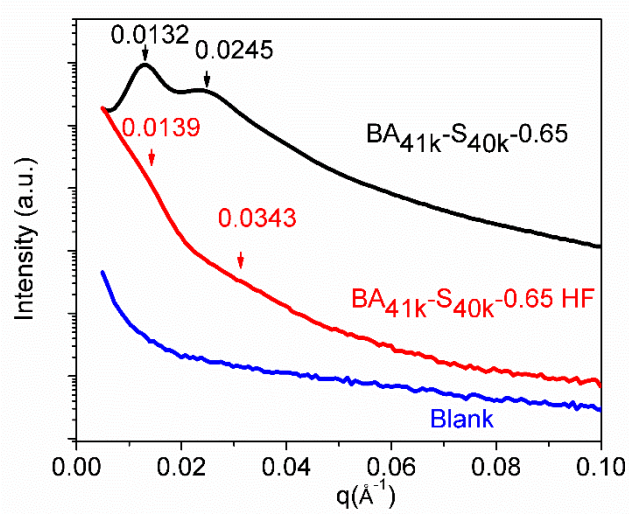

Figure 2.10 SAXS of BA_{41k}-S_{40k}-0.65 before and after HF etching

Effect of Graft Density on the Silica Nanoparticle Dispersion in Matrix-Free Nanocomposites.

SAXS and TEM measurements of the PS-*b*-PBA-*g*-SiO_2 films were used to characterize the dispersion of silica nanoparticles in the matrix-free polymer nanocomposite. Herein we investigated the graft density effect on the silica nanoparticle dispersion in BA_{42k}-S_{37k}-0.12, BA_{40k}-S_{41k}-0.24 and BA_{41k}-S_{40k}-0.65, which had similar

molecular weights of PBA and PS but different polymer graft densities. The SAXS and TGA data of PS-*b*-PBA-*g*-SiO_2 are summarized in **Table 2.3**. The higher polymer graft density resulted in lower silica weight percent in the polymer nanocomposite. SAXS data suggested that all the three samples, BA_{42k}-S_{37k}-0.12, BA_{40k}-S_{41k}-0.24, and BA_{41k}-S_{40k}-0.65, exhibited two scattering peaks representing a longer and shorter distance, which were characterized by domain spacing d_1 and d_2 ($d=2\pi/q$). Vaia et al. reported two scattering peaks in a matrix-free polymer nanocomposite film formed by polystyrene grafted silica nanoparticles with 0.05 ch/nm^2 graft density.[38] As the graft density decreased for the PS-*b*-PBA-*g*-SiO_2 NPs, the long interparticle distance increased while the short interparticle distance decreased. In addition, the scattering peaks became broader as the graft density decreased, which indicated silica nanoparticles entered into a broader distribution regime. The difference between d_1 and d_2, in this scenario, can be used to characterize the uniformity of distribution of silica nanoparticles. The $\Delta d= (d_1-d_2)$ was 40.0, 29.8, and 22.3 nm for the grafted densities 0.12, 0.24, and 0.65 ch/nm^2, respectively. This indicated that higher graft densities resulted in a more uniform distribution of silica nanoparticles. The TEM images of sectioned bulk PS-*b*-PBA-*g*-SiO_2 films showed the silica nanoparticles were randomly dispersed in the matrix-free polymer nanocomposite (**Figure 2.11**). The silica nanoparticles in the lower graft density nanocomposite were more densely packed than higher graft density samples. This was due to the higher silica content in lower graft density nanocomposites with 30.5, 20.3, and 9.4 wt% silica at 0.12, 0.24, and 0.65 ch/nm^2, respectively (**Table 3**). Despite the differences in the samples, the silica nanoparticles in the BA_{41k}-S_{40k}-0.65 sample, with a high graft density of 0.65 ch/nm^2, exhibited a more uniform distribution than lower graft density 0.12 and 0.24 ch/nm^2 samples. DSC and

SAXS studies showed microphase separation, which resulted in different interparticle distances (short and long distances). Nonetheless, the dispersion state of the silica nanoparticles with high graft density was dominated by the steric hindrance of the concentrated polymer brush (CPB) regimes, which resulted in relatively more uniform distribution of silica nanoparticles.[33,38,48]

Table 2.3 SAXS and TGA data of PS-*b*-PBA grafted silica nanoparticle with different densities.

Sample	Graft density (ch/nm^2)	SiO_2 (wt%)	q_1 (nm^{-1}) [a]	q_2 (nm^{-1})[a]	d_1 (nm)[b]	d_2 (nm)[b]
BA_{42k}-S_{37k}-0.12	0.12	30.5	0.110	0.361	57.4	17.4
BA_{40k}-S_{41k}-0.24	0.24	20.3	0.125	0.308	50.2	20.4
BA_{41k}-S_{40k}-0.65	0.65	9.4	0.133	0.253	47.2	24.9

[a] q_i represents the i^{th} scattering peak in the SAXS profile; [b] $d_i=2\pi/q_i$.

We also measured the silica dispersion in approximately monolayer films formed by drop casting PS-*b*-PBA-*g*-SiO_2 THF solution (~0.1 mg/mL) onto a TEM grid. The TEM images of these thin films are shown in **Figure 2.12**. For the low graft density 0.12 ch/nm^2, the distance between silica nanoparticles was 31.1 ± 0.5 nm. As the graft density increased to 0.24 ch/nm^2 and 0.65 ch/nm^2, the interparticle distance increased to 38.0 ± 0.5 nm and 55.9 ± 0.5 nm respectively as well as a more uniform silica nanoparticle dispersion. The TEM image of low graft density NPs showed some strings formed in the thin film of BA_{42k}-

S_{37k}-0.12. Moreover, the TEM image of BA_{41k}-S_{40k}-0.65 exhibited direct visual evidence of microphase separation of PBA and PS in the polymer nanocomposite (**Figure 2.12C**).

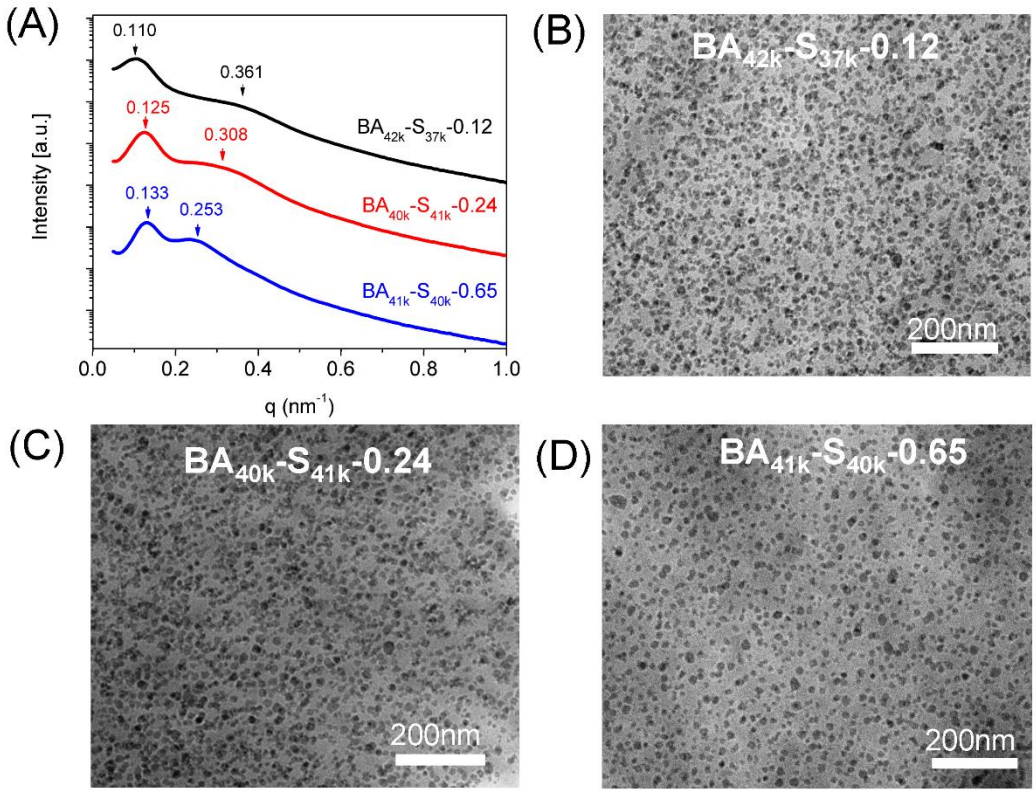

Figure 2.11 Characterization of bulk film of PS-*b*-PBA-*g*-SiO_2. (A) SAXS curves; Sectioned TEM images of (B) BA_{42k}-S_{37k}-0.12; (C) BA_{40k}-S_{41k}-0.24 and (D) BA_{41k}-S_{40k}-0.65 film. The films were formed by hot pressing with thickness ~0.3 mm. Scale bar was 200 nm.

The black dots in the TEM image were silica nanoparticles and white corona of silica nanoparticles was PBA while the grey area was PS. This indicated the PS phase formed a continuous domain and there were very few entanglements of PBA chains from adjacent silica nanoparticles.

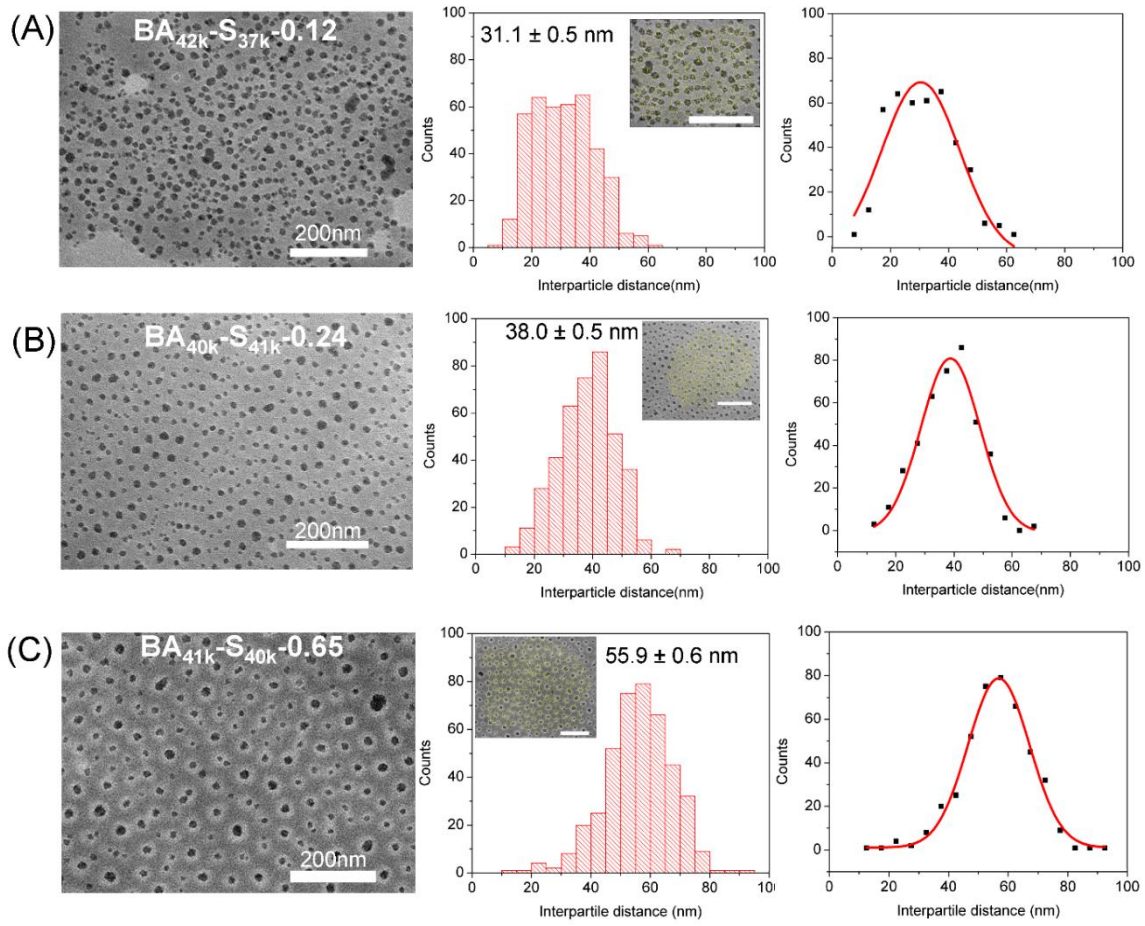

Figure 2.12 TEM images, inter-particle distance histograms and distribution of PS-*b*-PBA-*g*-SiO_2 monolayer films with different graft densities. (A) BA_{42k}-S_{37k}-0.12; (B) BA_{40k}-S_{41k}-0.24 and (C) BA_{41k}-S_{40k}-0.65. The approximately monolayer films of PS-*b*-PBA-*g*-SiO_2 were prepared by dissolving in THF with concentration ca. 0.1 mg/mL and then drop casting onto TEM grids. The histograms were generated by analyzing ~400 distances. The insets in the histograms showed the measured ligaments of interparticle distances.

Effect of Graft Density on the Microphase Separation of Polymer in the Nanocomposite.

DSC and DMA analysis were carried out to investigate the effect of graft density on the microphase separation of PBA and PS in films formed by BA_{42k}-S_{37k}-0.12, BA_{40k}-S_{41k}-0.24 and BA_{41k}-S_{40k}-0.65. The DSC curves showed that all the three samples had similar glass transition temperatures at *ca.* -44 ℃ and *ca.* 106 ℃, which were the T_gs for PBA and

PS, respectively (**Figure 2.13A**). This indicated that the PBA and PS were microphase separated in each of the samples. DMA, a more sensitive technique for detecting glass transitions, was used to more fully characterize the microphase separation (**Figure 2.13B-D**).[49]

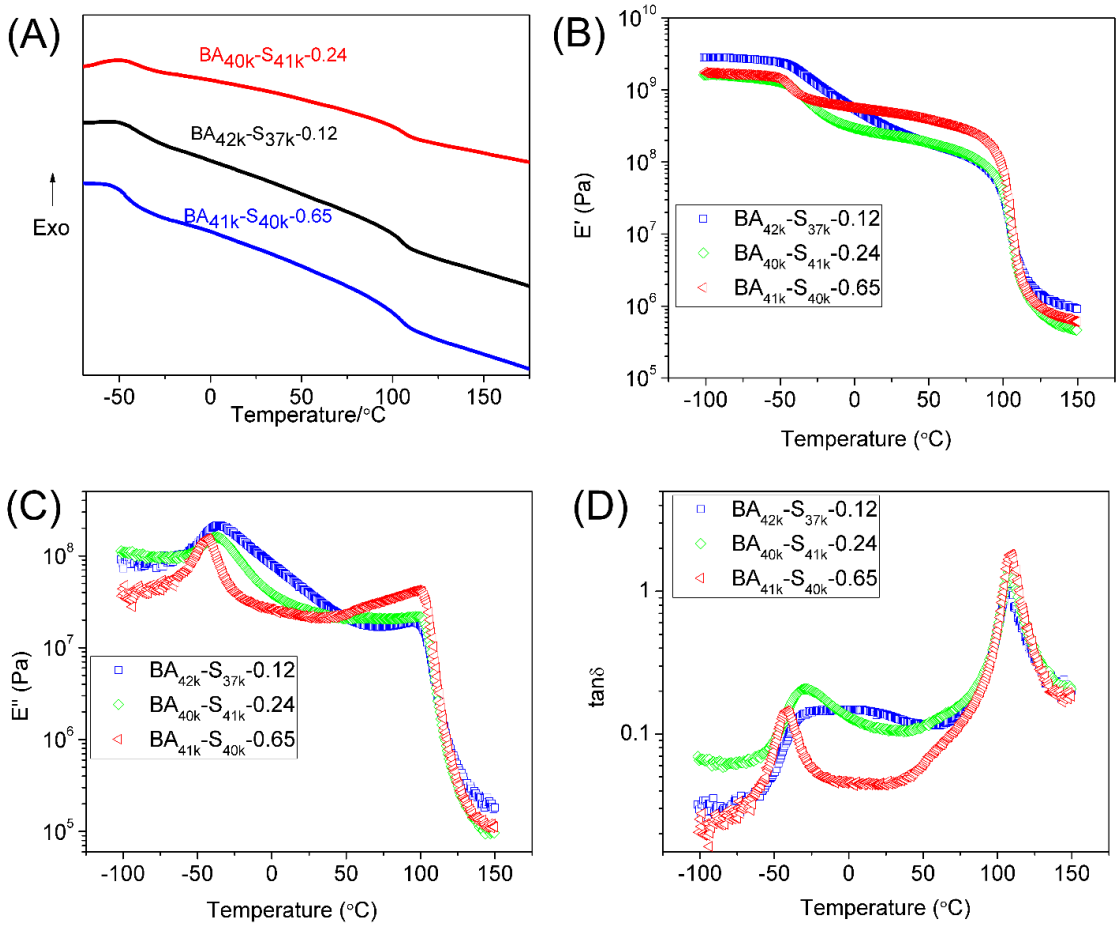

Figure 2.13 DSC and DMA characterization of PS-*b*-PBA-*g*-SiO_2 films with different graft densities. (A) DSC curves; (B) storage modulus; (C) loss modulus and (D) tan δ of DMA.

The storage modulus (E'), loss modulus (E'') and dissipation factor (tan δ) are summarized in **Table 2.4**. In the storage modulus-temperature curves, all three samples with different graft densities showed a decrease at ~ -49 ℃ and ~96 ℃, consistent with the T_gs of PBA and PS respectively. However, they had different PBA glass transition regions

at approximately -49 ℃ to 50 ℃, -48 ℃ to 24 ℃ and -51 ℃ to -19 ℃ for BA_{42k}-S_{37k}-0.12, BA_{40k}-S_{41k}-0.24 and BA_{41k}-S_{40k}-0.65 respectively (**Figure 2.13B**). This indicated that the block copolymer with the highest graft density had better microphase separation of PBA and PS than lower graft densities.[50] The rubbery plateau modulus can be related to the number of crosslinks or polymer chain length between entanglements.[49] The film formed by BA_{41k}-S_{40k}-0.65 had a higher rubbery plateau modulus than BA_{42k}-S_{37k}-0.12 and BA_{40k}-S_{41k}-0.24. The silica nanoparticles can serve as crosslinking points for PBA in the PS-*b*-PBA-*g*-SiO_2. The higher rubbery plateau modulus of higher graft density films may result from more crosslinks between PBA polymer chains. In the loss modulus vs temperature curves, all the samples showed two peaks at ~ -40 ℃ and ~98 ℃, which corresponded to T_gs of PBA and PS. However, the T_g peak of PBA became broader when the grafted density decreased from 0.65 ch/nm^2 to 0.12 ch/nm^2. In the tan δ vs temperature curves, all the samples exhibited two peaks as for the T_gs of PBA and PS. They had the similar T_gs for the PS at ~109 ℃. However, they exhibited different T_gs for the PBA. The 0.12 ch/nm^2 and 0.24 ch/nm^2 samples had similar T_gs at -29.8 ℃ and -28.4 ℃ respectively while 0.65 ch/nm^2 sample had T_g at -41.0 ℃ (**Figure 2.14**, **Table 2.4**).

Furthermore, the 0.65 ch/nm^2 sample had a narrow peak for PBA T_g with full width at half maximum (FWHM) 17.1 ℃, which was less than 0.12 ch/nm^2 (>81 ℃) and 0.24 ch/nm^2 (43.1 ℃). The T_g peaks for PBA became broader when the grafted density decreased from 0.65 ch/nm^2 to 0.12 ch/nm^2. All these results indicated a better microphase separation of block copolymers for higher graft density than lower graft density polymer nanocomposites.[50]

Table 2.4 T_gs and FWHM determined from DMA

Sample	Tg(E')/ ℃[a]		Tg(E'')/ ℃[b]		Tg(tan δ)/ ℃[b]		FWHM (tan δ)/ ℃[c]	
	PBA	PS	PBA	PS	PBA	PS	PBA	PS
BA_{42k}-S_{37k}-0.12	-46.6	95.2	-34.7	95.1	-29.8	107.6	-[d]	15.9
BA_{40k}-S_{41k}-0.24	-47.8	96.0	-36.5	98.7	-28.4	109.1	43.1	12.4
BA_{41k}-S_{40k}-0.65	-48.6	96.3	-43.0	98.0	-41.0	109.3	17.1	12.0

[a] T_g from the onset of E'; [b] T_g from the peaks of E'' and tan δ; [c]FWHM meant full width at half maximum; [d]The FWHM for BA_{42k}-S_{37k}-0.12 was too broad to be measured and it was more than 81.1 ℃.

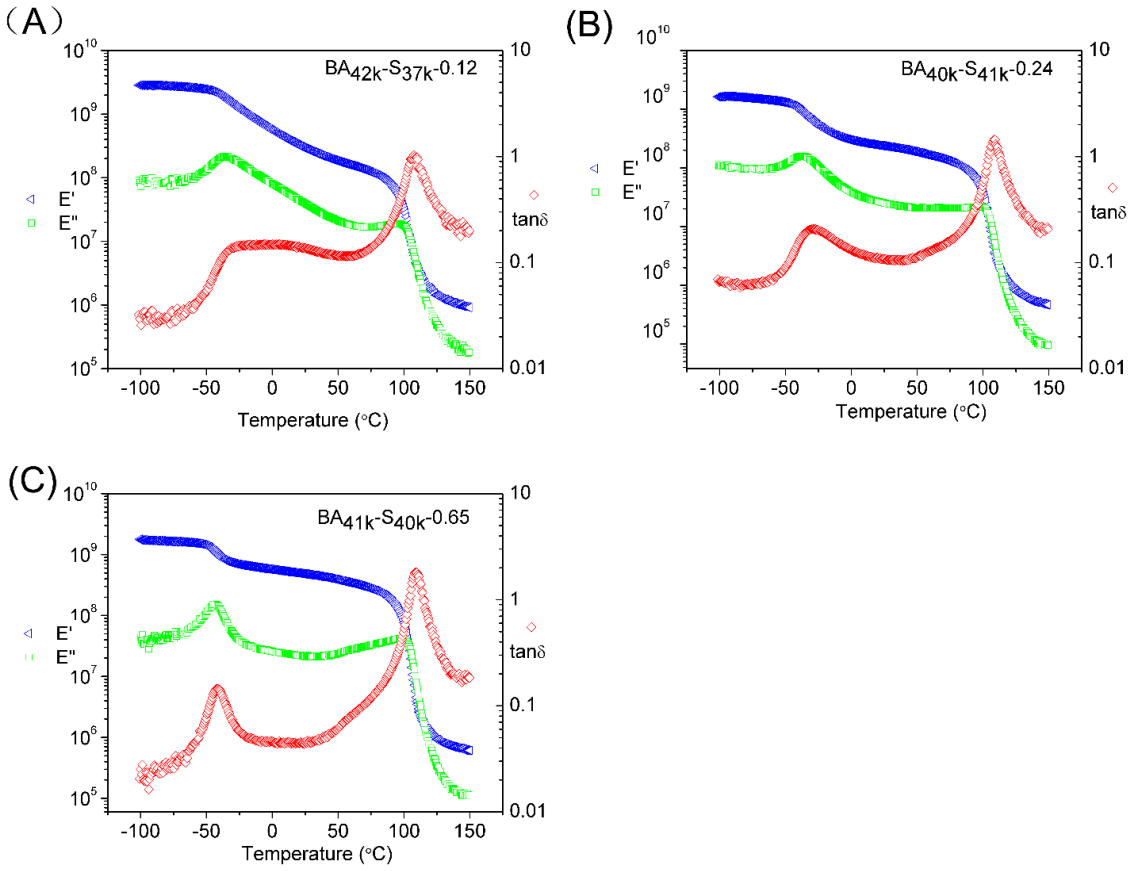

Figure 2.14 DMA of PS-*b*-PBA-*g*-SiO_2 with different graft densities. (A) BA_{42k}-S_{37k}-0.12; (B) BA_{40k}-S_{41k}-0.24 and (C) BA_{41k}-S_{40k}-0.65 film.

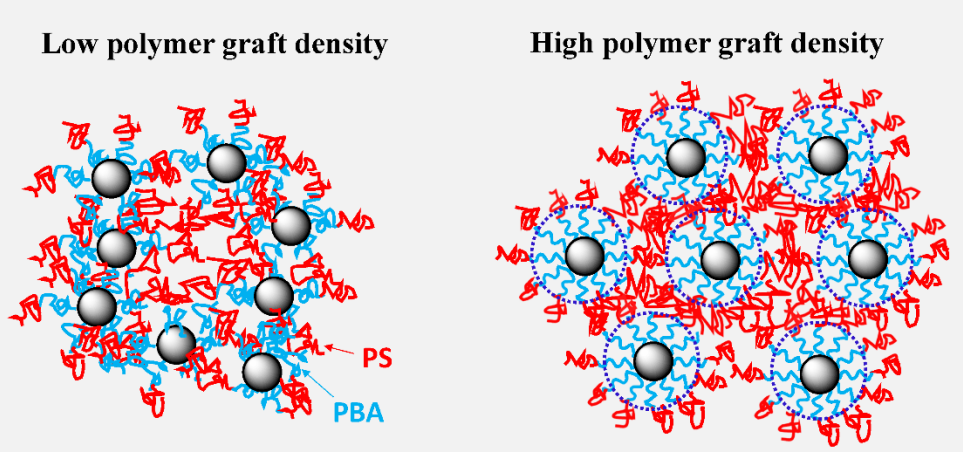

Figure 2.15 Proposed packing model of low and high graft densities with same polymer chain length and composition of PS-*b*-PBA-*g*-SiO_2 nanocomposite.

The proposed model for the graft density effect on the silica dispersion and microphase separation of PBA and PS in PS-*b*-PBA-*g*-SiO_2 nanocomposite is illustrated in **Figure 2.15**. The TEM images and SAXS data revealed high graft density nanocomposites had a more uniform silica nanoparticle dispersion than low graft density nanocomposites. The DMA data indicated block copolymers with higher graft density in polymer grafted nanoparticles had a better microphase separation than lower graft density when the block copolymers had similar molecular weights and composition. Here the molecular weight of PBA (~40 kg/mol) was greater than the chain entanglement molecular weight (M_e) (~28 kg/mol).[51] At low graft density (0.12 ch/nm^2), the NPs appeared to exhibit poor phase separation of the PBA and PS domains, which was confirmed by the DMA studies (**Figure 2.13**). The morphology of the corona of the high graft density (0.65 ch/nm^2) samples was mainly in the concentrated polymer brush (CPB) regime with highly extended polymer chains.[38,52] Thus, it was difficult for the adjacent PBA corona's to entangle with each other, which resulted in a better microphase separation of PBA and PS in high graft density

samples as compared to the low graft density samples. This was consistent with the data on particle distribution.

2.5 Conclusion

We prepared a series of thermoplastic elastomers formed by block copolymer grafted silica nanoparticles PS-*b*-PBA-*g*-SiO_2 with different chain lengths and graft densities via surface initiated RAFT polymerization. The effects of polymer chain length and polymer graft density on the mechanical properties were evaluated. The PS content was crucial to the ultimate tensile stress and elastic modulus. An increase in PS content resulted in an increase of ultimate tensile stress and elastic modulus. The longer PBA chain length resulted in a higher strain at break. The higher polymer graft density TPEs had similar tensile strain and stress to the lower graft density TPEs with similar block copolymer chain length. However, the higher graft density TPEs resulted in a higher elastic modulus than low graft density film. The highest ultimate tensile strength of PS-*b*-PBA-*g*-SiO_2 (*ca.* 17 MPa) was higher than the highest value of TPEs from triblock PS-*b*-PBA-*b*-PS (*ca.* 12 MPa) prepared by emulsion RAFT polymerization. DMA, SAXS and TEM data revealed the higher polymer graft density TPEs had a better microphase separation and more uniform nanoparticle dispersion than lower graft density TPEs with similar polymer chain lengths and composition. This versatile strategy to prepare thermoplastic elastomers by block copolymer grafted nanoparticles broadened the design of new TPEs. The mechanical properties of traditional TPEs formed by ABA triblock copolymers can only be tuned by chain length and composition of the block copolymers. In comparison, TPEs formed by block copolymer grafted nanoparticles introduces a new parameter, polymer chain graft

density, as a new tool to enhance microphase separation, and hence to tune the mechanical properties of TPEs.

2.6 References

(1) Matyjaszewski, K.; Gnanou, Y.; Leibler, L., Eds *Macromolecular Engineering. Precise Synthesis, Materials Properties, Applications;* **2007**, Wiley.

(2) Holden, G.; Legge, N. R.; Quirk, R. P.; Schroeder, H. E., Eds *Thermoplastic Elastomers, 2nd ed.* **1996**, Hanser/Gardner Publications: Cincinnati.

(3) Campos-Lopez, E.; McIntyre, D.; Fetters, L. J. *Macromolecules* **1973**, *6*, 415.

(4) Braunecker, W. A.; Matyjaszewski, K. *Prog. Polym. Sci.* **2007**, *32*, 93.

(5) Hawker, C. J.; Bosman, A. W.; Harth, E. *Chem. Rev.* **2001**, *101*, 3661.

(6) Per B. Zetterlund, Y. K., and Masayoshi Okubo *Chem. Rev.* **2008**.

(7) Moad, G.; Rizzardo, E.; Thang, S. H. *Aust. J. Chem.* **2005**, *58*, 379.

(8) Matyjaszewski, K.; Tsarevsky, N. V. *Nat. Chem.* **2009**, *1*, 276.

(9) Tong, J. D.; Moineau, G.; Leclere, P.; Bredas, J. L.; Lazzaroni, R.; Jerome, R. *Macromolecules* **2000**, *33*, 470.

(10) Luo, Y.; Wang, X.; Zhu, Y.; Li, B.-G.; Zhu, S. *Macromolecules* **2010**, *43*, 7472.

(11) Jeusette, M.; Leclere, P.; Lazzaroni, R.; Simal, F.; Vaneecke, J.; Lardot, T.; Roose, P. *Macromolecules* **2007**, *40*, 1055.

(12) Burns, A. B.; Register, R. A. *Macromolecules* **2016**, *49*, 9521.

(13) Dufour, B.; Tang, C. B.; Koynov, K.; Zhang, Y.; Pakula, T.; Matyjaszewski, K. *Macromolecules* **2008**, *41*, 2451.

(14) Wang, W.; Wang, W.; Lu, X.; Bobade, S.; Chen, J.; Kang, N.-G.; Zhang, Q.; Mays, J. *Macromolecules* **2014**, *47*, 7284.

(15) Schlegel, R.; Duan, Y. X.; Weidisch, R.; Hölzer, S.; Schneider, K.; Stamm, M.; Uhrig, D.; Mays, J. W.; Heinrich, G.; Hadjichristidis, N. *Macromolecules* **2011**, *44*, 9374.

(16) Weidisch, R.; Gido, S. P.; Uhrig, D.; Iatrou, H.; Mays, J.; Hadjichristidis, N. *Macromolecules* **2001**, *34*, 6333.

(17) Nese, A.; Mosnáček, J.; Juhari, A.; Yoon, J. A.; Koynov, K.; Kowalewski, T.; Matyjaszewski, K. *Macromolecules* **2010**, *43*, 1227.

(18) Jiang, F.; Wang, Z.; Qiao, Y.; Wang, Z.; Tang, C. *Macromolecules* **2013**, *46*, 4772.

(19) Kumar, S. K.; Krishnamoorti, R. *Annu. Rev. Chem. Biomol. Eng.* **2010**, *1*, 37.

(20) Zou, H.; Wu, S.; Shen, J. *Chem. Rev.* **2008**, *108*, 3893.

(21) Tjong, S. C. *Mater. Sci. Eng., R* **2006**, *53*, 73.

(22) Maillard, D.; Kumar, S. K.; Fragneaud, B.; Kysar, J. W.; Rungta, A.; Benicewicz, B. C.; Deng, H.; Brinson, L. C.; Douglas, J. F. *Nano Lett.* **2012**, *12*, 3909.

(23) Moll, J. F.; Akcora, P.; Rungta, A.; Gong, S.; Colby, R. H.; Benicewicz, B. C.; Kumar, S. K. *Macromolecules* **2011**, *44*, 7473.

(24) Fu, S.-Y.; Feng, X.-Q.; Lauke, B.; Mai, Y.-W. *Composites, Part B* **2008**, *39*, 933.

(25) Jancar, J.; Douglas, J. F.; Starr, F. W.; Kumar, S. K.; Cassagnau, P.; Lesser, A. J.; Sternstein, S. S.; Buehler, M. J. *Polymer* **2010**, *51*, 3321.

(26) Kumar, S. K.; Benicewicz, B. C.; Vaia, R. A.; Winey, K. I. *Macromolecules* **2017**, *50*, 714.

(27) Yu, X.; Yue, K.; Hsieh, I.-F.; Li, Y.; Dong, X.-H.; Liu, C.; Xin, Y.; Wang, H.-F.; Shi, A.-C.; Newkome, G. R.; Ho, R.-M.; Chen, E.-Q.; Zhang, W.-B.; Cheng, S. Z. D. *Proc. Natl. Acad. Sci. U. S. A.* **2013**, *110*, 10078.

(28) Zhang, W.-B.; Yu, X.; Wang, C.-L.; Sun, H.-J.; Hsieh, I. F.; Li, Y.; Dong, X.-H.; Yue, K.; Van Horn, R.; Cheng, S. Z. D. *Macromolecules* **2014**, *47*, 1221.

(29) Zheng, Y.; Huang, Y.; Abbas, Z. M.; Benicewicz, B. C. *Polym. Chem.* **2016**, *7*, 5347.

(30) Zheng, Y.; Huang, Y.; Abbas, Z. M.; Benicewicz, B. C. *Polym. Chem.* **2017**, *8*, 370.

(31) Bieligmeyer, M.; Taheri, S. M.; German, I.; Boisson, C.; Probst, C.; Milius, W.; Altstadt, V.; Breu, J.; Schmidt, H. W.; D'Agosto, F.; Forster, S. *J. Am. Chem. Soc.* **2012**, *134*, 18157.

(32) Cobo Sanchez, C.; Wahlander, M.; Taylor, N.; Fogelstrom, L.; Malmstrom, E. *ACS Appl. Mater. Interfaces* **2015**, *7*, 25669.

(33) Kumar, S. K.; Jouault, N.; Benicewicz, B.; Neely, T. *Macromolecules* **2013**, *46*, 3199.

(34) Akcora, P.; Liu, H.; Kumar, S. K.; Moll, J.; Li, Y.; Benicewicz, B. C.; Schadler, L. S.; Acehan, D.; Panagiotopoulos, A. Z.; Pryamitsyn, V.; Ganesan, V.; Ilavsky, J.; Thiyagarajan, P.; Colby, R. H.; Douglas, J. F. *Nat. Mater.* **2009**, *8*, 354.

(35) Khani, M. M.; Woo, D.; Mumpower, E. L.; Benicewicz, B. C. *Polymer* **2017**, *109*, 339.

(36) Zhao, D.; Di Nicola, M.; Khani, M. M.; Jestin, J.; Benicewicz, B. C.; Kumar, S. K. *ACS Macro Lett.* **2016**, *5*, 790.

(37) Garcıa, I.; Tercjak, A.; Rueda, L.; Mondragon, I. *Macromolecules* **2008**, *41*, 9295.

(38) Fernandes, N. J.; Koerner, H.; Giannelis, E. P.; Vaia, R. A. *MRS Commun.* **2013**, *3*, 13.

(39) Jiang, F.; Zhang, Y.; Wang, Z.; Fang, H.; Ding, Y.; Xu, H.; Wang, Z. *Ind. Eng. Chem. Res.* **2014**, *53*, 20154.

(40) Jiang, F.; Zhang, Y.; Fang, C.; Wang, Z.; Wang, Z. *RSC Adv.* **2014**, *4*, 60079.

(41) Jiang, F.; Zhang, Y.; Wang, Z.; Wang, W.; Xu, Z.; Wang, Z. *ACS Appl. Mater. Interfaces* **2015**, *7*, 10563.

(42) Li, C.; Han, J.; Ryu, C. Y.; Benicewicz, B. C. *Macromolecules* **2006**, *39*, 3175.

(43) Barbey, R.; Lavanant, L.; Paripovic, D.; Schuwer, N.; Sugnaux, C.; Tugulu, S.; Klok, H.-A. *Chem. Rev.* **2009**, *109*, 5437.

(44) Moraes, J.; Ohno, K.; Maschmeyer, T.; Perrier, S. *Chem. Commun.* **2013**, *49*, 9077.

(45) Laruelle, G.; Parvole, J.; Francois, J.; Billon, L. *Polymer* **2004**, *45*, 5013.

(46) Carrot, G.; Diamanti, S.; Manuszak, M.; Charleux, B.; Vairon, J. P. *J. Polym. Sci., Part A: Polym. Chem.* **2001**, *39*, 4294.

(47) Goel, V.; Pietrasik, J.; Dong, H.; Sharma, J.; Matyjaszewski, K.; Krishnamoorti, R. *Macromolecules* **2011**, *44*, 8129.

(48) Vaia, R. A.; Maguire, J. F. *Chem. Mater.* **2007**, *19*, 2736.

(49) Menard, K. P. *Dynamic Mechanical Analysis: A Practical Introduction. CRC Press: Boca Raton, FL* **2008**.

(50) Storey, R. F.; Baugh, D. W. *Polymer* **2001**, *42*, 2321.

(51) Tong, J.-D.; Jerôme, R. *Macromolecules* **2000**, *33*, 1479.

(52) Ohno, K.; Morinaga, T.; Takeno, S.; Tsujii, Y.; Fukuda, T. *Macromolecules* **2007**, *40*, 9143.

CHAPTER 3

POLYMER GRAFTED NANOPARTICLE MEMBRANES FOR GAS SEPARATION

3.1 Abstract

Polymer membranes have wide applications in gas separation. Here a novel type of polymer membrane formed only from merely polymer grafted silica nanoparticles (NPs) was developed to investigate the application in gas separation. Poly(methyl acrylate) (PMA) and poly(methyl methacrylate) (PMMA) grafted silica NPs were synthesized by surface initiated reversible addition-fragmentation chain transfer (SI-RAFT) polymerization. A versatile protocol was developed to remove ungrafted PMA from PMA grafted silica NP from RAFT polymerization, which was used in place of the traditional ultracentrifuge procedure. The membranes from neat polymer grafted silica NPs exhibited an enhanced gas permeability over neat polymers, which was related to the increased polymer free volume. The permeability can also be tuned by the grafted polymer molecular weight, which showed a "volcano plot" in permeability versus molecular weight. There was no aging effect on the membranes from polymer grafted NPs in the experimental measurement time line, which has practical applications in designing stable gas separation membranes.

3.2 Introduction

Polymer membranes are commercially available for gas separations, such as removal of CO_2 from natural gas[1], H_2/CO_2 separation in hydrocarbon fuel processing,[2] etc. The performance of the polymer membranes for gas separation are investigated on the parameters of permeability and selectivity. However, there is a trade-off between gas permeability and selectivity, which was described as the Robeson upper bound.[3-5] The diffusion model was used to explain the gas transport in membranes.[6] The permeability (P)

of gas in a polymer membrane is related to the diffusivity (D) and solubility (K), which was expressed as P=KD. The selectivity of a membrane is expressed as $\alpha_{ij}=P_i/P_j$. In order to obtain a high performance membrane for practical industrial gas separation applications, the membrane should possess high permeability difference for the gases while maintaining an appropriate gas permeability for output. Currently, there are a few series of new membranes which have crossed the upper bound of the Robeson plot, such as polymers of microporosity (PIMs), thermally rearranged (TR) polymers, and polybenzimidazoles (PBIs).[7-9] Mixed matrix membranes from nanofiller/matrix combinations showed unique properties in gas separation[10-13], such as metal-organic frameworks (MOFs)[14-16], graphene-based materials[17], silica[18], and carbon nanotube.[19]

A common phenomenon for gas separation membranes was the physical aging effect, which resulted in a decrease of gas permeability.[20,21] This decreased permeability was explained by the changes in free volume in glassy polymers.[22,23] The membranes formed by polymer grafted nanoparticles and polymer matrix composites showed a suppression of the aging effect, which originates from the interfacial interaction of well dispersed nanofillers and polymer matrix. [24] Durning et al. reported the effects of diameter and loading of silica nanoparticles on permeability by n-alkyl acetate in PMA/silica nanocomposites.[25] The permeability of penetrants in the composite decreased with the loading of silica nanoparticles, which was consistent with traditional composite theory using Maxwell's model: $P_c=P_b(1-\phi)/(1+\phi/2)$, where P_c is the permeability of composite, P_b is the permeability of neat polymer, and ϕ is the volume fraction of nanofiller.[12] Freeman et al. reported a surprising increase of permeability and selectivity from fumed silica particles and glassy poly(4-methyl-2-pentyne) polymers, which was in contrast to

Maxwell's model . This enhancement resulted from the increased free volume in the composite. [26] However, the permeability and selectivity of this kind of polymer/fumed silica composite was effected by different polymers and fumed silica particles, which had different dispersions of the fumed silica in the composites with different loadings and process methods.[27,28] Paul et al. investigated the permeability and selectivity of membranes from a different kind of glassy polymer, poly (ether imide) (ULTEM®), with fumed silica particles. The fumed silica agglomerated and formed voids in the membrane , which resulted in an enhanced permeability but decreased selectivity as compared to the neat polymer.[27]

The dispersion of nanoparticles in a polymer matrix can be improved by surface modification of the silica with ligands and polymers, which increases the miscibility of nanoparticle surface and polymer matrix. Recently developed controlled radical polymerization techniques enabled the synthesis of polymer modified nanoparticles.[29-32] It was reported that the silica nanoparticles had different morphologies by adjusting the grafted polymer chain lengths and graft densities.[33,34] Matrix-free polymer nanocomposites, which are formed only by polymer grafted NPs, have advantages over traditional NP/matrix composites since they minimize agglomeration of the NPs.[35] This worked aimed to investigate the gas permeability and selectivity of matrix-free polymer nanocomposite membranes.

3.3 Experimental

Materials. All chemicals were obtained from either Fisher or Acros and used as received unless otherwise specified. Spherical silica nanoparticles (14±4 nm diameter) were

obtained from Nissan Chemical. 3-Aminopropyldimethylethoxysilane was purchased from Gelest, Inc. and used as received. 2-(Dodecylthiocarbonothioylthio)propanoic acid (DoPAT) was purchased from Boron Molecular, Inc. 4-Cyanopentanoic acid dithiobenzoate (CPDB) was purchased from Strem Chemicals. Methyl acrylate (MA, 99%, Acros) and methyl methacrylate (MMA, 99%, Acros) were purified by filtration through an activated basic alumina column. Azobisisobutyronitrile (AIBN) was recrystallized from ethanol twice before use.

Characterization. ^{1}H NMR and ^{13}C NMR (Bruker Avance 300) were conducted using $CDCl_3$ as solvent. Molecular weights (Mn) and dispersity (Đ) were determined using gel permeation chromatography (GPC) equipped with a Varian 290-LC pump, a Varian 390-LC refractive index detector, and three Styragel columns (HR1, HR3 and HR4, molecular weight range of 100-5000, 500-30000, and 5000-500000, respectively). THF was used as eluent for GPC at 30℃ and a flow rate of 1.0 mL/min. GPC was calibrated with poly (methyl methacrylate) (PMMA) standards obtained from Polymer Laboratories. Thermogravimetric analysis (TGA) measurements were carried out on a TA Q5000 thermogravimetric analyzer (TA Instruments). All the samples were preheated to 150 ℃ and kept at this temperature for 10 min to remove residual solvents. After cooling to 40 ℃, the samples were heated to 800 ℃ with a heating rate of 10 ℃/min in a nitrogen atmosphere. The ultrasonication was performed in a Branson 1510 sonicator. The ultracentrifuge was carried out in Sorvall Evolution RC superspeed centrifuge SA-300 rotor with 23000 rpm at 4-10℃ for 30min.

Activation of RAFT agent.

RAFT agent 2-(dodecylthiocarbonothioylthio)propanoic acid (DoPAT) (1.75g, 5mmol) and 2-mercaptothiazoline (0.596 g, 5 mmol) were dissolved in 20mL dry CH_2Cl_2.

(Dimethylamino)pyridine (DMAP) (61 mg, 0.50 mmol) was added slowly to the solution. The solution was stirred for 10min at 0℃ in ice bath in N_2 atmosphere. Dicyclohexylcarbodiimide (DCC) (1.24 g, 6.00 mmol) in 10mL CH_2Cl_2 was added to the solution slowly and stirred at room temperature for another 1 hour. After the reaction, the salt was removed by filtration. The solvent was evaporated by vacuum and followed by silica gel column chromatography (hexane: ethyl acetate=5:1) to get activated DoPAT as yellow oil (2.10g, 93% yield). The oil turned into a yellow solid after storing in a freezer overnight. ^{1}H NMR (300 MHz, $CDCl_3$) δ (ppm): 6.46 (q, 1H, J =7.1 Hz), 4.62-4.70 (m, 1 H), 4.42-4.52 (m, 1H), 3.38-3.48 (m, 1H), 3.21-3.34 (m, 3H), 1.51-1.75 (m, 5 H), 1.25-1.42 (m, 18 H), 0.88 (t, 3H, J =7.0 Hz). ^{13}C NMR (75MHz, $CDCl_3$) δ (ppm): 222.80, 201.22, 173.25, 56.41, 48.73, 37.52, 31.93, 29.64, 29.56, 29.45, 29.36, 29.10, 28.97, 28.92, 27.91, 22.71, 16.44, and 14.15. Elemental Analysis: calculated for $C_{19}H_{33}NOS_5$: C, 50.51; H, 7.36; N, 3.10; S, 35.48; found C, 51.31; H, 7.36; N, 3.20; S, 34.46

Synthesis of DoPAT modified silica NPs.

Silica nanoparticles (50.0g, 30 wt% in MEK solution) were added to a 250mL round bottom flask with 150 mL THF and 3.0 mL 3-aminopropyldimethylethoxysilane. After purging with N_2 for 30min, the solution was refluxed at 75 ℃ for 5 hours. The solution was then cooled to room temperature and precipitated into 500mL hexane. The amine functional silica nanoparticles were recovered by centrifuge at 5000 rpm for 5 min. The dispersion-precipitation process were then repeated another two more times. The silica nanoparticles were then dispersed in 150mL dry THF and added to 1.25g activated DoPAT THF (3mL) solution in N_2 atmosphere. The solution was stirred overnight and precipitated into a large amount of methanol and re-dispersed in THF. This dispersion-precipitation

process was repeated until the supernatant solution was colorless. The nanoparticles were placed in a room temperature vacuum oven to dry. The grafted density of DoPAT-NP was 0.43 chains/nm^2 by measuring and calculated from the UV-Vis spectrum.

RAFT polymerization of MA on DoPAT modified Silica NP.

DoPAT-NP (1.0 g, graft density=0.47 chains/nm^2) was dispersed in 21 mL anhydrous DMF and 12.0 mL methyl acrylate (0.133 mol). The stock solution of AIBN in DMF (1.11 mL, 0.01 mol/L), was added to the solution, and finally the mixture was transferred into a dried Schlenk flask. The mixture was degassed by four freeze- pump- thaw cycles, backfilled with nitrogen, and then placed in an oil bath at 60 ℃. The polymerization solution was quenched in ice water after 1.67 hours. THF (40mL) was added to the flask and the solution was poured into hexanes (200mL) to precipitate PMA grafted silica nanoparticles. The PMA grafted silica nanoparticles were recovered by centrifuge at 4000 rpm for 10 min. The PMA grafted silica nanoparticles were redispersed in 100mL THF and precipitated in 200ml methanol. This dispersion-precipitation process was repeated for another four times. The cleavage of RAFT agent was achieved by reacting with 20eq AIBN in THF at 65 ℃ for 2 h.[36,37] The molecular weight (Mn) and dispersity (Đ) were measured by GPC. The sample was prepared by treating 50mg polymer grafted silica in 5mL THF and 200 μL HF solution overnight at room temperature. The solvent was evaporated in a Teflon petri dish for 24h and the residual was dissolved in THF for GPC analysis.

Synthesis of neat PMMA and PMMA grafted silica NPs.

The RAFT polymerization of MMA followed a similar procedure as previously reported.[38] CPDB RAFT agent was used for the polymerization. The PMMA-g-SiO_2 was purified by ultracentrifuge to remove ungrafted PMMA.

3.4 Results and Discussions

3.4.1 RAFT Polymerization of methyl acrylate (MA) by 4-cyanopentanoic acid dithiobenzoate (CPDB).

It was reported that 4-cyanopentanoic acid dithiobenzoate (CPDB) was used as the RAFT agent to synthesize poly(n-butyl acrylate), polystyrene, and poly(methyl methacrylate) grafted nanoparticles with narrow polydispersity.[38] A similar synthesis route was firstly designed to synthesize PMA grafted nanoparticles (**Scheme 3.1**).

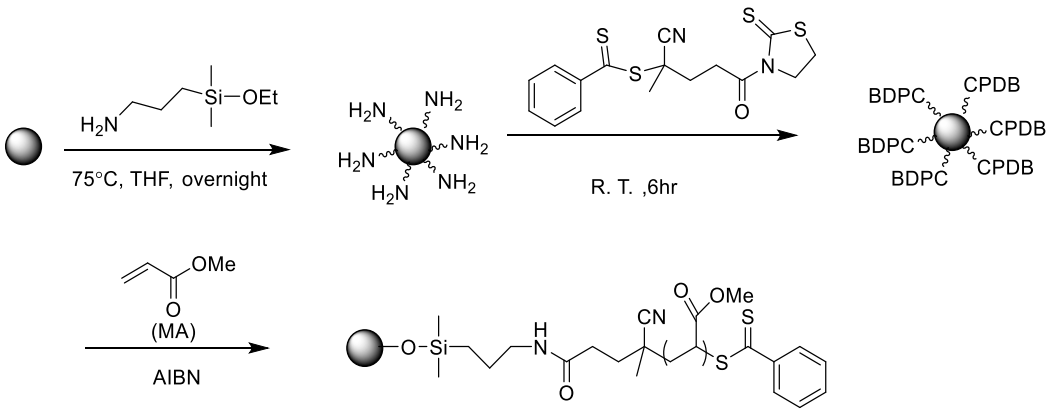

Scheme 3.1 Polymerization of methyl acrylate on silica nanoparticles by CPDB

The ratio of RAFT agent to initiator was set to 1:0.1-0.2 to obtain a narrow polymer molecular dispersity (Đ). The kinetic study of RAFT polymerization of methyl acrylate (MA) by CPDB is shown in **Figure 3.1**. It showed a linear fit of ln (M_0/M_t) (where M_0 is the initial concentration of monomer and M_t is concentration of monomer at t hour) vs polymerization time, which indicated a pseudo-first-order rate polymerization (a constant concentration of radicals in the solution). This is the characteristic of a controlled radical polymerization. However, the molecular weight measured by GPC was not in agreement with the theoretical calculation from monomer conversion after the monomer conversion was more than 0.05 (**Figure 3.1b**). Meanwhile, the dispersity (Đ) was more than 1.4 after conversion was more than 0.15. This suggested the polymerization of PMA was not well controlled by using CPDB as RAFT agent. The kinetic study of RAFT polymerization of methyl acrylate on silica nanoparticles also indicated a poor controlled polymerization by CPDB, which was similar to the free PMA polymerization (**Figure 3.2**).

Although the RAFT polymerization of methyl acrylate yielded narrow dispersity at very low conversion (<0.05), it was very difficult to synthesize the desired free PMA and PMA grafted nanoparticles with predictable Mn and narrow Đ.

In 2006, Patton *et al.* reported a versatile RAFT polymerization to synthesize polymers with α-functionalized norbornenyl, vinyl, and cinnamyl macromonomers using CPDB derivatives.[39] The CPDB derivatives showed a good control of polymerization of MA when the monomer conversion was less than 0.23 (Đ<1.2) with [MA]: [CPDB-derivatives]: [AIBN]= 500:1:0.48 at 65℃.

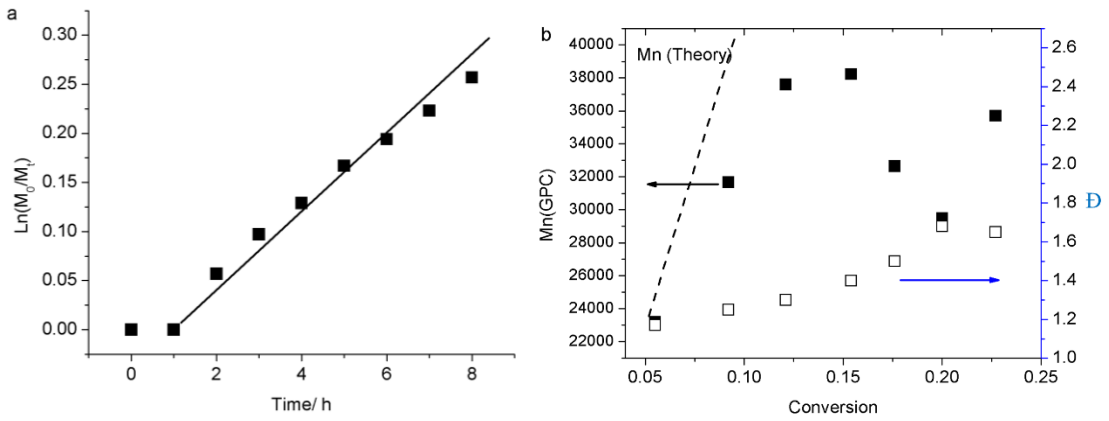

Figure 3.1 Free poly (methyl acrylate) by RAFT polymerization with CPDB. a) Kinetic plots of polymethyl acrylate; b) dependence of molecular weight and polydispersity on conversion of RAFT polymerization by CPDB. Dash line in (b) is the theoretical molecular weight. [MA]= 6.25M in anhydrous THF, [CPDB]=1.25 mM, [AIBN]=0.125 mM, [MA]: [CPDB]: [AIBN]=5000: 1: 0.1, 60℃

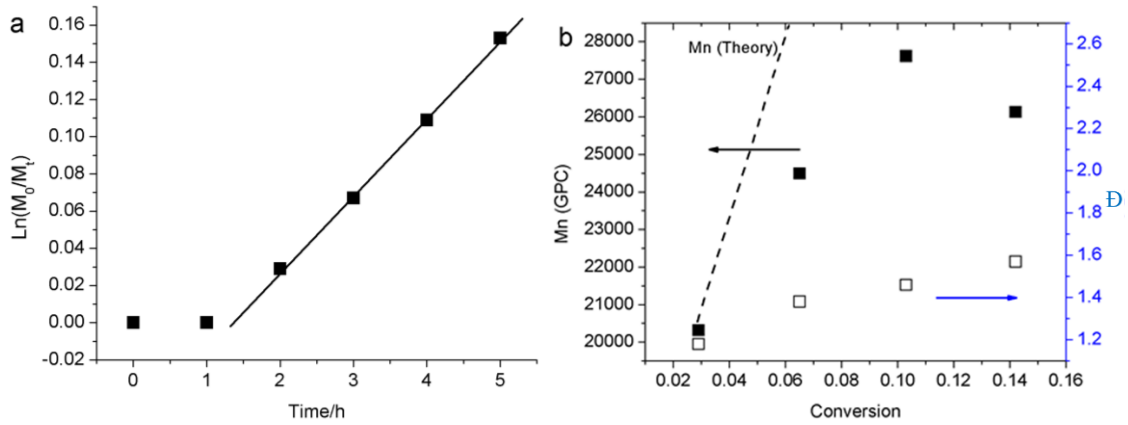

Figure 3.2 Poly(methyl acrylate) by RAFT polymerization with CPDB on silica nanoparticles (density= 0.097 chain/nm^2). a) Kinetic plots of polymethyl acrylate; b) dependence of molecular weight and polydispersity on conversion of RAFT polymerization by CPDB. Dash line in (b) is the theoretical molecular weight. [MA]= 4.08M in anhydrous THF, [CPDB]=0.51 mM, [AIBN]=0.051 mM, [MA]: [CPDB]: [AIBN]=8000: 1: 0.1, 60℃

In subsequent experiments, the ratio of AIBN/CPDB was increased to 0.5:1 for the RAFT polymerization of methyl acrylate. Both the Mn and Đ were well controlled when the conversion was less than 0.19, which was consistent with the literature (**Figure 3.3**).

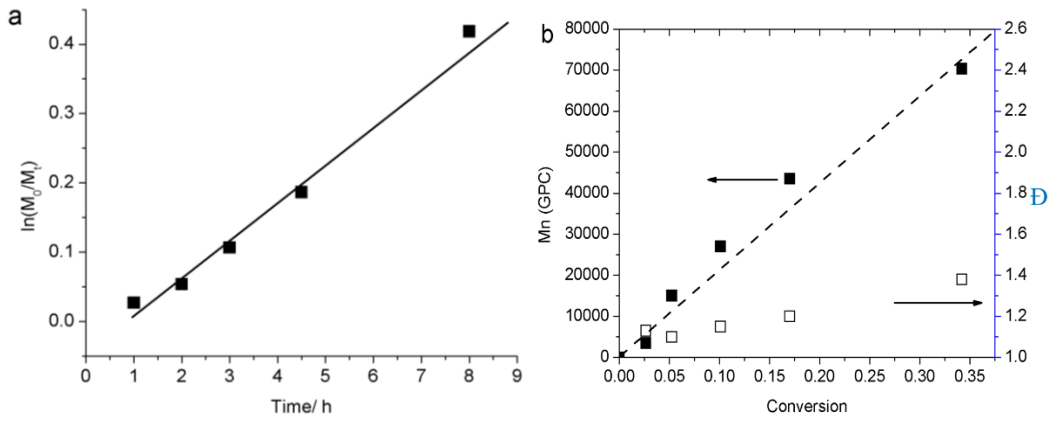

Figure 3.3 Free poly(methyl acrylate) by RAFT polymerization with CPDB. a) Kinetic plots of polymethyl acrylate; b) dependence of molecular weight and polydispersity on conversion of RAFT polymerization by CPDB. Dash line in (b) is the theoretical molecular weight. [MA]= 8.82M in anhydrous THF, [CPDB]=3.5 mM, [AIBN]=1.75 mM, [MA]: [CPDB]: [AIBN]=2500: 1: 0.5, 60℃

Table 3.1 shows the results for the RAFT polymerizaon for [CPDB]: [AIBN]= 1:0.5 and different [MA]/ [CPDB] ratios. PMA polymers with narrow dispersity and different molecular weights were synthesized by using the ratio [CPDB]: [AIBN]=1:0.5. A higher ratio of AIBN/CPDB (0.8:1) resulted in a broader Đ (Entry 7). Also the low ratio of AIBN to CPDB (0.1: 1) resulted in a broader Đ polymer (Entry 8).

However, the RAFT polymerization of methyl acrylate on silica nanoparticles showed poor control when the ratio [CPDB]:[AIBN]=1:0.5 was applied for the polymerization. After polymerization for 1-2 hours, the pink color disappeared in the solution. This indicated the RAFT agent CPDB was deactivated during the polymerization.

Table 3.1 RAFT polymerization of methyl acrylate by CPDB

Entry	Time (h)	[MA] (mol/L)	[MA]: [CPDB]: [AIBN]	Mn (GPC)	Đ
1	4.0	5.3	500:1:0.5	5100	1.10
2	4.0	7.1	1000:1:0.5	16200	1.10
3	4.0	8.7	2000:1:0.5	28900	1.14
4	5.0	9.1	2500:1:0.5	57200	1.20
5	4.0	10.0	5000:1:0.5	101800	1.23
6	4.0	10.3	7500:1:0.5	142500	1.15
7	5.0	8.2	2500:1:0.8	54700	1.40
8	5.0	6.5	5000:1:0.1	38200	1.40

3.4.2 RAFT polymerization of methyl acrylate by 2-(dodecylthiocarbonothioylthio)propanoic acid (DoPAT)

In order to synthesize PMA grafted silica nanoparticles by RAFT polymerization using similar strategy as CPDB, the RAFT agent should have a carboxylic acid end group for easily grafting to silica nanoparticles. 2-(Dodecylthiocarbonothioylthio)propanoic acid (DoPAT) is a trithiocarbonate RAFT agent which was reported to exhibit good control of the emulsion polymerization of methyl acrylate.[40] Initial results of RAFT polymerization

of methyl acrylate by DoPAT showed narrow dispersity when applied in bulk polymerization ([MA]: [DoPAT]: [AIBN]=1000:1:0.1, 60℃, 5h, Mn=24500, Đ=1.11). Thus, DoPAT was evaluated as RAFT agent for the synthesis of PMA grafted silica nanoparticles (**Scheme 3.2**).

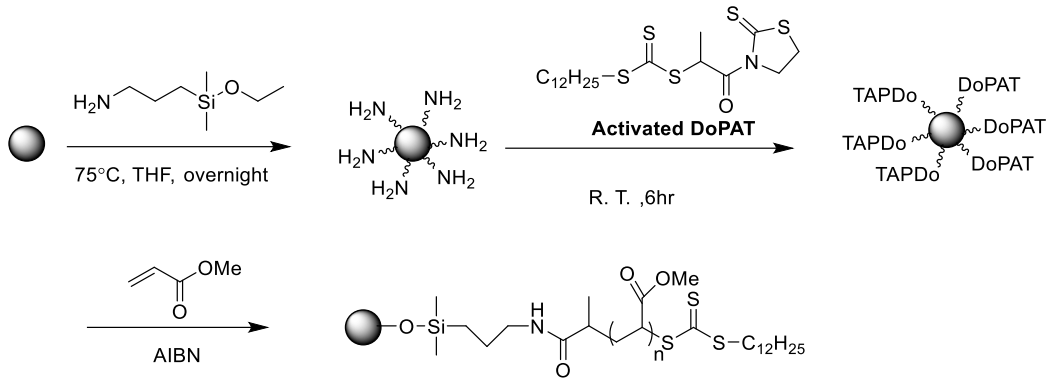

Scheme 3.2 RAFT polymerization of methyl acrylate on silica nanoparticles by DoPAT

The DoPAT-NPs with a chain density of 0.11 chain/nm^2 was synthesized. The ratio of [DoPAT]: [AIBN] was set to 1:0.1 in order to minimize the free polymers derived from initiator AIBN as well as eliminate the surface radical migration effect.[38] The general procedure for polymerization of methyl acrylate on particles was as follows: (1) dispersed the DoPAT-NPs with THF in a Schlenk tube; (2) added MA and AIBN (10mM in THF) to the Schlenk tube; (3) degased the solution by three freeze-pump-thaw cycles; (4) placed the tube into a 60℃ oil bath for polymerization. However, the polymerization of methyl acrylate on silica nanoparticles resulted in poor control over the dispersity in THF. The results were shown in **Table 3.2**.

The RAFT polymerization of methyl acrylate by DoPAT showed narrower Đ when the concentration of MA in THF increased. This indicated the broad Đ of PMA may result

from the solvent effect of THF. The PMA was synthesized with a very narrow Đ (1.06) in bulk polymerization of methyl acrylate. THF was good solvent to disperse RAFT-g-SiO_2. However, the RAFT polymerization of MA on silica nanoparticles in THF showed a broad dispersity of molecular weights. Thus, minimal amounts of THF solvent were used for the RAFT polymerization of methyl acrylate grafted silica nanoparticles (AIBN was dissolved in THF).

Table 3.2 RAFT polymerization of methyl acrylate by DoPAT

Polymers	[MA]: [DoPAT]: [AIBN]	Concentration of MA in THF/ wt %	Time/ h	Mn (GPC)	Đ
Free PMA by DoPAT	1000:1:0.1	30	4	13700	1.61
	1000:1:0.1	50	4	20100	1.55
	1000:1:0.1	90	4	24500	1.11
	1000:1:0.1	100	5	60600	1.06
DoPAT-NPs (Density=0.11)	1500:1:0.1	50	4	18300	1.54
	5000:1:0.1	50	6.5	37500	1.59
	1500:1:0.2	30	3.5	21300	1.49

Table 3.3 Polymerization of methyl acrylate on DoPAT-NPs

PMA on NPs	[MA]: [DoPAT]: [AIBN]	Concentration of MA in THF/ wt %[a]	Time/ h	Mn (GPC)	Đ
DoPAT-SiO_2 (Density=0.14)	3000:1:0.1	96	4	No Polymer	
	3000:1:0.1	96	5	No Polymer	
	3000:1:0.1	96	9.5[b]	95100	1.26
DoPAT-SiO_2 (Density=0.11)	450:1:0.1	81	2.5[b]	22900	1.18
	1500:1:0.1	93	4.5[b]	58900	1.21
	2400:1:0.1	96	4.5[b]	103200	1.17
	3000:1:0.1	96	10.5[b]	158300	1.18

[a]: No additional THF was added. AIBN was prepared in THF solution. [b]: At this time, the solution was "gelled" like and the polymerization was quenched at this time.

The DoPAT-g-SiO_2 was dispersed into methyl acrylate monomer with sonication. The results were shown in **Table 3.3**. The polymerization of methyl acrylate on DoPAT-SiO_2 showed an inhibition phenomenon. For the chain density 0.14 chain/nm^2 (32.5 μmol/g) DoPAT-SiO_2, there was an inhibition time for about 5h when [MA]: [DoPAT]: [AIBN] was set to 3000:1:0.1. However, the polymerization formed a gel-like state, which unexpectedly showed a narrow Đ. Inspired by this, several different ratios of [MA]: [DoPAT-SiO_2] were evaluated for the synthesis of specific molecular weights of PMA

grafted nanoparticles. This strategy worked well for the polymerization with low Đ (**Table 3.3**).

3.4.3 RAFT polymerization of methyl acrylate in DMF.

As discussed before, the bulk SI-RAFT polymerization of MA worked well with controlled Mn and dispersity. However, the bulk RAFT polymerization (without solvents) of MA often resulted in a very viscous gel, which was difficult to remove from the flask and disperse into solvent (**Figure 3.4**).

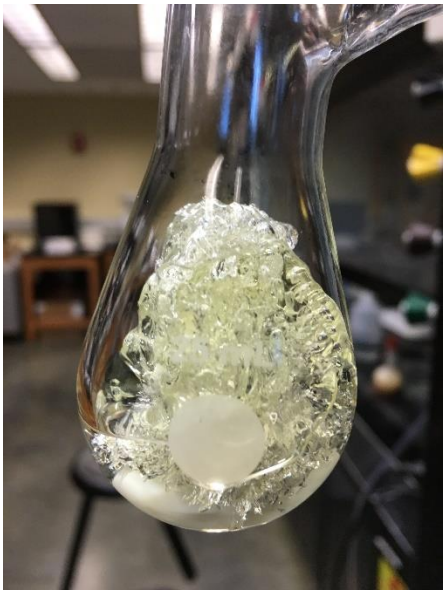

Figure 3.4 Photograph of SI-RAFT bulk polymerization of MA

The DoPAT-SiO_2 can also disperse in DMF well. DMF was used as the solvent for the polymerization of MA by DoPAT. The polymerization conditions were: [MA]: [DoPAT]: [AIBN]=1000:1:0.1, [MA]=5.6 mol/L in DMF, 60℃. The results showed the RAFT polymerization of methyl acrylate in DMF could achieve a narrow Đ even at 90% monomer

conversion (**Table 3.4**). Similarly, the RAFT polymerization of MA by DoPAT in DMF showed an inhibition time about 4h.

Table 3.4 RAFT polymerization of MA with DoPAT in DMF

Time/ h	Monomer conversion	Mn (Theory)	Mn (GPC)	Đ
2	0	-	-	-
4	0	-	-	-
6	0.467	40500	38400	1.17
7	0.628	54400	53300	1.17
8	0.730	63100	55300	1.15
12	0.901	77800	82000	1.13

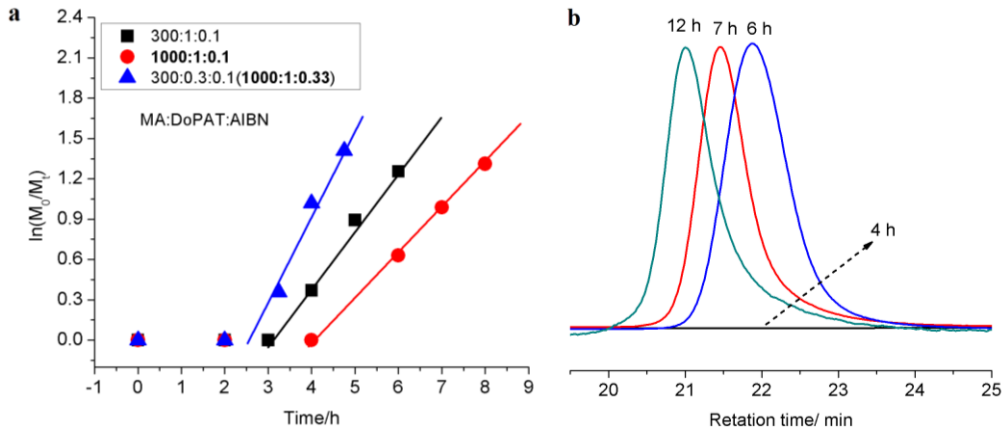

Figure 3.5 a) The kinetic study of different ratios of MA/DoPAT/AIBN with [MA]= 5.6M; b) GPC trace of RAFT polymerization of MA at [MA]:[DoPAT]:[AIBN] = 1000:1:0.1 in DMF

The rate of RAFT polymerization ideally should not be affected by the RAFT agent since the radicals are neither destroyed nor generated during the RAFT equilibrium.[41] However, there are many reports related to inhibition/retardation in RAFT

polymerization.[42] The inhibition may come from poor choice of R group, impurities in the RAFT agent and the presence of air/oxygen. Also the slow fragmentation of the intermediate, or the slow re-initiation by $R\cdot$ may result in inhibition.[43] Perrier *et al.* investigated the origin of inhibition effects in RAFT polymerization of methyl acrylate by different dithioesters[44], and suggested the inhibition may come from the slow fragmentation of the intermediate. However, the origin of inhibition of RAFT polymerization was still unclear.[43] The RAFT polymerization of methyl acrylate by DoPAT showed a 4h inhibition time when [MA]: [DoPAT]:[AIBN]=1000:1:0.1 with [MA]=5.6 mol/L in DMF (**Figure 3.5a**). The GPC trace indicated there was no polymer at 4 h (**Figure 3.5b**). Also the ^{1}H NMR confirmed the lack of polymerization (no PMA protons at δ=1.48-2.37 ppm) at 4 hour. When the [AIBN]/[DoPAT] ratio was increased to 0.33, the inhibition time was shortened to about 2.5h. The higher concentration of initiator may contribute to a faster propagation rate. The higher concentration of RAFT agent also resulted in a longer inhibition time, which was consistent with the literature. [42]

3.4.4 Separation of un-grafted PMA from PMA grafted silica nanoparticles.

Surface initiated controlled radical polymerization also generated some un-grafted free polymers. Our group reported there was 5.2 wt% un-grafted PMMA with 12% monomer conversion in RAFT polymerization of MMA from CPDB grafted SiO_2. The ratio of un-grafted PMMA increased into 13.4 wt% with 22% monomer conversion. The un-grafted PMMA polymer might come from radical polymerization by initiator AIBN.[38] Matyjaszewski et al. reported surface-initiated atom transfer radical polymerization (SI-ATRP) generated un-grafted PS from thermal self-initiated polymerization.[45,46] The ultracentrifuge was typically used to separate the un-grafted polymer from polymer grafted

nanoparticles. The separation was based on the different densities between silica core (~2.07 g/cm^3) and polymers (0.9-1.4 g/cm^3). A good solvent was used to disperse the grafted and un-grafted polymers and ultracentrifuge with high speed (40,000 rpm) for 30 min. The sediment was collected and redispered in good solvent to re-run the unltracentrifuge another 3 times for a good separation.[45,47] This procedure suffered from low efficiency as well as low recovery yield, which resulted from a fraction of polymer grafted silica nanoparticles still dispersed in the good solvent.

In order to investigate the permeability of gas in "pure" PMA grafted silica nanoparticles (without any ungrafted PMA) with different graft densities and molecular weights, an effective and high recovery yield process was needed. It would be efficient if there was a combination of solvents, which can dissolve free PMA while precipitate PMA grafted silica nanoparticles. This would facilitate the separation by using normal speed centrifuge in a short time. THF is a good solvent for PMA while hexane and methanol are not. Firstly, the THF and hexane combination was investigated as shown in **Figure 3.6**. Neat PMA (51KDa) was dissolved in 10mL THF at 10mg/mL. The PMA THF solution was still clear after adding 3mL hexane. The solution became opaque after 5mL hexane was added. The free PMA started to precipitate quickly after 12mL hexane was added. This indicated the THF/Hexane combination was not suitable for the design.

Secondly, THF and methanol solvents were used, which is shown in **Figure 3.7**. The PMA was dissolved in 10mL THF at 10 mg/mL. The solution was still clear even after 25mL methanol was added. The solution became opaque after 35mL methanol was added. This suggested the PMA was soluble in the solvent mixture with less than 71 vol% MeOH (THF: MeOH = 1: 2.5).

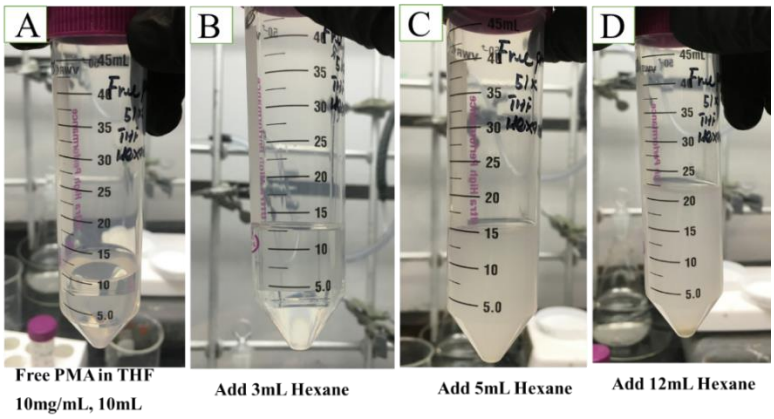

Figure 3.6 Photographs of free PMA (51kDa) in THF/Hexane mixture

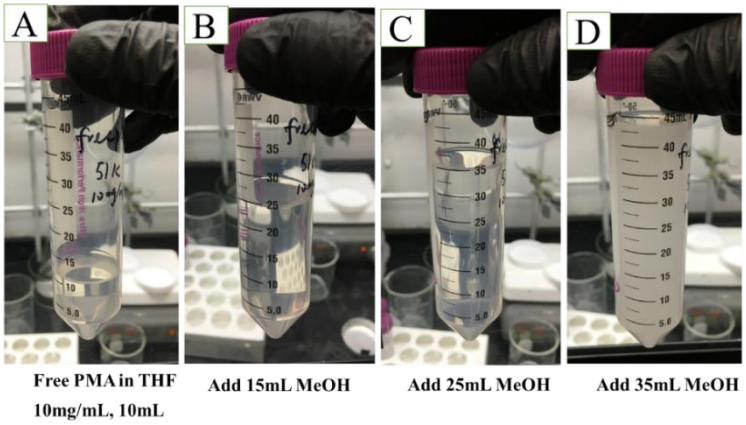

Figure 3.7 Photographs of free PMA (Mn=51000) in THF/MeOH mixture

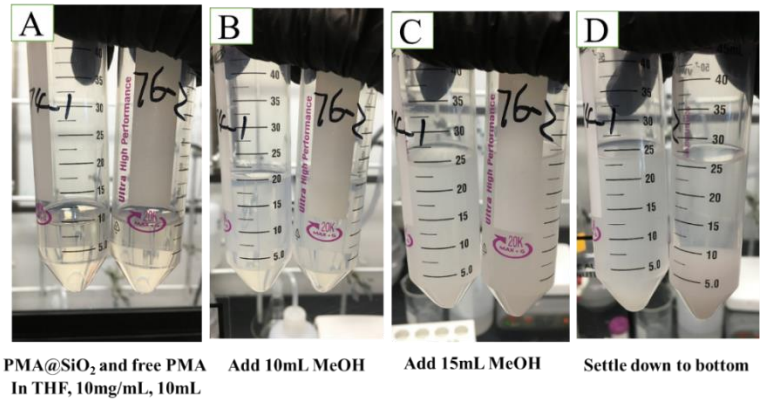

Figure 3.8 Photographs of PMA grafted SiO_2 with free PMA in THF/MeOH mixture

Finally, two PMA grafted silica nanoparticles (Mn=52200 (right tube) and 66300 (left tube), graft density=0.43 ch/nm^2), which were prepared by SI-RAFT polymerization, were worked up in the THF/methanol mixture (**Figure 3.8**). The PMA grafted silica nanoparticles, which contained free PMA polymer from SI-RAFT polymerization, were dispersed in 10mL THF at 10mg/mL each. After 10mL methanol was added, the solution became slightly opaque. The solution turned opaque after 15mL methanol was added and the precipitation settled down to the bottom (**Figure 3.8D**). This indicated only the PMA grafted SiO_2 precipitated while the ungrafted PMA was still dissolved in the solvent with THF: MeOH=1:1.5 mixture.

A new protocol to remove ungrafted PMA from PMA grafted silica nanoparticles was developed as follows: PMA grafted SiO_2 from SI-RAFT polymerization was dispersed in THF with concentration 10-25 g/mL in 50mL centrifuge tubes. Methanol (1.5-2eq volume of THF) was added into the solution. The PMA-grafted silica nanoparticles were recovered by centrifuge at 3000-6000 rpm for 5min. The nanoparticles were redispersed in THF and precipitated in methanol. This dispersion-precipitation process was repeated for another four times.

TGA was used to characterize the removal efficiency of ungrafted PMA from PMA grafted silica nanoparticle (**Figure 3.9**). The sample was also purified by using ultracentrifuge (23000 rpm at 4-10℃ for 60min, 4 cycles) for comparison. TGA showed PMA grafted silica nanoparticles (Mn=81000, Đ=1.23, 0.47 ch/nm^2) had 7.71 wt% silica content after polymerization, which contained both ungrafted and grafted PMA. The silica content increased into 13.02 wt% after ultracentrifuge purification, which resulted from the removal of ungrafted PMA. The silica content increased into 13.30 wt% after being treated

with THF/MeOH by the developed procedure, which showed the same efficiency as the ultracentrifuge procedure. The combination of THF/Hexane can partially remove ungrafted PMA as the silica content increased to 10.74 wt% (**Figure 3.9A**). After removal of ungrafted PMA, the GPC result showed the grafted PMA with Mn=92900, Đ=1.16 while before purification with Mn=81000, Đ=1.23. Another PMA grafted silica nanoparticle (Mn=132100, 0.43 ch/nm^2) also showed the same efficiency in removing ungrafted PMA by THF/MeOH as ultracentrifuge (**Figure 3.9B**).

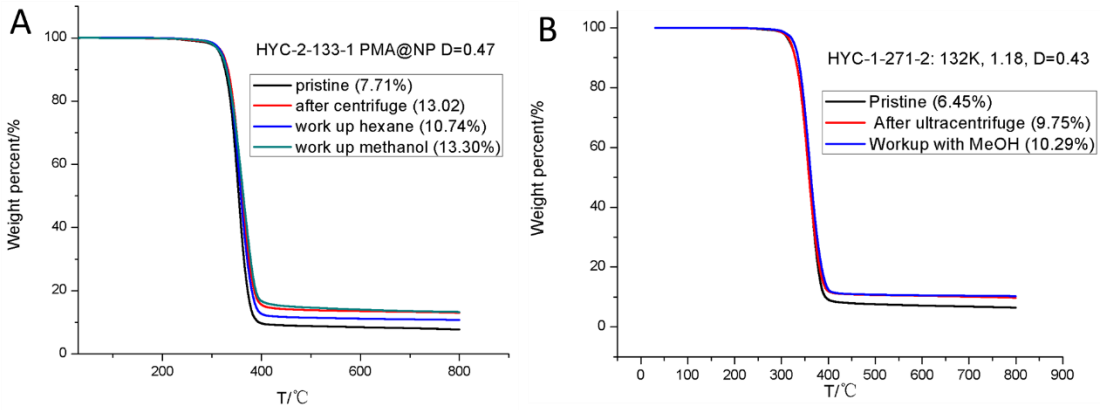

Figure 3.9 TGA of PMA grafted silica nanoparticle with different purification procedures. The percentages indicated the SiO_2 content of the different samples and procedures.

Ultrasonication effect on PMA grafted silica nanoparticle.

Ultrasonication is widely used in lab for dissolving chemicals and dispersion of nanoparticles in solvents. However, ultrasonication can cause polymer chain scission due to the mechanical force called cavitation.[48] It was reported the molecular weight of polystyrene changed from 282,000 to 252,000 Da and from 92,000 to 90,000 Da after sonication for 2min.[49] Moore et al. reported sonication can mechanochemically activate the heterointerface with maleimide-anthracene cycloadduct PMA grafted silica

nanoparticles.[47] We prepared PMA grafted silica nanoparticles by SI-RAFT polymerization with polymer chains covalently attached onto the silica surface with Si-O-Si bonding. It was necessary to investigate the ultrasonication effect on PMA grafted silica nanoparticles for proper processing.

The PMA grafted silica nanoparticles were purified by the newly developed THF/MeOH procedure, which had a Mn=92900, Đ=1.16, and graft density=0.47 chain/nm^2. After dispersion in THF with 10mg/mL, the solution was separated into 3 vials. Two of them were treated with sonication for 5min and 30min. The samples were repurified by THF/MeOH method to remove any cleaved ungrafted PMA. After treatment with HF, the grafted PMA after sonication was analyzed by GPC. TGA and GPC were used to characterize the polymers and grafted Nps(**Figure 3.10**). The TGA showed there was almost no change of silica content after sonication for 5min with silica content changing from 13.02 wt% to 13.24 wt%. However, the silica content increased from 13.02 wt% to 14.64 wt% after sonication for 30min, which indicated PMA chains were partially cleaved from the silica surface. GPC was used to investigate the chain cleavage mechanism. It showed there was no difference in molecular weight and dispersity of grafted PMA after sonication for 5min and 30min (**Figure 3.10B**). The TGA and GPC data indicated that 30min sonication can cleave PMA chains from the silica surface in PMA grafted silica nanoparticles with 0.47 chain/nm^2. It also illustrated there was almost no change in PMA grafted silica nanoparticles after sonication for 5min. Thus, we can use sonication for a short time (less than 5min) to treat PMA grafted silica nanoparticles for dispersion in solvents or processing.

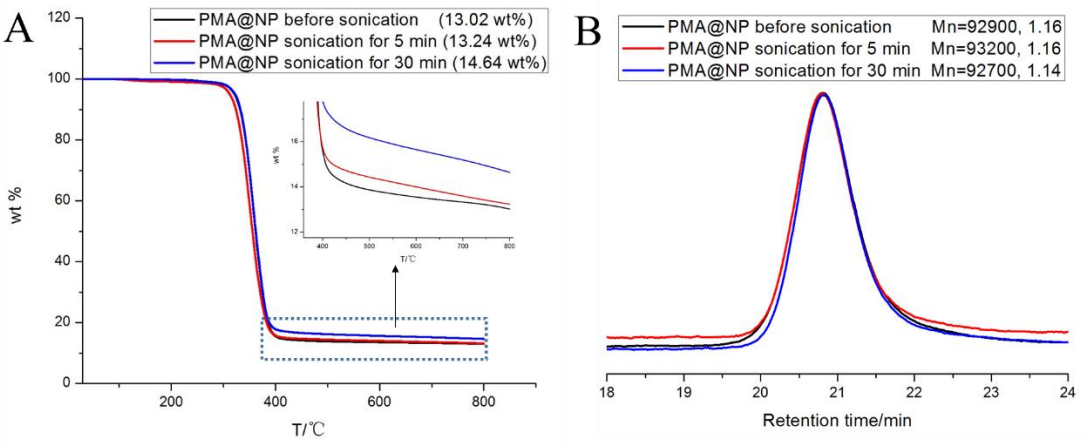

Figure 3.10 TGA and GPC analysis of PMA-g-SiO_2 for sonication effect

3.4.5 Gas separation testing.

PMA-g-SiO_2, PMMA-g-SiO_2 samples and neat PMA, PMMA polymers used for gas separation testing are listed in **Table 3.5**.

The tests were performed by our collaborators at Columbia University. The transport properties were measured by steady-state permeability tests and s nonsteady-state quartz crystal microbalance (QCM) technique.[50] **Figure 3.11** showed the performance of polymer grafted silica nanoparticle membranes comparing permeability of CO_2 and CH_4 in Robeson plots. The plots suggested that all the membranes from polymer grafted silica nanoparticles had a higher permeability than neat polymers in CO_2/CH_4. This was contrast to the conventional composite theory that mixtures of bare silica nanoparticles and PMA polymer exhibited a decrease of permeability.[25] Furthermore, the membrane with highest permeability (92kDa) had very little decrease in selectivity of CO_2/CH_4, indicating that the permeability can be tuned by tethering different polymer chain lengths to the NPs while keeping a comparable selectivity. The permeability of CO_2 over CH_4 in 92kDa membrane

increased by over 800% while the selectivity deceased by about 35%. The PMMA-g-SiO_2 showed a similar trend in the Robeson Plot (**Figure 3.11B**). The membranes generated from polymer grafted silica nanoparticles showed a nearly horizontal right shift in the Robenson Plot by adjusting the molecular weights with the best membrane in PMMA-*g*-SiO_2 nearly reaching the 1991 upper bound.

Table 3.5 The list of neat and grafted polymers

PMA			PMMA		
Graft density (chain/nm^2)	Mn	Đ	Graft density (chain/nm^2)	Mn	Đ
0.43	26,900	1.14	0.44	25,300	1.07
	38,100	1.11		62,400	1.08
	62,000	1.13		69,200	1.10
	77,100	1.15		78,200	1.13
	92,100	1.13		90,400	1.13
	132,100	1.18		113,600	1.17
Neat PMA	25,600	1.07	Neat PMMA	24,100	1.13
	46,100	1.11		60,400	1.08
	65,000	1.14		111,600	1.14
	77,600	1.12			
	96,500	1.16			
	135,000	1.20			

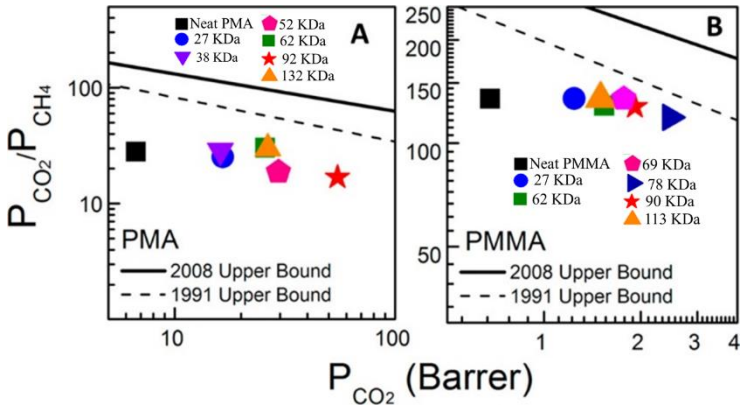

Figure 3.11 Performance of polymer-grafted NP membranes (Graft density = 0.43 chains/nm^2). Robeson plots comparing the permeabilities of CO_2 and CH_4 in (A) PMA- and (B) PMMA-grafted NP composites for various brush Mn.

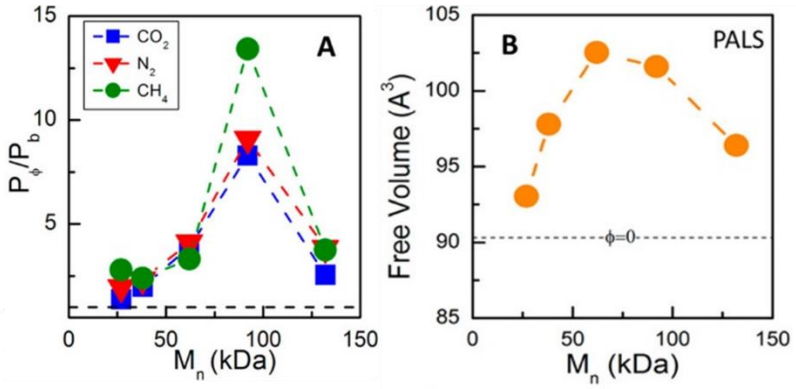

Figure 3.12 a) Increases in measured gas permeability relative to that of neat PMA (for grafted systems. Neat PMA is presented as a dashed line at Pϕ/Pb = 1. B) Measured free volume element size from PALS experiments as a function of the composite brush Mn. (ϕ represented the PMA-g-SiO_2 composite, b represented neat PMA)

The enhancement of the permeability of polymer grafted silica nanoparticles was dependent on the grafted polymer chain length. In **Figure 3.12A**, the ratio of permeability of PMA-g-SiO_2 (Pϕ) over neat PMA (Pb) are higher than 1 at graft density of 0.43 chain/nm^2 for CO_2, CH_4, and n-C_4H_{10}, which indicated an increase of permeability of grafted systems. In addition, it showed a "volcano plot" dependence of permeability of grafted over neat PMA. The permeability of PMA-*g*-SiO_2 over neat PMA increased as the

molecular weights increased, with the maximum permeability at an intermediate Mn of 92kDa for PMA-*g*-SiO_2. The Pϕ/Pb started to decrease as the molecular weight increased higher than 92 kDa. However, the Pϕ/Pb is still higher than 1, which indicated a higher permeability than neat PMA. Positron annihilation lifetime spectroscopy (PALS) can be used to measure the free volume of materials. [26] The free volume of PMA-g-SiO_2 nanocomposite membrane showed a similar volcano plot (**Figure 3.12B**), which suggested the enhanced permeability of PMA-g-SiO_2 was related to the free volume.

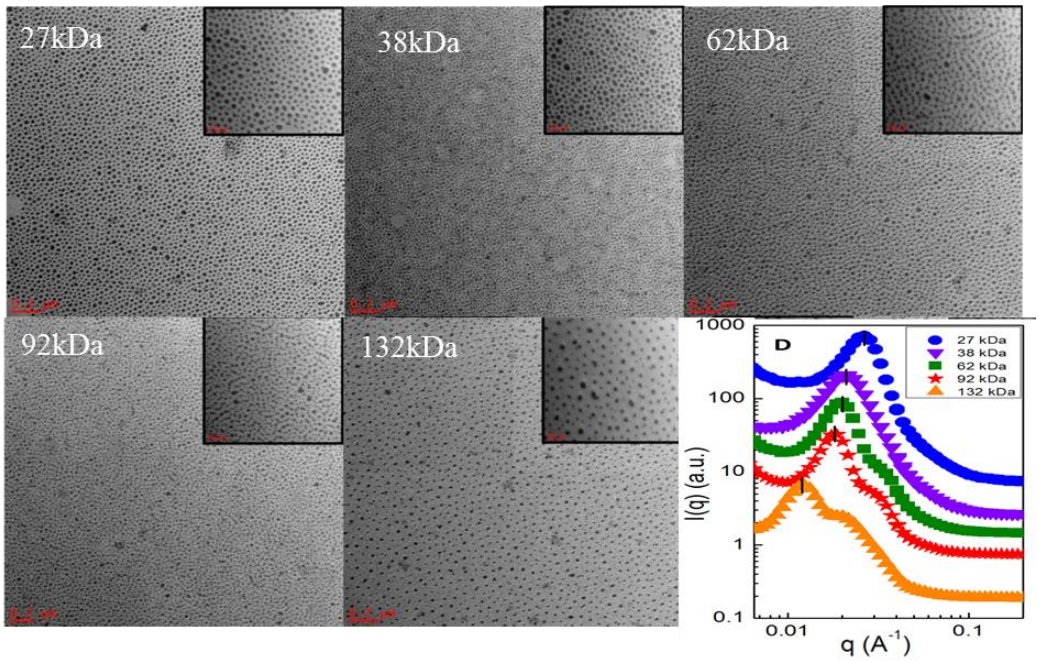

Figure 3.13 TEM and SANS characterization of PMA-g-SiO_2 with different molecular weights at 0.43 chain/nm^2. Scale bars on the large images were 0.2μm, and inset images were 100nm.

Transmission electron microscopy (TEM) was used to characterize the microstructure of the PMA-*g*-SiO_2 (**Figure 3.13**). The samples were prepared by drop casting the THF solution onto TEM grids. The TEM images showed that there were no agglomerations of silica nanoparticles in the films, which resulted from the fact that these were matrix-free

polymer nanocomposites. In addition, no observable defects of the films were detected from the TEM images. Small-angle neutron scattering (SANS) was used to characterize the dispersion of silica nanoparticles in the composite. It showed the nanoparticle distance increased (lower q_1*, the first peak in SANS) with the increase of grafted polymer chain lengths.

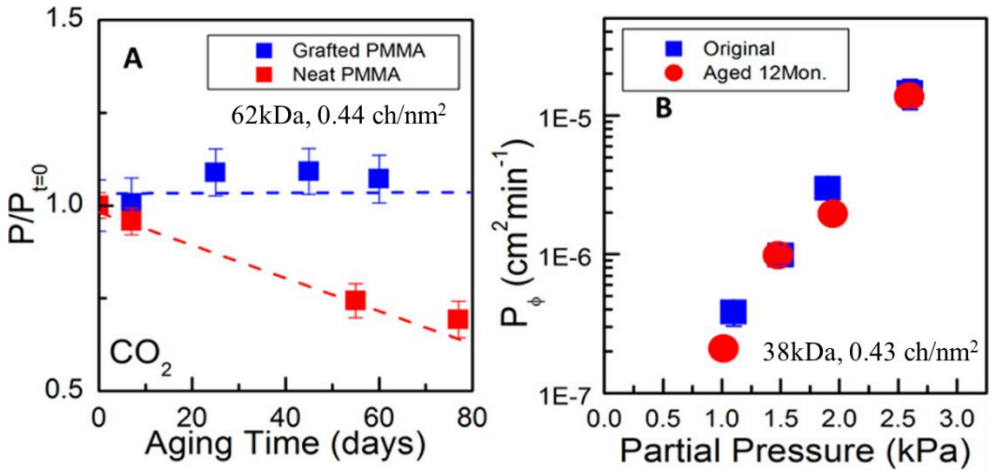

Figure 3.**14** Aging of neat and NP composite polymer films. (A) Effect of aging time on CO_2 permeability in neat PMMA and PMMA-g-SiO_2. (B) Time dependence of ethyl acetate permeability in a PMA-g-SiO_2.

Glassy polymer membranes are known to experience an aging effect, which resultes in the change of membrane performance.[20,51] The permeability of CO_2 in neat PMMA polymer decreased 25% in 10 weeks (**Figure 3.14A**). To the contrary, the PMMA-*g*-SiO_2 with 62kDa and 0.44 ch/nm^2 showed no measurable changes in permeability of CO_2 up to 60 days. This indicated the aging effect of glassy polymers can be lowered by chemically bonding the polymer chains to nanoparticles. **Figure 3.14B** showed there was almost no aging effect on PMA-g-SiO_2 with acetyl acetate for up to 1 year.

3.5 Conclusion

We have developed the well-controlled synthesis of poly(methyl acrylate) grafted silica nanoparticles (PMA-*g*-SiO_2) by surface-initiated reversible addition fragmentation chain-transfer polymerization. Different RAFT agents, 4-cyanopentanoic acid dithiobenzoate (CPDB) and 2-(dodecylthiocarbonothioylthio)propanoic acid (DoPAT), and solvent effects were investigated for the polymerization. The PMA-*g*-SiO_2 was successfully synthesized with DoPAT-SiO_2 in DMF solvent. The kinetic study suggested an inhibition time 2.5-4 hours in different conditions. An effective and timesaving strategy was developed to separate the ungrafted PMA polymer from PMA-*g*-SiO_2. By using a combination of THF and methanol, the removal efficiency of ungrafted PMA was the same as multiple ultracentifugations, which afforded a possible strategy for scale up for practical applications. Ultrasonication effects on the PMA-*g*-SiO_2 were also investigated. The membrane formed by matrix free PMA-*g*-SiO_2 and PMMA-*g*-SiO_2 showed an enhancement of the permeability in CO_2 while the selectivity of CO_2 over CH_4 had minor changes when compared to the neat polymers. This is contrary to the traditional composite theory. The most permeable membrane of PMA-*g*-SiO_2 had an increase over 800% in permeability while the selectivity decreased about 35%. The permeability of polymer grafted silica nanoparticles can also be tuned by polymer chain length, which showed a "volcano plot" in the permeability relative to neat polymer versus PMA molecular weight. The free volume measured by PALS exhibited a similar volcano shape versus PMA Mn, which strongly suggested the permeability was related to the free volume. TEM images showed the PMA-*g*-SiO_2 had no agglomeration of nanoparticles and SANS showed increased nanoparticle distance with longer grafted PMA chain length. The grafted PMMA

and PMA silica nanoparticles exhibited no aging effects. This provided an advantageous strategy for designing new industrial membranes with long life times. The membranes from polymer grafted nanoparticles exhibited significantly enhanced performance over neat polymers, which motivated us to design other glassy polymer grafted nanoparticle systems with potentially even better separation properties.

3.6 Acknowledgements

This work was performed in collaboration with Connor R. Bilchak, Eileen Buenning, and Dr. Sanat K. Kumar group at Columbia University who conducted the gas separation results.

3.7 References

(1) Xiao, Y.; Low, B. T.; Hosseini, S. S.; Chung, T. S.; Paul, D. R. *Prog. Polym. Sci.* **2009**, *34*, 561.

(2) Li, X.; Singh, R. P.; Dudeck, K. W.; Berchtold, K. A.; Benicewicz, B. C. *J. Membr. Sci.* **2014**, *461*, 59.

(3) Robeson, L. M. *J. Membr. Sci.* **2008**, *320*, 390.

(4) Park, H. B.; Kamcev, J.; Robeson, L. M.; Elimelech, M.; Freeman, B. D. *Science* **2017**, *356*.

(5) Galizia, M.; Chi, W. S.; Smith, Z. P.; Merkel, T. C.; Baker, R. W.; Freeman, B. D. *Macromolecules* **2017**, *50*, 7809.

(6) Baker, R. W.; Low, B. T. *Macromolecules* **2014**, *47*, 6999.

(7) Park, H. B. J., C. H.; Lee, Y. M.; Hill, A. J.; Pas, S. J.; Mudie, S. T.; Van Wagner, E.; Freeman, B. D.; Cookson, D. J. *Science* **2007**, *318*, 254.

(8) Park, H. B.; Han, S. H.; Jung, C. H.; Lee, Y. M.; Hill, A. J. *J. Membr. Sci.* **2010**, *359*, 11.

(9) Singh, R. P.; Li, X.; Dudeck, K. W.; Benicewicz, B. C.; Berchtold, K. A. *Polymer* **2017**, *119*, 134.

(10) Chung, T.-S.; Jiang, L. Y.; Li, Y.; Kulprathipanja, S. *Prog. Polym. Sci.* **2007**, *32*, 483.

(11) Goh, P. S.; Ismail, A. F.; Sanip, S. M.; Ng, B. C.; Aziz, M. *Sep. Purif. Technol.* **2011**, *81*, 243.

(12) Cong, H.; Radosz, M.; Towler, B.; Shen, Y. *Sep. Purif. Technol.* **2007**, *55*, 281.

(13) Rezakazemi, M.; Ebadi Amooghin, A.; Montazer-Rahmati, M. M.; Ismail, A. F.; Matsuura, T. *Prog. Polym. Sci.* **2014**, *39*, 817.

(14) Rodenas, T.; Luz, I.; Prieto, G.; Seoane, B.; Miro, H.; Corma, A.; Kapteijn, F.; Llabres, I. X. F. X.; Gascon, J. *Nat. Mater.* **2015**, *14*, 48.

(15) Bae, T. H.; Lee, J. S.; Qiu, W.; Koros, W. J.; Jones, C. W.; Nair, S. *Angew. Chem. Int. Ed.* **2010**, *49*, 9863.

(16) Zhang, Y.; Feng, X.; Yuan, S.; Zhou, J.; Wang, B. *Inorg. Chem. Front.* **2016**, *3*, 896.

(17) Li, X.; Ma, L.; Zhang, H.; Wang, S.; Jiang, Z.; Guo, R.; Wu, H.; Cao, X.; Yang, J.; Wang, B. *J. Membr. Sci.* **2015**, *479*, 1.

(18) Ahn, J.; Chung, W.-J.; Pinnau, I.; Guiver, M. D. *J. Membr. Sci.* **2008**, *314*, 123.

(19) Kim, S.; Chen, L.; Johnson, J. K.; Marand, E. *J. Membr. Sci.* **2007**, *294*, 147.

(20) Huang, Y.; Paul, D. R. *Polymer* **2004**, *45*, 8377.

(21) Rowe, B. W.; Freeman, B. D.; Paul, D. R. *Polymer* **2009**, *50*, 5565.

(22) Staiger, C. L.; Pas, S. J.; Hill, A. J.; Cornelius, C. J. *Chem. Mater.* **2008**, *20*.

(23) Tiwari, R. R.; Smith, Z. P.; Lin, H.; Freeman, B. D.; Paul, D. R. *Polymer* **2014**, *55*, 5788.

(24) Rittigstein, P.; Torkelson, J. M. *J. Polym. Sci., Part B: Polym. Phys.* **2006**, *44*, 2935.

(25) Janes, D. W.; Durning, C. J. *Macromolecules* **2013**, *46*, 856.

(26) Merkel, T. C.; Freeman, B. D.; Spontak, R. J.; He, Z.; Pinnau, I.; Meakin, P.; Hill, A. J. *Science* **2002**, *296*, 519.

(27) Takahashi, S.; Paul, D. R. *Polymer* **2006**, *47*, 7519.

(28) Takahashi, S.; Paul, D. R. *Polymer* **2006**, *47*, 7535.

(29) Zoppe, J. O.; Ataman, N. C.; Mocny, P.; Wang, J.; Moraes, J.; Klok, H. A. *Chem. Rev.* **2017**.

(30) Chen, W.-L.; Cordero, R.; Tran, H.; Ober, C. K. *Macromolecules* **2017**.

(31) Wu, L.; Glebe, U.; Böker, A. *Polym. Chem.* **2015**, *6*, 5143.

(32) Edmondson, S.; Osborne, V. L.; Huck, W. T. *Chem. Soc. Rev.* **2004**, *33*, 14.

(33) Kumar, S. K.; Jouault, N.; Benicewicz, B.; Neely, T. *Macromolecules* **2013**, *46*, 3199.

(34) Akcora, P.; Liu, H.; Kumar, S. K.; Moll, J.; Li, Y.; Benicewicz, B. C.; Schadler, L. S.; Acehan, D.; Panagiotopoulos, A. Z.; Pryamitsyn, V.; Ganesan, V.; Ilavsky, J.; Thiyagarajan, P.; Colby, R. H.; Douglas, J. F. *Nat. Mater.* **2009**, *8*, 354.

(35) Fernandes, N. J.; Koerner, H.; Giannelis, E. P.; Vaia, R. A. *MRS Commun.* **2013**, *3*, 13.

(36) Rungta, A.; Natarajan, B.; Neely, T.; Dukes, D.; Schadler, L. S.; Benicewicz, B. C. *Macromolecules* **2012**, *45*, 9303.

(37) Perrier, S.; Takolpuckdee, P.; Mars, C. A. *Macromolecules* **2005**, *38*, 2033.

(38) Li, C.; Han, J.; Ryu, C. Y.; Benicewicz, B. C. *Macromolecules* **2006**, *39*, 3175.

(39) Patton, D. L.; Advincula, R. C. *Macromolecules* **2006**, *39*, 8674.

(40) Ferguson, C. J. H., R. J.; Nguyen, D.; Pham, B. T. T.; Gilbert, R. G.; Serelis, A. K.; Such, C. H.; Hawkett, B. S. *Macromolecules* **2005**, *38*, 2191.

(41) Chong, Y. K. K., J.; Le, T. P. T.; Moad, G.; Postma, A.; Rizzardo, E.; Thang, S. H. *Macromolecules* **2003**, *36*, 2256.

(42) Moad, G. C., J.; Chong, Y. K.; Krstina, J.; Mayadunne, R. T. A.; Postma, A.; Rizzardo, E.; Thang, S. H. *Polym. Int.* **2000**, *49*, 993.

(43) Moad, G. *Macromol. Chem. Phys.* **2014**, *215*, 9.

(44) Davis, S. P. C. B.-K. J. F. Q. P. V. T. P. *Macromolecules* **2002**, *35*, 8300.

(45) Tchoul, M. N.; Dalton, M.; Tan, L.-S.; Dong, H.; Hui, C. M.; Matyjaszewski, K.; Vaia, R. A. *Polymer* **2012**, *53*, 79.

(46) Hui, C. M.; Dang, A.; Chen, B.; Yan, J.; Konkolewicz, D.; He, H.; Ferebee, R.; Bockstaller, M. R.; Matyjaszewski, K. *Macromolecules* **2014**, *47*, 5501.

(47) Li, J.; Shiraki, T.; Hu, B.; Wright, R. A.; Zhao, B.; Moore, J. S. *J. Am. Chem. Soc.* **2014**, *136*, 15925.

(48) May, P. A.; Moore, J. S. *Chem. Soc. Rev.* **2013**, *42*, 7497.

(49) Bansal, A.; Yang, H.; Li, C.; Cho, K.; Benicewicz, B. C.; Kumar, S. K.; Schadler, L. S. *Nat. Mater.* **2005**, *4*, 693.

(50) Bilchak, C. R.; Buenning, E.; Asai, M.; Zhang, K.; Durning, C. J.; Kumar, S. K.; Huang, Y.; Benicewicz, B. C.; Gidley, D. W.; Cheng, S.; Sokolov, A. P.; Minelli, M.; Doghieri, F. *Macromolecules* **2017**, *50*, 7111.

(51) Dorkenoo, K. D.; Pfromm, P. H. *J. Polym. Sci., Part B: Polym. Phys.* **1999**, *37*, 2239.

CHAPTER 4

A Versatile Approach to Different Colored Photonic Films Generated from Block Copolymers and Their Conversion into Polymer-Grafted Nanoplatelets*

*This chapter was reproduced and adapted from Huang et al. *J. Mater. Chem. C*, **2017**, *5*, 9873.

4.1 Abstract

One-dimensional photonic crystals can be formed by self-assembly of block copolymers. However, such materials are still difficult to make due to the synthetic challenge of making high molecular weight block copolymers and the slow self-assembly characteristics of these block copolymers to form high domain spacings (d >150 nm). Herein we report a new strategy to construct two different photonic crystals with different solvent responses and reflecting colors from the films of a single block copolymer. Initially, films made from poly(3-(triethoxysilyl)propyl methacrylate)-*block*-poly(stearyl methacrylate) with moderate molecular weight ($PTEPM_{666}$-*b*-$PSMA_{553}$ film) were responsive to alcohol with an observed stop band change from 365 nm (dry film) to 458 nm (film in ethanol), displaying a blue color. After conversion of the PTEPM domain to form SiO_2 nanoplatelets, the $PSMA_{553}$-*g*-SiO_2 nanoplatelet film showed a larger stop band change from 365 nm (dry film) to 591 nm (film in THF), which reflected a bright orange color.

4.2 Introduction

Block copolymers (BCPs) can self-assemble into well-ordered microstructures by tuning the molecular weight and copolymer composition.[1] Self-assembly of BCPs into lamellar, hexagonally packed cylinders, and double gyroid morphologies have been used as a platform to form photonic crystals.[2-6] Different photonic crystals have been fabricated to respond to stimuli including solvents[7-10], ions[11], electric fields[12-14], pH[15], heat[16,17], ionic liquids[18], etc. Responsive photonic crystals have a wide array of applications in display devices, sensing and bio-sensing.[19] Creating

photonic crystals formed by one-dimensional self-assembly necessitates the use of ultrahigh molecular weight of BCPs (Mn>500 kDa), which can form ordered microstructures with high inter-domain (d) spacing. However, self-assembly of high molecular weight BCPs usually requires long annealing times to reach thermodynamic equilibrium, which is due to slow reptation of highly entangled polymer chains. In addition, the synthesis of ultrahigh molecular weight BCPs is still challenging. Anionic polymerization is the most common polymerization method used to synthesize ultrahigh molecular weight BCPs for photonic crystals.[7,12,20,21] Grubbs et al. reported the synthesis of brush BCPs by ring-opening metathesis polymerization (ROMP), which could lead to rapid self-assembly to form one dimensional photonic crystals.[22-25] Rzayev et al. recently reported the use of a combination of Cu-mediated reversible-deactivation radical polymerization (RDRP) and reversible addition-fragmentation chain transfer (RAFT) polymerization to synthesize ultrahigh molecular weight (Mn=800 - 1600 kDa) BCPs, which self-assembled into an ordered morphology with large d-spacing to form photonic nanomaterials.[26] Thomas et al. reported a hydrophobic-hydrophilic BCP with modest molecular weight, which self-assembled into a one-dimensional lamellar morphology to construct chemically tunable photonic crystal gels with broad wavelength range. [27]

The properties of one dimensional polymeric photonic crystals are related to the domain size and refractive index contrast between the two domains.[28] Low molecular weight homo-polymers can be co-assembled with BCPs to increase the volume of one domain which could in turn tune the stop band of the photonic

crystals.[21] However, the amount of added homo-polymer must be carefully selected so that the volume fraction of that domain does not change too significantly, or a change in the morphology of the ordered system may be induced. Inorganic nanoparticles (NPs) can be selectively blended into one domain to increase the refractive index contrast.[29-32] Kang et al. reported a full color stop band photonic crystal formed by block polymer PS-*b*-P2VP/silica hybrid. The block copolymer self-assembled into a lamellar morphology and tetraethoxysilane (TEOS) was blended into the P2VP domain in methanol to form SiO_2 by gelation of TEOS. This film showed full color stop bands by aging at different time intervals.[33]

Herein we have designed a facile way to construct two different kinds of photonic crystals with different solvent responses and reflected colors using the same batch of synthesized block copolymer. The films had different responses to solvents before and after conversion of one domain to SiO_2 nanoplatelets, which resulted in different reflecting colors (**Scheme 4.1**). The BCP, poly(3-(triethoxysilyl)propyl methacrylate)$_{666}$-*block*-poly(stearyl methacrylate)$_{553}$ (PTEPM$_{666}$-*b*-PSMA$_{553}$), self-assembled into a lamellar structure. The PTEPM block contained silane groups which could be converted upon exposure to HCl to form inorganic SiO_2 platelets.[34,35] The d-spacing of the BCP film and polymer grafted nanoplatelet film can be tuned by immersion in selective solvents, ethanol and THF respectively. This system can form photonic crystals with different stop bands in visible light.

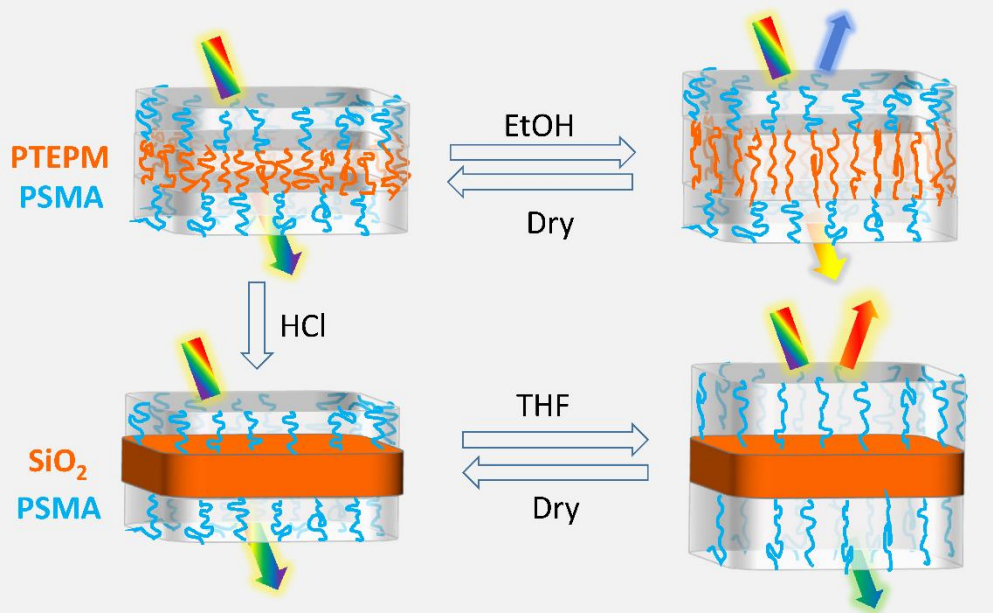

Scheme 4.1 Schematic of tunable photonic crystals formed by PTEPM-*b*-PSMA self-assembly

4.3 Experimental

Materials.

All chemicals were obtained from either Fisher or Acros and used as received unless otherwise specified. 3-(Trimethoxysilyl)propyl methacrylate (98%) was purchased from Sigma-Aldrich. 2-(2-Cyanopropyl)dithiobenzoate (CPDB) was purchased from Strem Co. Ltd. Stearyl methacrylate (SMA, >95%, TCI) was purified by passing through an activated basic alumina column. Azobisisobutyronitrile (AIBN) was recrystallized from ethanol twice before use.

Instrumentation.

^{1}H NMR (Bruker Avance III-HD 300 MHz and 400MHz) were conducted using $CDCl_3$ as solvent. Molecular weights (Mn) and dispersities (Đ) were determined using a gel permeation chromatograph (GPC) equipped with a Varian 290-LC pump, a Varian 390-LC refractive index detector, and three Styragel columns(HR1, HR3

and HR4, molecular weight range of 100-5000, 500-30000, and 5000-500000, respectively). THF was used as eluent for GPC at 30℃ and a flow rate of 1.0 mL/min. GPC was calibrated with polystryrene (PS) standards obtained from Polymer Laboratories. UV-vis transmission spectra were measured on Shimadzu UV-2450. FT-IR spectra were measured on PerkinElmer Spectrum 100 spectrometer. Thermogravimetric analysis (TGA) measurements were carried out on a TA Q5000 thermogravimetric analyzer (TA Instruments). The samples were preheated to 150 ℃ and kept at this temperature for 10 min to remove residual solvents. After cooling to 40 ℃, the samples were heated to 800 ℃ with a heating rate 10 ℃/min in nitrogen atmosphere. Differential scanning calorimetry (DSC) measurements were conducted using a TA Q2000 DSC (TA Instruments) under nitrogen atmosphere at a heating rate 10 ℃/min from -80 ℃ to 80 ℃. Extreme-small angle X-ray scattering (ESAXS) experiments were conducted using a SAXSLab Ganesha instrument at the South Carolina SAXS Collaborative. A Xenocs GeniX3D microfocus source was used with a Cu target to generate a monochromic beam with a 0.154 nm wavelength. The instrument was calibrated using National Institute of Standard and Technology (NIST) reference material 640c silicon powder with the peak position at total scattering angle of 2θ of 28.44˚. A Pilatus 300 K detector (Dectris) was used to collect the two-dimensional (2D) scattering pattern. The 2D images were azimuthally integrated to yield the scattering vector and intensity. All ESAXS experiments were conducted for 1 hour with an X-ray flux of 1.8 M photons/s incident up on the sample with a sample-to-detector distance of 1502 mm. Scanning electron microscopy (SEM) images of films were

observed with a Zeiss Ultraplus thermal field emission SEM using an acceleration voltage of 6 kV. Samples were prepared by freezing the film in liquid nitrogen and fracturing films. The cross sections were taken for SEM imaging. The transmission electron microscopy (TEM) was performed on a Hitachi H8000 TEM at an accelerating voltage of 200 KV. Samples were prepared by stirring the film in THF for one week and the supernatant was dropped onto a copper grid. All the photographs were taken on a black background.

Synthesis of PSMA-*b*-PTEPM block copolymer.

The synthesis of PTEPM-*b*-PSMA block copolymer is illustrated in **Scheme 4.2**.

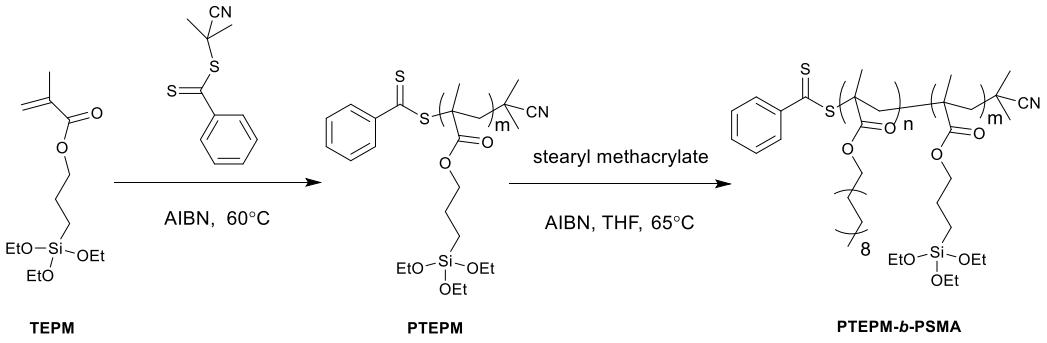

Scheme 4.2 Synthesis of PTEPM-*b*-PSMA

Synthesis of PTEPM.

3-(Triethoxysilyl) propyl methacrylate (TEPM) was synthesized from 3-(trimethoxysilyl)propyl methacrylate with ethanol.[36] A general polymerization procedure is described here: TEPM (12.0 g, 0.041 mol), 2-(2-cyanopropyl)dithiobenzoate (CPDB) (4.57 mg, 0.021 mmol) and 0.041mL AIBN in DMF solution (0.1 M) were transferred into a 50mL Schlenk tube. The mixture was degassed by three freeze- pump- thaw cycles, backfilled with nitrogen, and then

placed in an oil bath at 60 ℃. The polymerization solution was stopped by submerging the tube in ice after 17 hours. A 50 μL solution was taken for ^{1}H NMR analysis to calculate the monomer conversion.[34] The polymer was precipitated in methanol/water mixture (1:1) and recovered by centrifugation. The purification was repeated for another three times. The PTEPM polymer was dried in vacuum overnight. The resulting polymer was analyzed by GPC to get Mn=124400 with dispersity Đ=1.15.

Synthesis of PTEPM-*b*-PSMA.

PTEPM (0.84 g, 0.0043 mmol) and stearyl methacrylate (SMA) (2.93 g, 0.0087 mol) were dissolved in 7mL THF. AIBN in THF solution (43 μL, 0.01 M) was added into the solution. The mixture was transferred into a Schlenk flask and degassed by three freeze- pump- thaw cycles, backfilled with nitrogen, and then placed in an oil bath at 65 ℃ for 18 h. The polymerization solution was quenched in ice. The polymer was precipitated in methanol and recovered by centrifugation. The polymer was washed with methanol until there was no SMA monomer, which was characterized by ^{1}H NMR. The resulting block copolymer was measured with GPC to get Mn=237400 with Đ=1.37.

Film preparation.

A solution of PTEPM-*b*-PSMA in THF (~40 mg/mL) was poured into a petri dish and evaporated at room temperature over 24 hours. The resulting film was dried in vacuum oven at R.T. overnight to remove the residual solvent. The cast film was annealed in 60 ℃ in a vacuum oven for 12 hours and cooled slowly to room temperature with thickness ca. 0.2 mm.

Conversion of the BCP film into grafted nanoplatelets.

A PTEPM-*b*-PSMA film was placed in an HCl atmosphere for 12 hours. After that, the film was placed in 60 ℃ vacuum oven for another 12 hours to complete the conversion.

4.4 Results and Discussion

We synthesized a modest molecular weight block copolymer, $PTEPM_{666}$-*b*-$PSMA_{553}$, by RAFT polymerization (**Scheme 4.2**). The composition of the BCP and molecular weight were characterized by ^{1}H NMR (**Figure 4.1**, **4.2**) and gel permeation chromatography (GPC) (Mn ($PTEPM_{666}$) =124400, Đ=1.15; Mn ($PTEPM_{666}$-*b*-$PSMA_{553}$) =237400, Đ=1.37) (**Figure 4.3**).

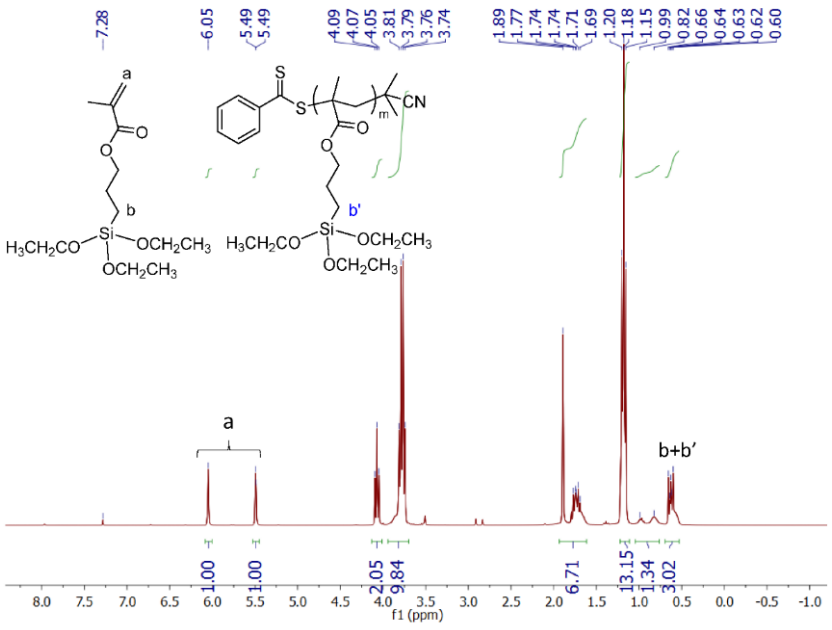

Figure 4.1 ^{1}H NMR ($CDCl_3$, 300MHz) of $PTEPM_{666}$ polymer solution

The monomer conversion p was calculated by:

$$p = \frac{I(b+b') - I(a)}{I(b+b')}$$, I is the integration of peak

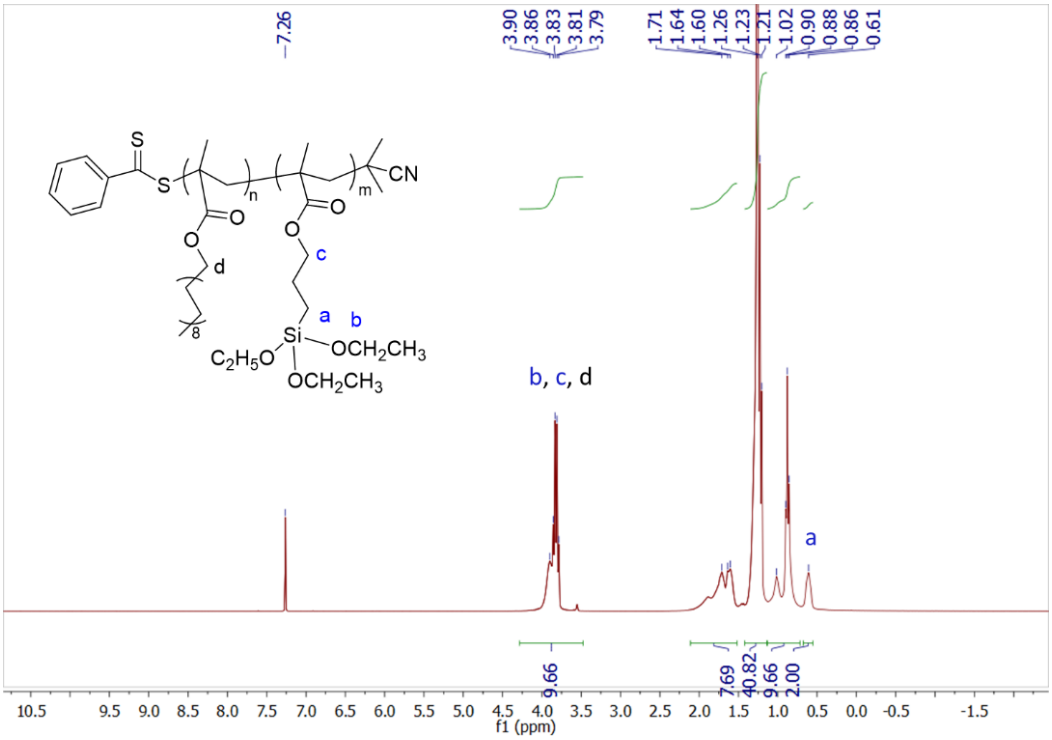

Figure 4.2 ^{1}H NMR ($CDCl_3$, 300M) of $PTEPM_{666}$-*b*-$PTEPM_{553}$ block copolymer

The ratio of degree of polymerization (DP) of TEPM (m) and DP of SMA (n) can be calculated by: $\frac{m}{n} = \frac{I(a)}{I(b,c,d)-4I(a)}$, I is the integration of peak

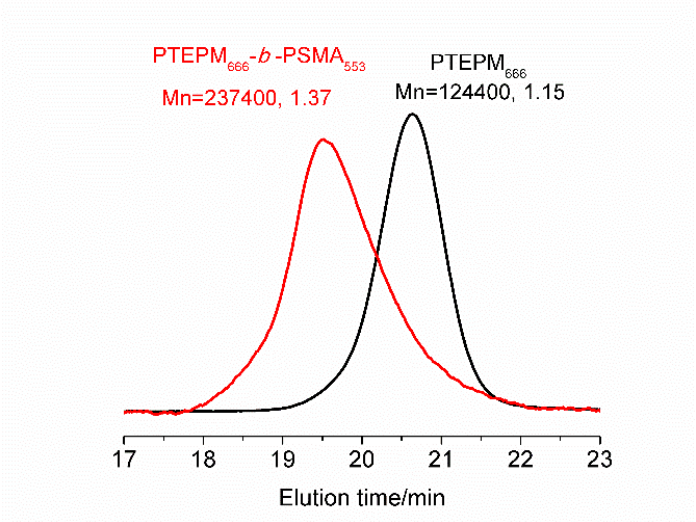

Figure 4.3 GPC curves of $PTEPM_{666}$ and $PTEPM_{666}$-*b*-$PSMA_{553}$

The BCP was dissolved in THF and drop-cast to form a film. After annealing at 60 ℃ for 12h, the film was exposed to an HCl atmosphere to convert the PTEPM domain to $PSMA_{553}$-graft-silica ($PSMA_{553}$-*g*-SiO_2) nanoplatelets. The conversion process was confirmed by Fourier Transform infrared spectroscopy (FT-IR) (**Figure 4.4**). For $PTEPM_{666}$-*b*-$PSMA_{553}$, the peaks at 1103 and 1077 cm^{-1} were from the Si-O-C vibration as well as 1165 and 956 cm^{-1} were from ethoxyl group. After conversion to form $PSMA_{553}$-*g*-SiO_2 nanoplatelets, the peaks for the ethoxy group (1165 and 956 cm^{-1}) disappeared and a new strong broad region appeared at 1059 to 1145 cm^{-1} resulting from the Si-O-Si vibration.[34] Thermogravimetric analysis (TGA) showed there was 12.6 wt% silica in the $PSMA_{553}$-*g*-SiO_2 nanoplatelet, which also indicated successful conversion of PTEPM (**Figure 4.5**).

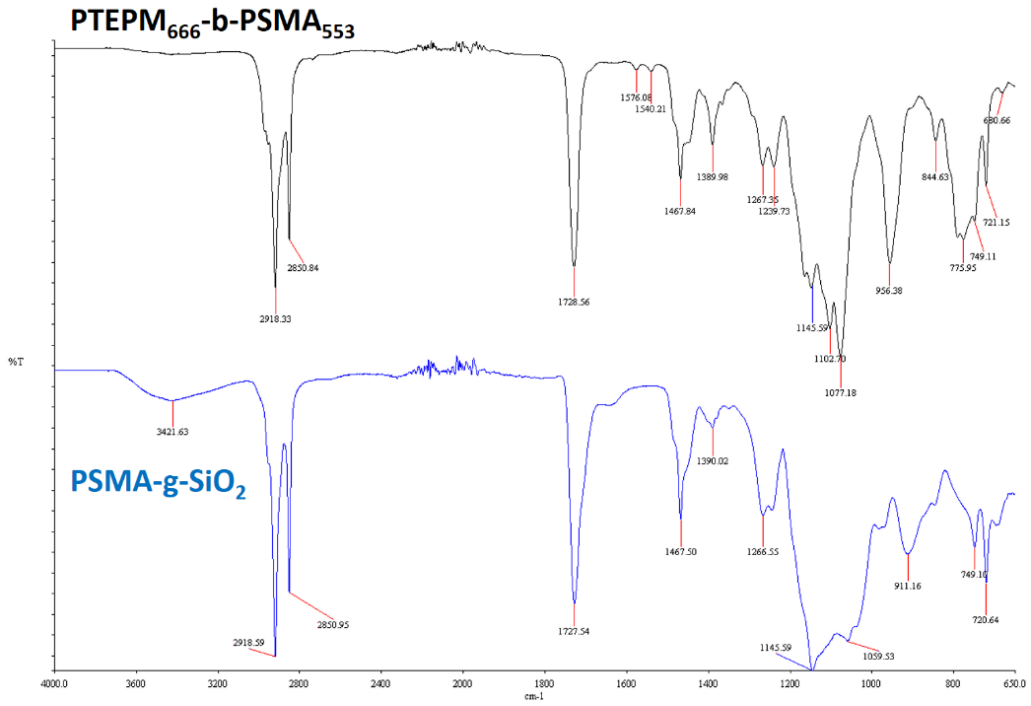

Figure 4.4 FT-IR spectra of $PTEPM_{666}$-*b*-$PSMA_{553}$ and $PSMA_{553}$-*g*-SiO_2

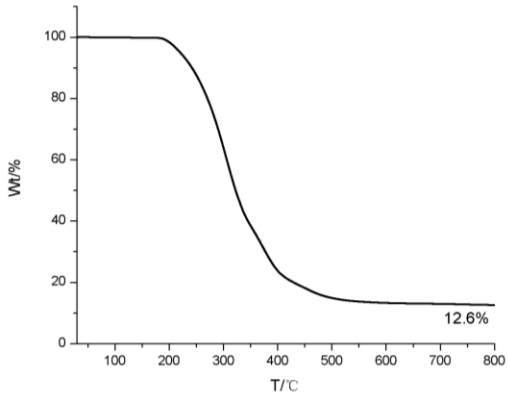

Figure 4.5 TGA of $PSMA_{553}$-*g*-SiO_2

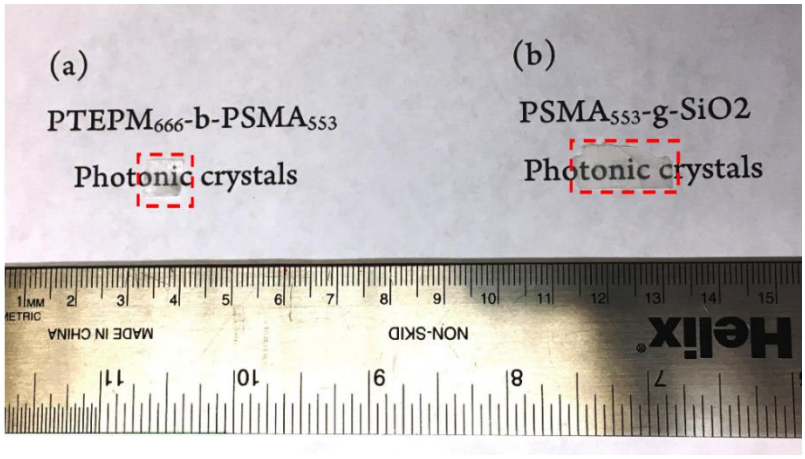

Figure 4.6 Photographs of dry films a) $PTEPM_{666}$-*b*-$PSMA_{553}$; b) $PSMA_{553}$-*g*-SiO_2. The dotted lines area shows the placement of the films.

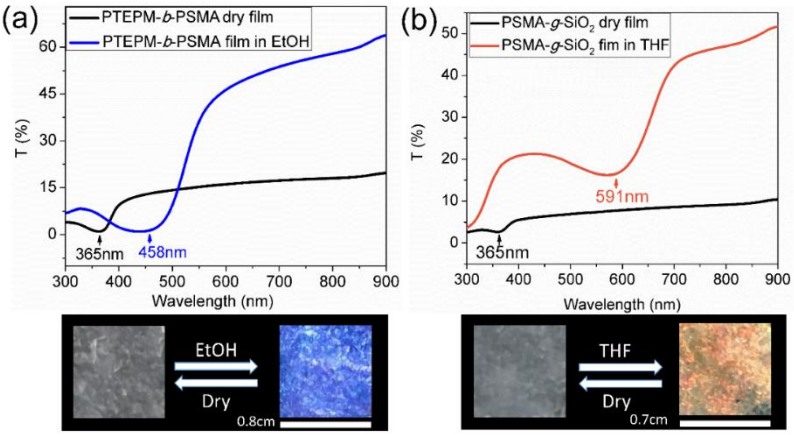

Figure 4.7 Transmission spectra and photographs of (a) $PTEPM_{666}$-*b*-$PSMA_{553}$ dry film and film in EtOH; (b) $PSMA_{553}$-*g*-SiO_2 dry film and film in THF.

Both the $PTEPM_{666}$-*b*-$PSMA_{553}$ and $PSMA_{553}$-*g*-SiO_2 film were slightly opaque in visible light (**Figure 4.6**).The transmittance data is the sum of both reflectance and absorbance. However, the contribution to this sum from absorbance is minimal in the visible light region. In this case, the inverse transmittance closely approximates the reflectance of the films. The dry film $PTEPM_{666}$-*b*-$PSMA_{553}$ was colorless and showed a stop band at 365 nm in the transmission spectrum. However, the film gradually changed to a blue color when immersed in ethanol with the stop band shifting from 365 nm to 458 nm (**Figure 4.7a**).The stop band changed to 417 nm after 4 min and stabilized at 458 nm after 45 min. During this process, the stop band shifted to longer wavelength region while the intensity had little change (**Figure 4.8a**). The wavelength of reflecting light from the 1D photonic crystal was related to the layer distance and refractive index contrast between the layers.[4] EtOH was a good solvent for PTEPM, which caused the swelling of the PTEPM and resulted in a larger layer distance. The blue color slowly disappeared with the evaporation of the solvent. This process was reversible. After conversion of the PTEPM domain, the $PSMA_{553}$-*g*-SiO_2 nanoplatelet film was colorless in visible light with a stop band at 365 nm. However, the $PSMA_{553}$-*g*-SiO_2 film didn't show any color change when immersed in ethanol. This was ascribed to the unfavorable interactions of the PSMA grafted nanoplatelets with EtOH. Interestingly, the $PSMA_{553}$-*g*-SiO_2 nanoplatelet film had a large shift in the stop band from 365 nm to 591 nm after immersion in THF, resulting in a bright orange-colored film (**Figure 4.7b**). The stop band changed to 529 nm after 5 min and stabilized at 591 nm after 25 min (**Figure 4.8b**). During this process, the color of the film changed from

colorless (dry film) to blue, green and finally orange (**Figure 4.9**). THF is a good solvent for PSMA but not for the silica nanoplatelets. This indicated the PSMA between the nanoplatelets gradually swelled in THF, which increased the layer distance and resulted in reflecting different colors. The film gradually changed to a colorless film with evaporation of THF. The orange color film was stable in THF for more than five months.

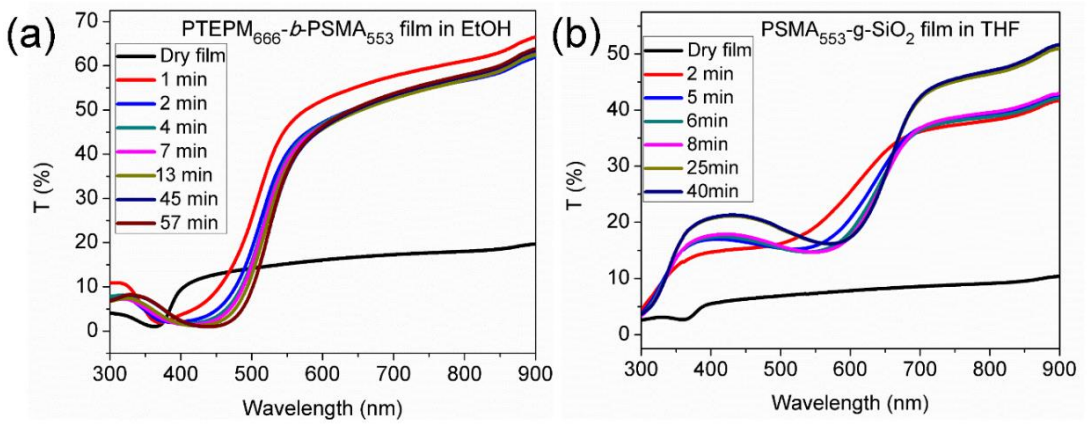

Figure 4.8 Transmission spectra of films immersed in solvents with different time. (a) $PTEPM_{390}$-*b*-$PSMA_{553}$ film in EtOH; (b) $PSMA_{353}$-*g*-SiO_2 film in THF.

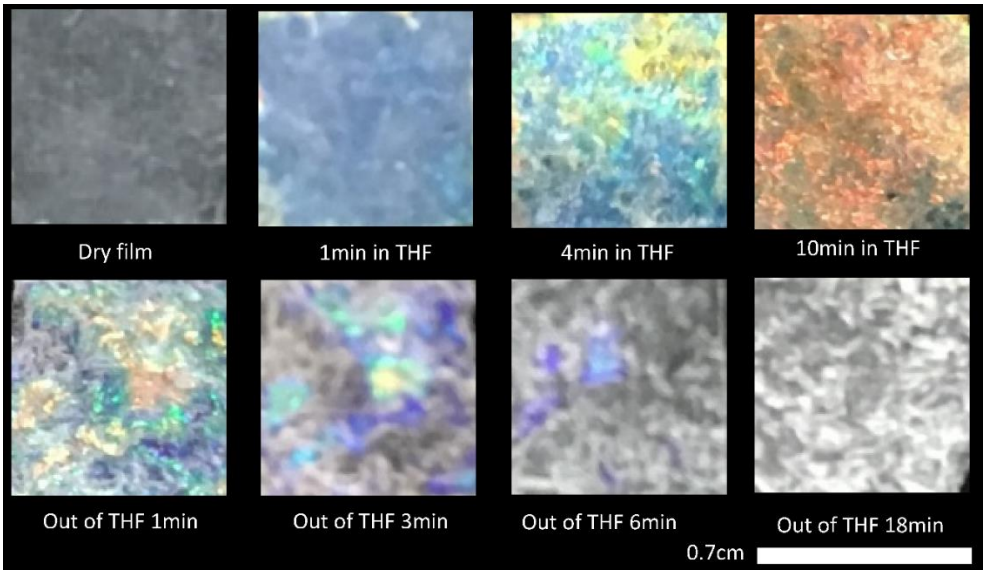

Figure 4.9 Photography of $PSMA_{553}$-g-SiO_2 dry film and film in THF at different times

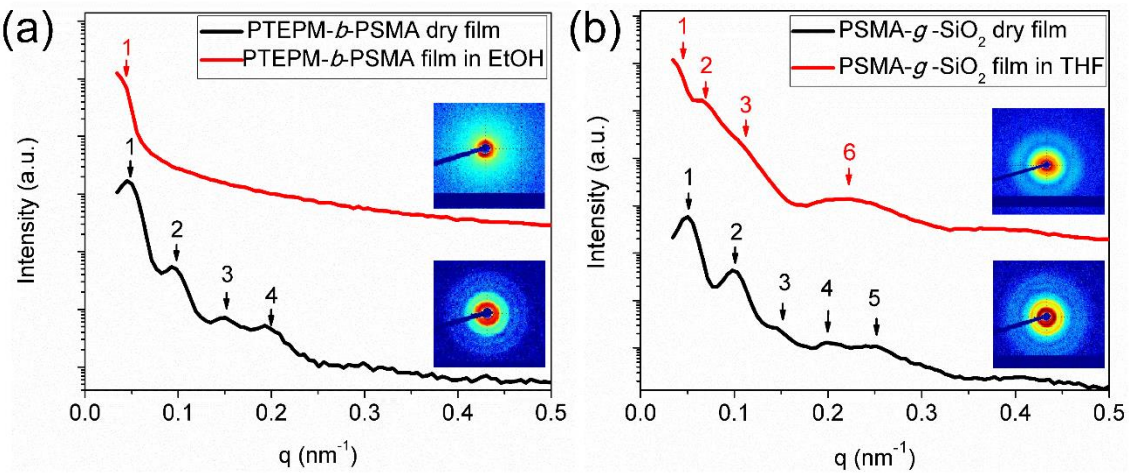

Figure 4.10 ESAXS spectra of (a) $PTEPM_{666}$-*b*-$PSMA_{553}$ dry film and film in EtOH; (b) $PSMA_{553}$-*g*-SiO_2 dry film and film in THF. (The insets are 2D patterns)

Extreme-small angle X-ray scattering (ESAXS) was used to characterize the micro-phase separation of $PTEPM_{666}$-*b*-$PSMA_{553}$ block copolymer and $PSMA_{553}$-*g*-SiO_2 nanoplatelet films (**Figure 4.10**). The ESAXS spectra of $PTEPM_{666}$-*b*-$PSMA_{553}$ film showed a principal scattering peak (q) at 0.0495 nm^{-1}, which corresponded to a d-spacing of about 127 nm ($d=2\pi/q$). Also present were the higher-ordered peaks 2q, 3q and 4q, which indicated well-ordered asymmetric lamellar morphology. The d-spacing of $PTEPM_{666}$-*b*-$PSMA_{553}$ film in ethanol increased to *ca.* 145 nm. The $PTEPM_{666}$-*b*-$PSMA_{553}$ film displayed a blue color after immersion in ethanol while the dry film was colorless. This was due to the swelling of the PTEPM in ethanol, which increased the domain thickness of PTEPM. After ethanol evaporation, the ESAXS spectra of vacuum dried $PTEPM_{666}$-*b*-$PSMA_{553}$ film was almost identical to the virgin dry film. This indicated the lamellar structure was preserved after being immersed in ethanol. The ESAXS data of $PSMA_{553}$-*g*-SiO_2 also showed a highly ordered lamellar morphology (1:2:3:4:5) with d-spacing of *ca.*

126 nm. The ESAXS profile of the $PSMA_{553}$-g-SiO_2 film in ethanol showed no difference from the dry film (**Figure 4.11**). This was consistent with the absence of any color change after the $PSMA_{553}$-*g*-SiO_2 film was immersed in ethanol. After the $PSMA_{553}$-*g*-SiO_2 film was immersed in THF, a selective solvent for PSMA, the film displayed a bright orange color. The ESAXS data showed a principal peak at 0.0364 nm^{-1} with high ordered peaks 2q, 3q and 6q. This high d-spacing (*ca.* 173 nm) contributed to the reflection of an orange color.

We also found that both the $PTEPM_{666}$-*b*-$PSMA_{553}$ and $PSMA_{553}$-*g*-SiO_2 nanoplatelet films had a broader bandwidth in the solvents than the respective dry films (**Figure 4.7**). The ESAXS profile showed the disappearance of higher order scattering peaks as well as lower intensity of scattering peaks after the films were immersed in solvents (**Figure 4.10**). This indicated that the solvation of films resulted in a less ordered lamellar microstructure than the dry films. The swelling of PTEPM domain in ethanol may cause a distortion of the lamellar structure of self-assembled $PTEPM_{666}$-*b*-$PSMA_{553}$ film in ethanol, which resulted in a less ordered microstructure. The $PSMA_{553}$-*g*-SiO_2 nanoplatelet film was formed by the HCl induced conversion of the PTEPM domain in the BCP into nanoplatelets. However, not all of the PTEMP reacted with HCl to form perfect silica nanoplatelets, which resulted in a small portion of PSMA-*b*-PTEPM grafted on the surface of the silica nanoplatelets. This contributed to the slight disruption of nanoplatelet ordering after the film was immersed in THF.

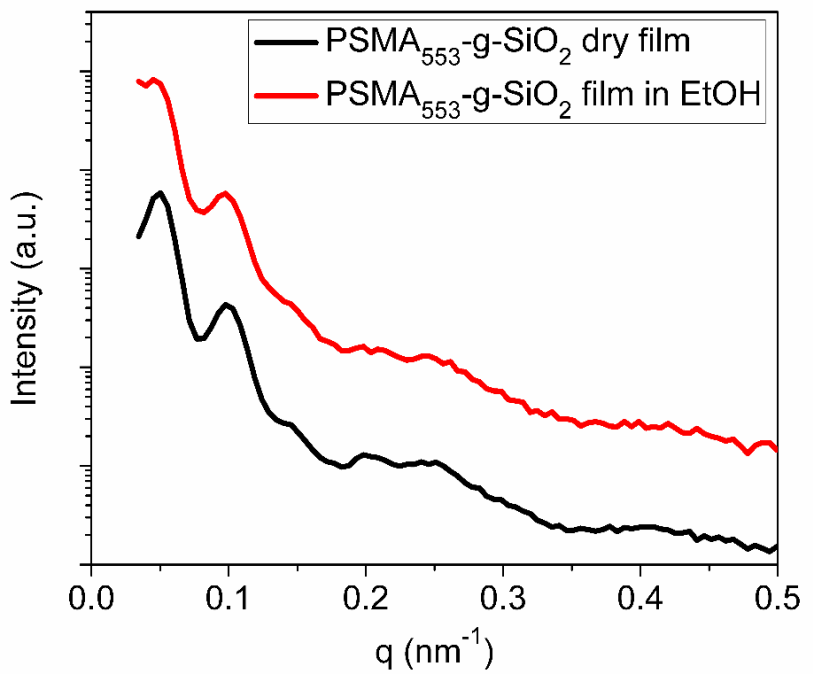

Figure 4.11 ESAXS of $PSMA_{553}$-*g*-SiO_2 dry film and film in ethanol.

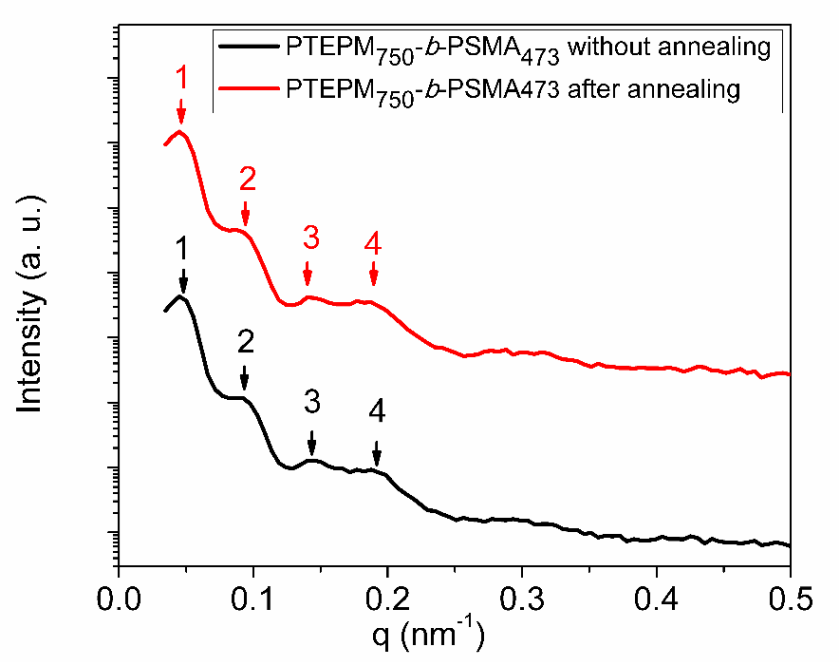

Figure 4.12 ESAXS of $PSMA_{750}$-*b*-$PSMA_{473}$ film formed by rapid THF evaporation before and after thermal annealing.

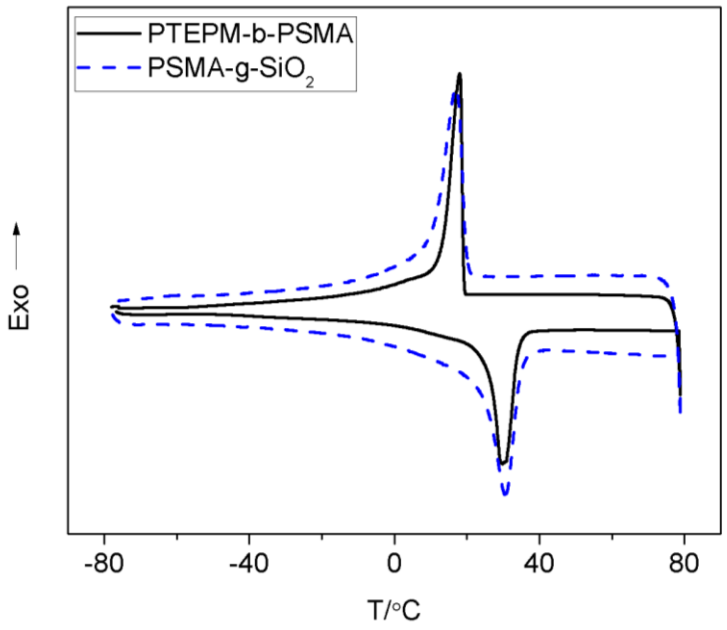

Figure 4.13 DSC PTEPM$_{666}$-*b*-PSMA$_{553}$ and PSMA$_{553}$-*g*-SiO$_2$

The PTEPM-*b*-PSMA BCP could rapidly self-assemble into well-ordered micro-structure without annealing. The PTEPM$_{750}$-*b*-PSMA$_{473}$ BCP in THF solution was drop cast to form a film with rapid THF evaporation. The ESAXS profile indicated highly ordered lamellar structure (1:2:3:4) was formed without any thermal or solvent vapor annealing. Moreover, the ESAXS data of PTEPM$_{750}$-*b*-PSMA$_{473}$ BCP with thermal annealing at 60 ℃ for 12 hours was almost identical to the film without annealing (**Figure 4.12**). We believe crystallization of the PSMA regions contributed to the rapid self-assembly of the BCP. Differential scanning calorimetry (DSC) showed the PTEPM$_{666}$-*b*-PSMA$_{553}$ and PSMA$_{553}$-*g*-SiO$_2$ crystallized at 17.9 ℃ and 17.0 ℃, respectively (**Figure 4.13**).

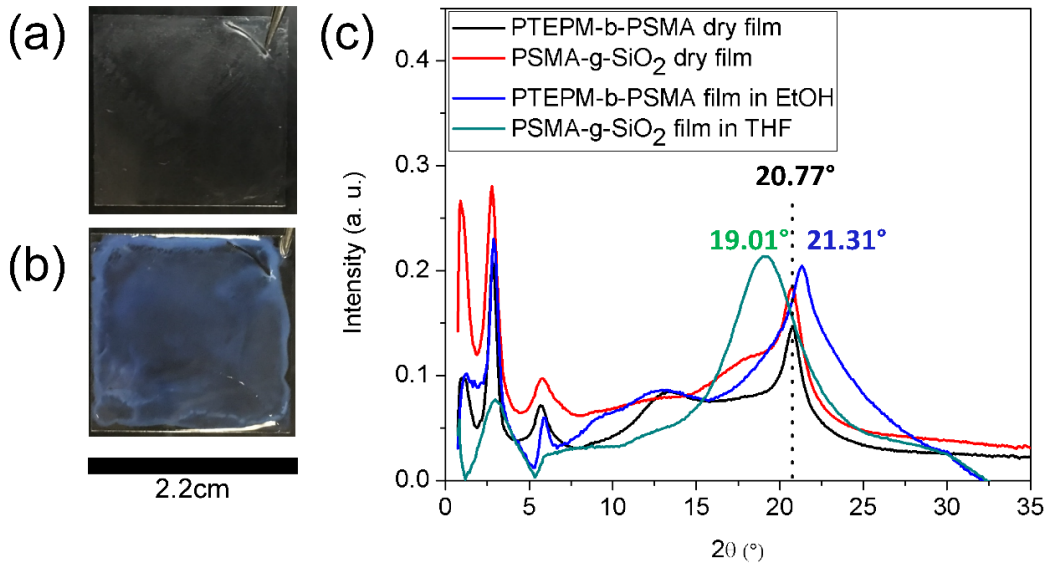

Figure 4.14 Photographs of (a) $PTEPM_{666}$-*b*-$PSMA_{553}$ film by solvent casting on a glass slide without annealing; (b) $PTEPM_{666}$-*b*-$PSMA_{553}$ film after spraying with EtOH; (c) WAXS data of dry films and films in different solvents.

Wide-angle X-ray scattering (WAXS) was used to characterize the crystallization behavior of PSMA (**Figure 4.14**). Both the $PTEPM_{666}$-*b*-$PSMA_{553}$ and $PSMA_{553}$-*g*-SiO_2 dry films showed a sharp peak at 2θ=20.77° ascribed to the PSMA crystallinity.[37] The peaks became broader after the $PTEPM_{666}$-*b*-$PSMA_{553}$ and $PSMA_{553}$-*g*-SiO_2 films were immersed in ethanol and THF, respectively. This indicated the crystallite size was smaller after immersion in solvents.[38] After the $PTEPM_{666}$-*b*-$PSMA_{553}$ film was immersed in ethanol, the inter-planar spacing decreased from 4.27 Å to 4.17 Å, which was due to the slight shrinkage of the PSMA domain in ethanol. For the $PSMA_{553}$-*g*-SiO_2 film, the inter-planar spacing increased from 4.27 Å to 4.67 Å, which was due to the swelling of PSMA domain in THF. The film displayed a blue color in one minute after ethanol was sprayed onto the surface of film (**Figure 4.14**).

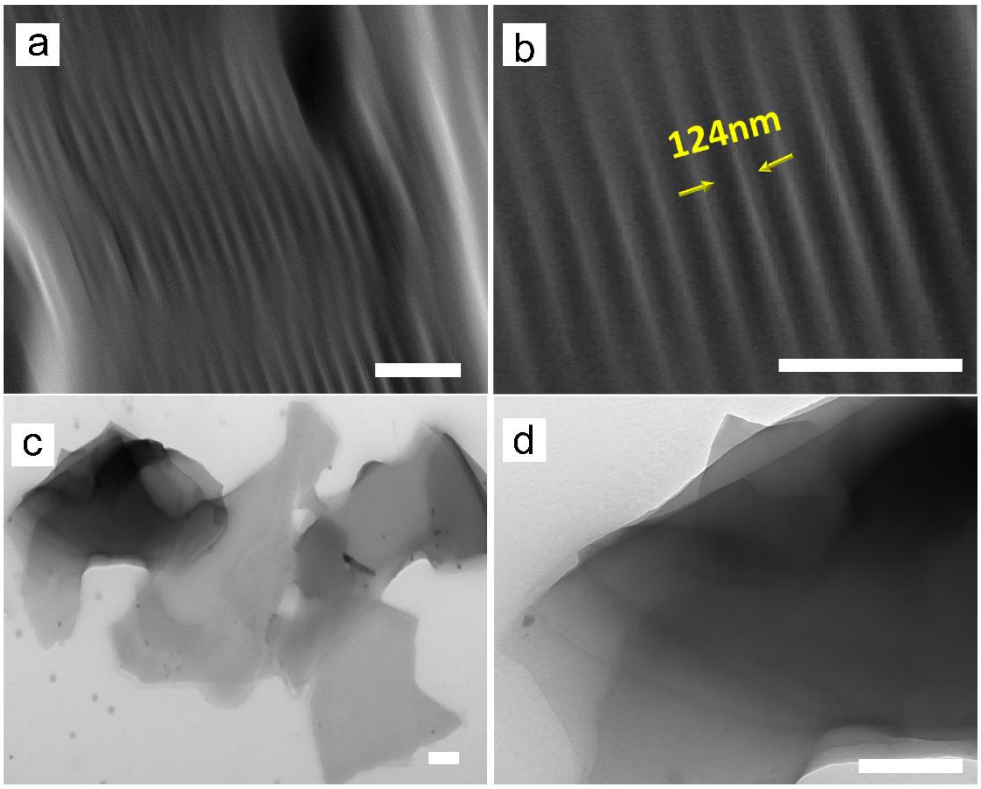

Figure 4.15 Microscopic characterization of polymer grafted silica nanoplatelets. (a) and (b) Cross sectional SEM of $PSMA_{553}$-*g*-SiO_2. Samples were prepared by freezing the film in liquid nitrogen and fracturing films; (c) and (d) TEM of $PSMA_{553}$-*g*-SiO_2. Samples were prepared by stirring the film in THF for one week and supernatant was dropped onto a copper grid. (Scale bars are 500 nm)

Scanning electron microscopy (SEM) and transmission electron microscopy (TEM) were used to characterize the microstructure of $PSMA_{553}$-*g*-SiO_2 film (**Figure 4.15**). It was observed from the SEM images that the film formed a well-ordered lamellar morphology. The distance between two silica nanoplatelets was *ca.* 124 nm, which was consistent with ESAXS data (d=126 nm). The TEM images showed that there were large pieces of silica nanoplatelets (diameter of pieces were larger than 2 μm) with several layers packing together.

The reflected color of the photonic crystals formed by in situ silica formation of self-assembled block copolymer can be tuned by the molecular weight of the

PTEPM-*b*-PSMA. A lower molecular weight block copolymer, $PTEPM_{390}$-*b*-$PSMA_{353}$ (Mn ($PTEPM_{390}$) =75000, Đ=1.14; Mn ($PTEPM_{390}$-*b*-$PSMA_{353}$) =139300, Đ=1.25), was synthesized to investigate the photonic property response to solvents (**Figure 4.16-4.18**).

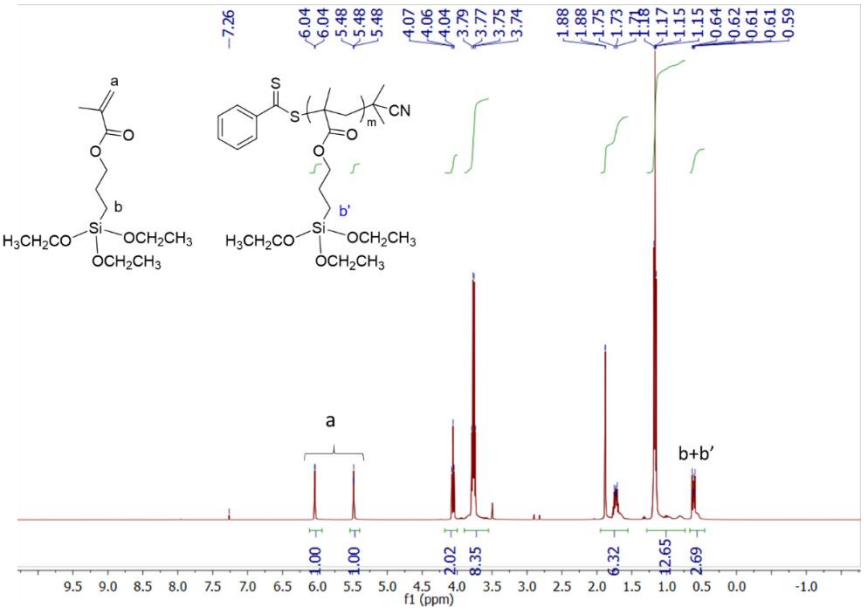

Figure 4.16 ^{1}H NMR ($CDCl_3$, 400MHz) of $PTEPM_{390}$ polymer solution

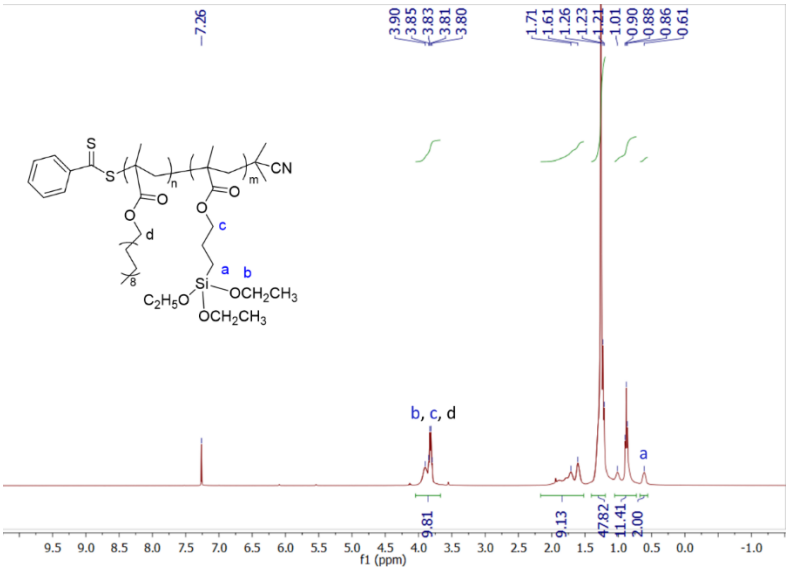

Figure 4.17 ^{1}H NMR ($CDCl_3$, 400MHz) of $PTEPM_{390}$-*b*-$PTEPM_{353}$ block copolymer

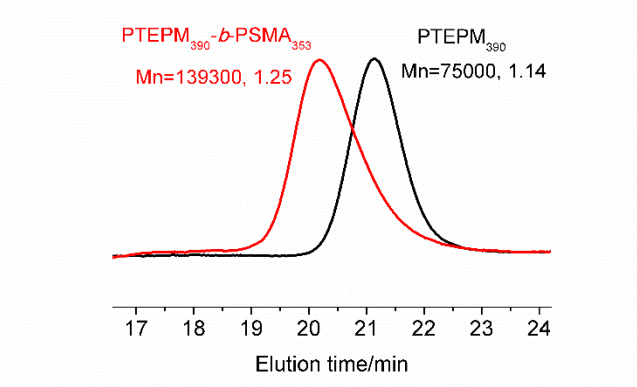

Figure 4.18 GPC curves of $PTEPM_{390}$ and $PTEPM_{390}$-*b*-$PSMA_{353}$

The ESAXS profile showed $PTEPM_{390}$-*b*-$PSMA_{353}$ self-assembled into a lamellar structure with d-spacing ca. 109 nm (**Figure 4.19**). The film displayed no obvious color change after immersion into ethanol, while the transmission spectra indicated no stop band in the visible light wavelength range. After conversion to silica nanoplatelets, $PSMA_{353}$-*g*-SiO_2 changed from colorless (dry film) to green (film in THF) with a stop band at 568 nm (**Figure 4.20**). The ESAXS profile showed the d-spacing increased from 102 nm (dry film) to 159 nm (film in THF).

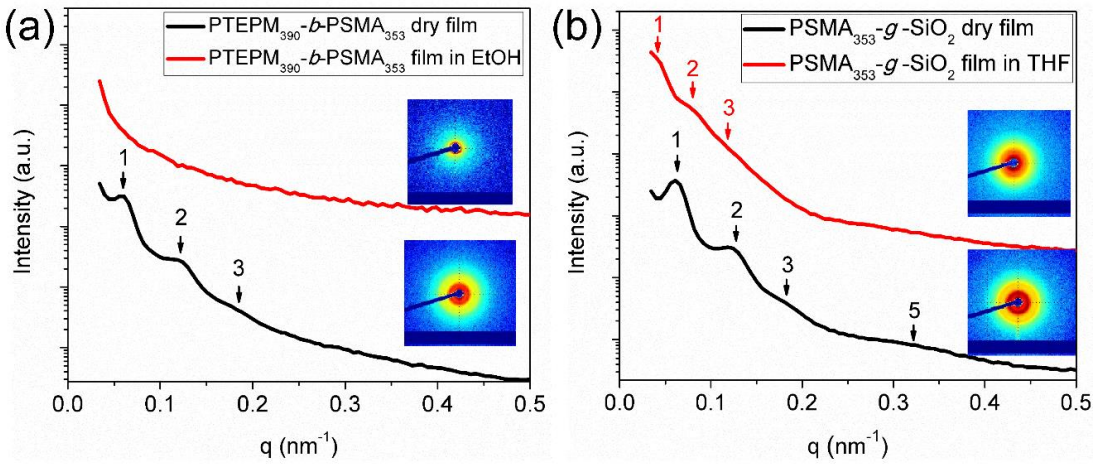

Figure 4.19 ESAXS of (a) $PTEPM_{390}$-*b*-$PSMA_{353}$ dry film and film in EtOH; (b) $PSMA_{353}$-*g*-SiO_2 dry film and film in THF. (The inserts are 2D patterns)

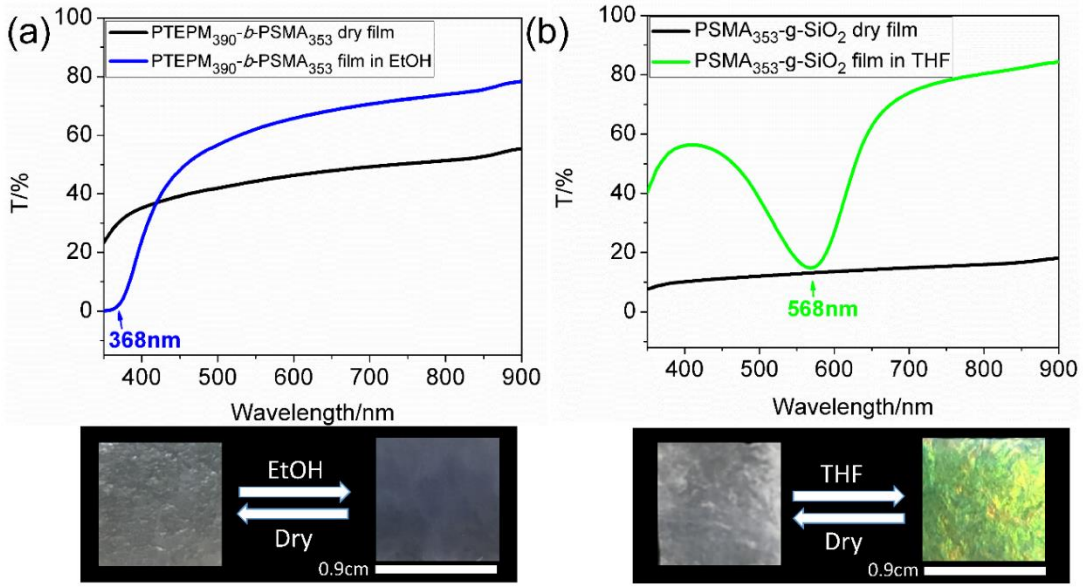

Figure 4.20 Transmission spectra and photographs of (a) $PTEPM_{390}$-*b*-$PSMA_{353}$ dry film and film in EtOH; (b) $PSMA_{353}$-*g*-SiO_2 dry film and film in THF.

4.5 Conclusion

We have demonstrated a facile strategy to synthesize two different kinds of photonic crystals, a block copolymer with modest molecular weight and polymer grafted silica nanoplatelets. Although prepared from the same batch of BCP, the two materials exhibited different solvent responses and reflecting colors. The film formed by self-assembly of $PTEPM_{666}$-*b*-$PSMA_{553}$ reflected blue color in ethanol. A new photonic crystal was generated by in situ conversion of the PTEPM domain of the BCP into silica to form $PSMA_{553}$-*g*-SiO_2 nanoplatelets, which reflected an orange color in THF. The $PSMA_{553}$-*g*-SiO_2 nanoplatelet film showed long-term stability even in good solvents for the grafted polymer PSMA. Different molecular weight block copolymers were investigated to construct different colors of photonic crystals. The crystalline domain contributed to rapid self-assembly of the block copolymer, which could be used in surface coatings for photonic applications.

4.6 References

(1) Bates, F. S.; Fredrickson, G. H. *Annu. Rev. Phys. Chem.* **1990**, *41*, 525.

(2) Stefik, M.; Guldin, S.; Vignolini, S.; Wiesner, U.; Steiner, U. *Chem. Soc. Rev.* **2015**, *44*, 5076.

(3) Moon, J. H.; Yang, S. *Chem. Rev.* **2010**, *110*, 547.

(4) Edrington, A. C.; Urbas, A. M.; DeRege, P.; Chen, C. X.; Swager, T. M.; Hadjichristidis, N.; Xenidou, M.; Fetters, L. J.; Joannopoulos, J. D.; Fink, Y.; Thomas, E. L. *Adv. Mater.* **2001**, *13*, 421.

(5) Yue, Y.; Gong, J. P. *J. Photochem. Photobiol., C* **2015**, *23*, 45.

(6) Hustad, P. D.; Marchand, G. R.; Garcia-Meitin, E. I.; Roberts, P. L.; Weinhold, J. D. *Macromolecules* **2009**, *42*, 3788.

(7) Chiang, Y.-W.; Chou, C.-Y.; Wu, C.-S.; Lin, E.-L.; Yoon, J.; Thomas, E. L. *Macromolecules* **2015**, *48*, 4004.

(8) Matsushita, A.; Okamoto, S. *Macromolecules* **2014**, *47*, 7169.

(9) Fan, Y.; Walish, J. J.; Tang, S.; Olsen, B. D.; Thomas, E. L. *Macromolecules* **2014**, *47*, 1130.

(10) Lee, W.; Yoon, J.; Thomas, E. L.; Lee, H. *Macromolecules* **2013**, *46*, 6528.

(11) Lim, H. S.; Lee, J.-H.; Walish, J. J.; Thomas, E. L. *ACS Nano* **2012**, *6*, 8933.

(12) Park, T. J.; Hwang, S. K.; Park, S.; Cho, S. H.; Park, T. H.; Jeong, B.; Kang, H. S.; Ryu, D. Y.; Huh, J.; Thomas, E. L.; Park, C. *ACS Nano* **2015**, *9*, 12158.

(13) Hwang, K.; Kwak, D.; Kang, C.; Kim, D.; Ahn, Y.; Kang, Y. *Angew. Chem., Int. Ed.* **2011**, *50*, 6311.

(14) Lu, Y.; Xia, H.; Zhang, G.; Wu, C. *J. Mater. Chem.* **2009**, *19*, 5952.

(15) Kim, E.; Kang, C.; Baek, H.; Hwang, K.; Kwak, D.; Lee, E.; Kang, Y.; Thomas, E. L. *Adv. Funct. Mater.* **2010**, *20*, 1728.

(16) Yoon, J.; Lee, W.; Thomas, E. L. *Macromolecules* **2008**, *41*, 4582.

(17) Valkama, S.; Kosonen, H.; Ruokolainen, J.; Haatainen, T.; Torkkeli, M.; Serimaa, R.; Ten Brinke, G.; Ikkala, O. *Nat. Mater.* **2004**, *3*, 872.

(18) Noro, A.; Tomita, Y.; Shinohara, Y.; Sageshima, Y.; Walish, J. J.; Matsushita, Y.; Thomas, E. L. *Macromolecules* **2014**, *47*, 4103.

(19) Serpe, M. J.; Kang, Y.; Zhang, Q. M. *Photonic Materials for Sensing, Biosensing and Display Devices*; Springer, Switzerland, 2016.

(20) Kim, E. A., H.; Park, S.; Lee, H.; Lee, M.; Lee, S.; Kim, T.; Kwak, E.-A.; Lee, J. H.; Lei, X.; Huh, J.; Bang, J.; Lee, B.; Ryu, D. Y. *ACS Nano* **2013**, *7*, 1952.

(21) Urbas, A.; Sharp, R.; Fink, Y.; Thomas, E. L.; Xenidou, M.; Fetters, L. J. *Adv. Mater.* **2000**, *12*, 812.

(22) Xia, Y.; Olsen, B. D.; Kornfield, J. A.; Grubbs, R. H. *J. Am. Chem. Soc.* **2009**, *131*, 18525.

(23) Miyake, G. M.; Weitekamp, R. A.; Piunova, V. A.; Grubbs, R. H. *J. Am. Chem. Soc.* **2012**, *134*, 14249.

(24) Macfarlane, R. J.; Kim, B.; Lee, B.; Weitekamp, R. A.; Bates, C. M.; Lee, S. F.; Chang, A. B.; Delaney, K. T.; Fredrickson, G. H.; Atwater, H. A.; Grubbs, R. H. *J. Am. Chem. Soc.* **2014**, *136*, 17374.

(25) Sveinbjornsson, B. R.; Weitekamp, R. A.; Miyake, G. M.; Xia, Y.; Atwater, H. A.; Grubbs, R. H. *Proc. Natl. Acad. Sci. U.S.A.* **2012**, *109*, 14332.

(26) Mapas, J. K. D.; Thomay, T.; Cartwright, A. N.; Ilavsky, J.; Rzayev, J. *Macromolecules* **2016**, *49*, 3733.

(27) Kang, Y.; Walish, J. J.; Gorishnyy, T.; Thomas, E. L. *Nat. Mater.* **2007**, *6*, 957.

(28) Bonifacio, L. D.; Lotsch, B. V.; Puzzo, D. P.; Scotognella, F.; Ozin, G. A. *Adv. Mater.* **2009**, *21*, 1641.

(29) Song, D.-P.; Shahin, S.; Xie, W.; Mehravar, S.; Liu, X.; Li, C.; Norwood, R. A.; Lee, J.-H.; Watkins, J. J. *Macromolecules* **2016**, *49*, 5068.

(30) Bockstaller, M. R.; Lapetnikov, Y.; Margel, S.; Thomas, E. L. *J. Am. Chem. Soc.* **2003**, *125*, 5276.

(31) Song, D. P.; Li, C.; Li, W.; Watkins, J. J. *ACS Nano* **2016**, *10*, 1216.

(32) Jeon, S.-J.; Chiappelli, M. C.; Hayward, R. C. *Adv. Funct. Mater.* **2016**, *26*, 722.

(33) Kang, C.; Kim, E.; Baek, H.; Hwang, K.; Kwak, D.; Kang, Y.; Thomas, E. L. *J. Am. Chem. Soc.* **2009**, *131*, 7538.

(34) Zhang, K.; Gao, L.; Chen, Y. *Macromolecules* **2007**, *40*, 5916.

(35) Chen, Y. *Macromolecules* **2012**, *45*, 2619.

(36) Ozaki, H.; Hirao, A.; Nakahama, S. *Macromolecules* **1992**, *25*, 1391.

(37) Jian, Y.; He, Y.; Wang, J.; Xu, B.; Yang, W.; Nie, J. *New J. Chem.* **2013**, *37*, 444.

(38) Langford, J. I.; Wilson, A. J. C. *J. Appl. Crystallogr.* **1978**, *11*, 102.

CHAPTER 5

CONCLUSION AND FUTURE WORK

CONCLUSION

Matrix free polymer nanocomposites were designed, synthesized, characterized, and applied in various aspects: thermoplastic elastomers, gas separation membranes, and photonic crystals. Reversible addition fragmentation chain transfer (RAFT) polymerization was used to synthesize functional block copolymers and polymer grafted silica nanoparticles.

The thermoplastic elastomers were formed by block copolymer grafted silica nanoparticles PS-*b*-PBA-*g*-SiO_2 with different chain lengths and graft densities via surface initiated RAFT polymerization. The effects of polymer chain length and polymer graft density on the mechanical properties were evaluated. The PS content was crucial to the ultimate tensile stress and elastic modulus. An increase in PS content resulted in an increase of ultimate tensile stress and elastic modulus. The longer PBA chain length resulted in a higher strain at break. The higher polymer graft density TPEs had similar tensile strain and stress to the lower graft density TPEs with similar block copolymer chain length. However, the higher graft density TPEs resulted in a higher elastic modulus than low graft density film. The highest ultimate tensile strength of PS-*b*-PBA-*g*-SiO_2 (*ca.* 17 MPa) was higher than the highest value of TPEs from triblock PS-*b*-PBA-*b*-PS (*ca.* 12 MPa) prepared by emulsion RAFT polymerization. DMA, SAXS and TEM data revealed the higher polymer graft density TPEs had a better microphase separation and more uniform nanoparticle dispersion than lower graft density TPEs with similar polymer chain lengths and composition. This versatile strategy to prepare thermoplastic elastomers by block

copolymer grafted nanoparticles broadened the design of new TPEs. The mechanical properties of traditional TPEs formed by ABA triblock copolymers can only be tuned by chain length and composition of the block copolymers. In comparison, TPEs formed by block copolymer grafted nanoparticles introduces a new parameter, polymer chain graft density, as a new tool to enhance microphase separation, and hence to tune the mechanical properties of TPEs.

Matrix-free polymer nanocomposites were also applied in gas separation membranes. Polymerization conditions were developed for the controlled high molecular weight synthesis of poly(methyl acrylate) grafted silica nanoparticles (PMA-g-SiO_2) by surface-initiated RAFT polymerization. Different RAFT agents and solvent effects were investigated on the RAFT polymerization. The PMA-g-SiO_2 was successfully synthesized with DoPAT-SiO_2 in DMF solvent. An effective and timesaving strategy was developed to separate the ungrafted PMA polymer from PMA-g-SiO_2. Ultrasonication effects on the PMA-g-SiO_2 were also investigated for proper processing. The membrane formed by matrix free PMA-g-SiO_2 and PMMA-g-SiO_2 showed an enhancement of the permeability in CO_2 while the selectivity of CO_2 over CH_4 had minor changes when compared to neat polymers, which was contrary to the traditional composite theory. The most permeable membrane of PMA-g-SiO_2 had an increase over 800% in permeability while the selectivity decreased about 35%. The permeability of polymer films showed a "volcano plot" in the permeability relative to neat polymer versus PMA molecular weight. The free volume measured by PALS exhibited a similar volcano shape to relative permeability versus PMA Mn, which indicated the permeability was related to the free volume. TEM images showed the PMA-g-SiO_2 had no agglomeration of nanoparticles in the membranes. The grafted

PMMA and PMA silica nanoparticles exhibited no aging effect, which provided an advantageous strategy for designing new industrial membranes with long time life. The membranes from polymer grafted nanoparticles exhibited significantly enhanced performance than neat polymers, which motivated us to design other glassy polymer grafted nanoparticle systems for potential better separation.

Self-assembled block copolymers with lamellar structure and *in situ* generated polymer grafted silica nanoplatelets formed photonic crystals. Although prepared from the same batch of block copolymer, the two materials exhibited different solvent responses and reflecting colors. The film formed by self-assembly of $PTEPM_{666}$-*b*-$PSMA_{553}$ reflected blue color in ethanol. A new photonic crystal was generated by *in situ* conversion of the PTEPM domain of the block copolymer into silica to form $PSMA_{553}$-*g*-SiO_2 nanoplatelets, which reflected an orange color in THF. The reflecting of visible lights from films in solvents resulted from the enhanced layer distance, which were characterized by ESAXS of dry films and films in solvents. The $PSMA_{553}$-*g*-SiO_2 nanoplatelet film showed long-term stability even in good solvents for the grafted polymer PSMA. Different molecular weight block copolymers were investigated to construct different colors of photonic crystals. The crystalline domain contributed to rapid self-assembly of the block copolymer, which could be used in surface coatings for photonic applications.

FUTURE WORK

This thesis focused on the design, synthesis, characterization and applications matrix of free polymer nanocomposites in different aspects: thermoplastic elastomers, gas

separation films, and photonic crystals. Further work could be done with other different functional polymer grafted nanoparticles with various properties.

Currently we have investigated the thermoplastic elastomers formed by matrix free block copolymer PS-b-PBA grafted silica nanoparticles, which showed a higher stress at break (*ca.* 17 MPa) than the thermoplastic elastomers formed by PS-b-PBA-PS triblock copolymers (ca. 14 MPa). This grafting of block copolymers onto silica nanoparticles enhanced the stress as compared to neat triblock copolymer. The commercially available styrene-butadiene-styrene (SBS) thermoplastic elastomer had stress at 30MPa and 800% strain at break. It could be interesting to synthesize poly(styrene-*block*-butadiene) grafted silica nanoparticles for new thermoplastic elastomers with higher stress at break than current SBS type thermoplastic elastomers. Another research direction could probe methods for better alignment of silica nanoparticles in the block copolymer grafted silica nanocomposite. We used the commercial Nissan spherical silica nanoparticles (MET-ST) with broad size distribution (14 ± 4 nm). Even though the TEM images of high polymer graft density showed good dispersion of nanoparticles in the block copolymer matrix, it didn't form perfect hexagonal morphology, which might be due to the broad size distribution of silica nanoparticles. It would be interesting to synthesize uniform size of nanoparticles for the investigation of mechanical properties of thermoplastic elastomers from block copolymer grafted nanoparticles, which can dissipate the applied mechanical force more evenly to achieve higher tensile stress and strain at break.

The matrix free polymer grafted silica nanoparticle membranes showed an enhancement of 10-fold for CO_2 permeability while still maintaining its selectivity of CO_2/CH_4. Even though this enhancement was still below the Robeson upper bound, we

can utilize this grafting technique to design and synthesize new polymer nanocomposite membranes for better performance. This grafting technique offered a versatile strategy to tune the free volume, resulting in an increase of gas permeability in both PMA and PMMA grafted silica nanoparticle membranes. This provides inspiration to design grafted polymer candidates located close to Robeson upper bound (cellulose acetates and polyimides types), which could exceed the upper bound. Another pathway for design of better gas separation membranes is to graft chemical functional group polymers onto silica nanoparticles. CO_2 is an acidic gas, which has stronger interaction with amines than CH_4 or other neutral gases. The polymers with primary and secondary amine groups could be grafted onto silica nanoparticles for a new design of matrix free polymer nanocomposite gas separation membranes.

Photonic crystals were formed by block copolymers and the *in situ* gelation of polymer grafted silica nanoplatelets and exhibited responsiveness to different solvents. After gelation, the polymer grafted silica nanoplatelets showed a high stop band shift from 365nm to 591nm. New architectures could be designed for faster and longer wavelength reflection based on the polymer grafted nanoplatelets, such as polymer brushes. The poly(stearyl methacrylate) grafted silica nanoplatelets can also be compounded with polyethylene for gas barrier applications.

APPENDIX A

PERMISSION TO REPRINT

Chapter 2 Reproduced by permission of ACS Publications

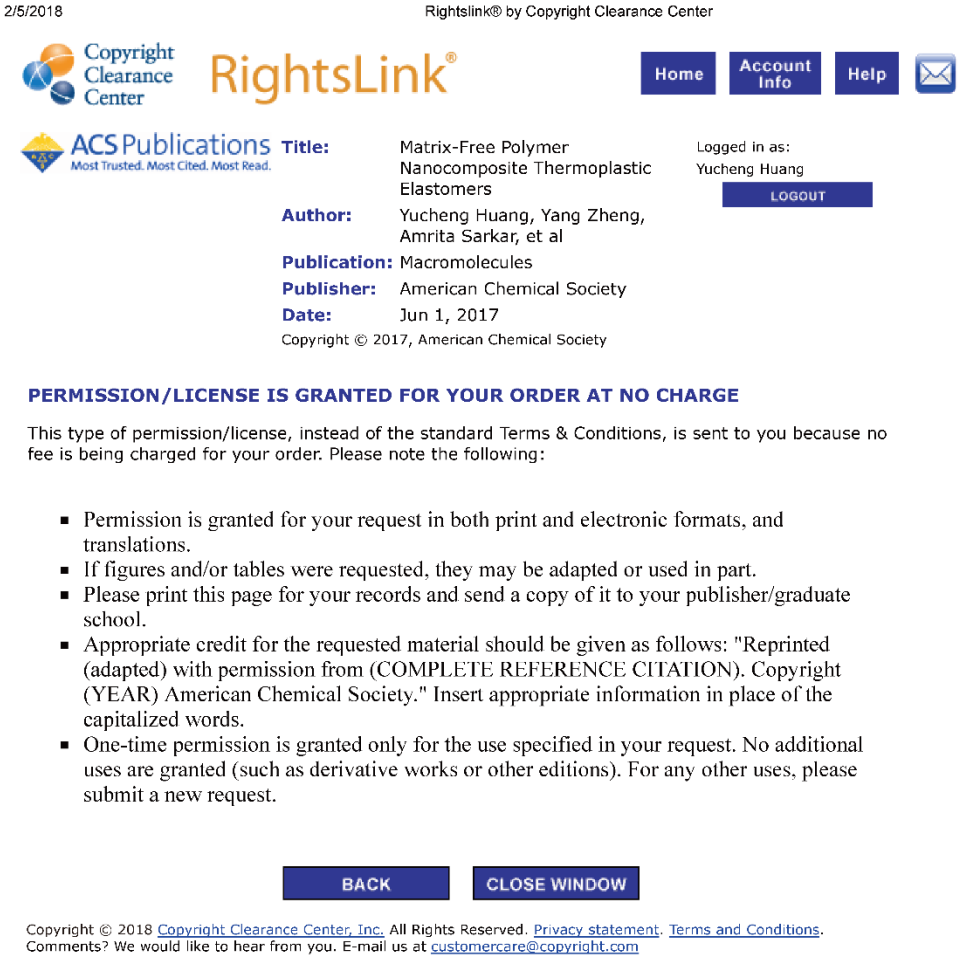

2/5/2018 Rightslink® by Copyright Clearance Center

Copyright Clearance Center RightsLink® Home Account Info Help

ACS Publications Most Trusted. Most Cited. Most Read.

Title: Matrix-Free Polymer Nanocomposite Thermoplastic Elastomers

Author: Yucheng Huang, Yang Zheng, Amrita Sarkar, et al

Publication: Macromolecules

Publisher: American Chemical Society

Date: Jun 1, 2017

Copyright © 2017, American Chemical Society

Logged in as: Yucheng Huang LOGOUT

PERMISSION/LICENSE IS GRANTED FOR YOUR ORDER AT NO CHARGE

This type of permission/license, instead of the standard Terms & Conditions, is sent to you because no fee is being charged for your order. Please note the following:

- Permission is granted for your request in both print and electronic formats, and translations.
- If figures and/or tables were requested, they may be adapted or used in part.
- Please print this page for your records and send a copy of it to your publisher/graduate school.
- Appropriate credit for the requested material should be given as follows: "Reprinted (adapted) with permission from (COMPLETE REFERENCE CITATION). Copyright (YEAR) American Chemical Society." Insert appropriate information in place of the capitalized words.
- One-time permission is granted only for the use specified in your request. No additional uses are granted (such as derivative works or other editions). For any other uses, please submit a new request.

BACK CLOSE WINDOW

Copyright © 2018 Copyright Clearance Center, Inc. All Rights Reserved. Privacy statement. Terms and Conditions.
Comments? We would like to hear from you. E-mail us at customercare@copyright.com

Chapter 4 Reproduced by permission of The Royal Society of Chemistry

A versatile approach to different colored photonic films generated from block copolymers and their conversion into polymer-grafted nanoplatelets

Y. Huang, Y. Zheng, J. Pribyl and B. C. Benicewicz, *J. Mater. Chem. C*, 2017, **5**, 9873
DOI: 10.1039/C7TC02562A
http://pubs.rsc.org/en/content/articlelanding/2017/tc/c7tc02562a#!divAbstract

contracts-copyright@rsc.org

Dear Yucheng Huang,

The Royal Society of Chemistry (RSC) hereby grants permission for the use of your paper(s) specified below in the printed and microfilm version of your thesis. You may also make available the PDF version of your paper(s) that the RSC sent to the corresponding author(s) of your paper(s) upon publication of the paper(s) in the following ways: in your thesis via any website that your university may have for the deposition of theses, via your university's Intranet or via your own personal website. We are however unable to grant you permission to include the PDF version of the paper(s) on its own in your institutional repository. The Royal Society of Chemistry is a signatory to the STM Guidelines on Permissions (available on request).

Please note that if the material specified below or any part of it appears with credit or acknowledgement to a third party then you must also secure permission from that third party before reproducing that material.

Please ensure that the thesis states the following:

Reproduced by permission of The Royal Society of Chemistry and include a link to the paper on the Royal Society of Chemistry's website.

Please ensure that your co-authors are aware that you are including the paper in your thesis.

Best wishes,

Chloe Szebrat
Contracts and Copyright Executive
Royal Society of Chemistry
Thomas Graham House
Science Park, Milton Road
Cambridge, CB4 0WF, UK
Tel: +44 (0) 1223 438329
www.rsc.org